THE THERMODYNAMIC PROPERTIES OF LEAD FILTERS

A thesis submitted to the University of Manchester for the degree of
Ph.D. in the Faculty of Technology
by
A.L. Jones

Department of Chemistry
UMIST
October, 1991

All of the work described in this thesis is the original work of the author, except where acknowledged by reference or special recognition. No portion of the work referred to in this thesis has been submitted in support of an application for another degree or qualification of this or any other university or other institution of learning.

Signed .....
Certified .....
Date .....

Acknowledgements

I thank Dr. Bob Simmons for his guidance and perseverance over the many years! I would also like to thank Dr Ting-Man Li and Dr J.R. Grove from The Associated Octel Company Ltd. for their help and encouragement, and SERC and The Associated Octel Company Ltd. for funding this research. Finally, thanks to Eric the glass, Max the computer, Terry the tools, Walter the stores, Robin the X-ray and all other members of the staff at UMIST who contributed in any way whatsoever!

Abstract

The vapour pressure and enthalpy of sublimation of lead bromide, 1:1 lead oxybromide and 2:1 lead oxybromide have been measured using the transpiration method and in all cases the evaporating species was lead bromide. Table 1 contains a summary of the vapour pressure data and shows the temperature ranges over which the data were obtained, the corresponding enthalpies of sublimation are given in Table 2. The lead oxybromides used in

Table 1: The vapour pressure data for lead bromide, 1:1 lead oxybromide and 2:1 lead oxybromide. $\log_{10}$ (p/mmHg) = $A + B\ K/T$

	Temperature Range K	A	B
lead bromide	613 - 645	12.0 ± 0.7	-9200 ± 480
1:1 lead oxybromide	630 - 770	10.0 ± 0.13	-8293 ± 91
2:1 lead oxybromide	803 - 919	11.4 ± 0.18	-11240 ± 149

Table 2: The enthalpy of sublimation of lead bromide from lead bromide, 1:1 lead oxybromide and 2:1 lead oxybromide

	Temperature Range K	$\Delta H_{sublimation}$ kJ mol^{-1}
lead bromide	613 - 645	176 ± 9
1:1 lead oxybromide	630 - 770	159 ± 2
2:1 lead oxybromide	803 - 919	215 ± 2

the vapour pressure experiments were characterised using X-ray powder crystallography and differential thermal analysis. The temperature dependence of the phases formed when mixtures of lead oxide and lead bromide were heated was also studied using these techniques.

Contents

List of Tables

List of Figures

Chapter 1

Introduction

1.1 The Background to the Present Study

This present study was concerned with the possible improvement of an existing lead filter developed by the Associated Octel Company Ltd., and it was begun before the decision was taken to remove completely lead based anti-knock agents from petrol. This decision followed a survey entitled Lead and Health [6] carried out by the Department of Health and Social Security (DHSS). The report contained data which gave the amount of lead entering the body by a number of different routes and provided suggestions as to ways in which the intake could be reduced. The data showed quite clearly that the majority of the lead found in the body was ingested with food and that the contribution from airborne lead was minimal. The working party found no indication that raised blood lead levels were due to lead in petrol, however, they were unanimous in recommending to the government that it would be prudent to reduce emissions of lead into the air.

At that time the existing exhaust filters were capable of efficiently trapping the majority of the lead species from the exhaust gases during urban driving, but unfortunately the emission increased under subsequent high speed driving conditions when the temperature of the filter rose. As a consequence a considerable amount of effort was being channelled into improving the performance of these filters.

The lead based anti-knock agents added to petrol consist mainly of tetraethyllead and tetramethyllead. Both of these compounds are highly toxic, foul smelling and volatile liquids. Neat tetramethyllead is known to explode violently and for this reason it is usually supplied in a solution of toluene. In addition, the anti-knock agent contains brominated and chlorinated hydrocarbons namely, dibromoethane and dichloroethane. These compounds are often referred to as "scavengers" because their sole purpose is to prevent the build up of lead deposits on the colder sections of the combustion chamber.

Thus, the combustion products of particular interest in this study are lead oxide and lead, from the lead alkyls and hydrogen halides from the scavengers.

A theoretical examination of the gaseous lead compounds in the exhaust stream from a petrol engine [36] showed that both lead oxide and lead were formed in the combustion process, with gaseous lead oxide predominating in lean and stoichiometric mixtures and gaseous lead predominating in rich mixtures. During the power stroke, however, the conversion of lead to lead oxide is sufficiently fast, even in rich mixtures, that by the end of the power stroke at least 90 % of the lead is converted to lead oxide. Thus, for all practical purposes, the lead species leaving the cylinder is lead oxide whether the engine is running fuel rich or under lean conditions. It was also shown that the exhaust gas becomes supersaturated with lead oxide before any significant formation of lead halide can occur, so that the solid initially deposited in the filter must be lead oxide. This then reacts with the hydrogen halide present in the exhaust gas to form the relevant oxybromide or oxychloride,

Examination of the solid deposit on a filter with an inlet temperature of 787 K showed that approximately equal amounts of lead sulphate and lead oxide were present (the latter from the sulphur present in the original fuel), but there was very little lead bromide. Deposits collected at 679 K still contained approximately equal amounts of lead sulphate and lead oxide, but the ratio of lead oxide to lead bromide was 2:1. At this temperature the lead bromide could not have condensed from the gas stream and this showed that it must have been formed by the reaction of solid lead oxide with the hydrogen bromide present in the gas stream. The latter reaction is known to proceed rapidly. It is important to note that at a temperature of 679 K a significant amount of the lead bromide produced would evaporate back into the gas stream.

The formation of lead oxyhalides is known to play an important role in the scavenging of lead deposits from the cooler regions of the combustion chamber. For example, Buck and Ryason [4] had previously explained qualitatively the composition of the deposits found in combustion engines which had been operating under specified conditions by treating the burnt gas and deposits as though they were in true thermodynamic equilibrium. The reactions suggested for the formation of the lead oxybromides were:

$$7PbO_{(s)} + 2HBr_{(g)} \rightleftharpoons 6PbO.PbBr_{2(s)} + H_2O_{(g)} \quad (1.1)$$

$$4(6PbO.PbBr_{2(s)}) + 6HBr_{(g)} \rightleftharpoons 7(3PbO.PbBr_{2(s)}) + 3H_2O_{(g)} \quad (1.2)$$

$$3(3PbO.PbBr_{2(s)}) + 2HBr_{(g)} \rightleftharpoons 4(2PbO.PbBr_{2(s)}) + H_2O_{(g)} \quad (1.3)$$

$$2(2PbO.PbBr_{2(s)}) + 2HBr_{(g)} \rightleftharpoons 3(PbO.PbBr_{2(s)}) + H_2O_{(g)} \quad (1.4)$$

$$2PbO.PbBr_{2(s)} + 4HBr_{(g)} \rightleftharpoons 3PbBr_{2(s)} + 2H_2O_{(g)} \quad (1.5)$$

$$PbO.PbBr_{2(s)} + 2HBr_{(g)} \rightleftharpoons 2PbBr_{2(s)} + H_2O_{(g)} \quad (1.6)$$

Thus, given sufficient hydrogen bromide gas the overall reaction becomes

$$PbO_{(s)} + 2HBr_{(g)} \rightleftharpoons PbBr_{2(s)} + H_2O_{(g)} \quad (1.7)$$

At any time the extent to which the conversion of lead oxide to lead bromide will proceed is determined by the partial pressures of water vapour and hydrogen bromide gas and for Reaction 1.1 the formation of $6PbO.PbBr_{2(s)}$ is controlled by

$$\Delta G^{\ominus} = -RT \ln(pH_2O/(pHBr)^2) \quad (1.8)$$

The standard Gibbs energy changes for the formation of the oxybromides at their melting point from lead bromide and lead oxide have been calculated by Buck and Ryason. The Gibbs energy change for the reaction

$$6PbO_{(s)} + PbBr_{2(s)} \rightarrow 6PbO.PbBr_{2(s)} \quad (1.9)$$

was calculated as -58 kJ mol^{-1} at 948 K and is believed to remain constant in the temperature range of interest (700-1000 K). The Gibbs energy change of Reaction 1.1 is related to this calculated value by

$$\Delta G_{1.1} = \Delta G_{1.9} - 58 \text{ kJ mol}^{-1} \quad (1.10)$$

Similar relationships exist for the other lead oxybromides.

Ting-Man Li and Simmons extended this analysis to show that the composition of the deposits could be explained quantitatively for a given level of lead and dibromoethane in the fuel. They calculated the variation of the Gibbs energy of the reactions with temperature, and then used these values to predict how far the transformation of lead oxide to lead oxybromide would proceed at any given temperature, air/fuel ratio and scavenger concentration. The results showed that the proportion of lead bromide in the solid phase increased with decreasing temperature, i.e. the lower oxybromides do not form at the higher temperatures. Figure 1.1 gives the theoretical change in the lead species in the exhaust gas [40], calculated assuming that the fuel was iso-octane containing 0.4 g l^{-1} Pb, 1 theory of dibromoethane and that the air fuel ratio was 15 (stoichiometric). The term "theory" is often used in the petrochemical industry to represent the stoichiometric amount of dibromoethane which is required to convert all of the lead to lead bromide.

Studies of the behaviour of the filters, performed with petrol engines on test beds, showed that with the engine running under low load, the majority of the lead species entering the

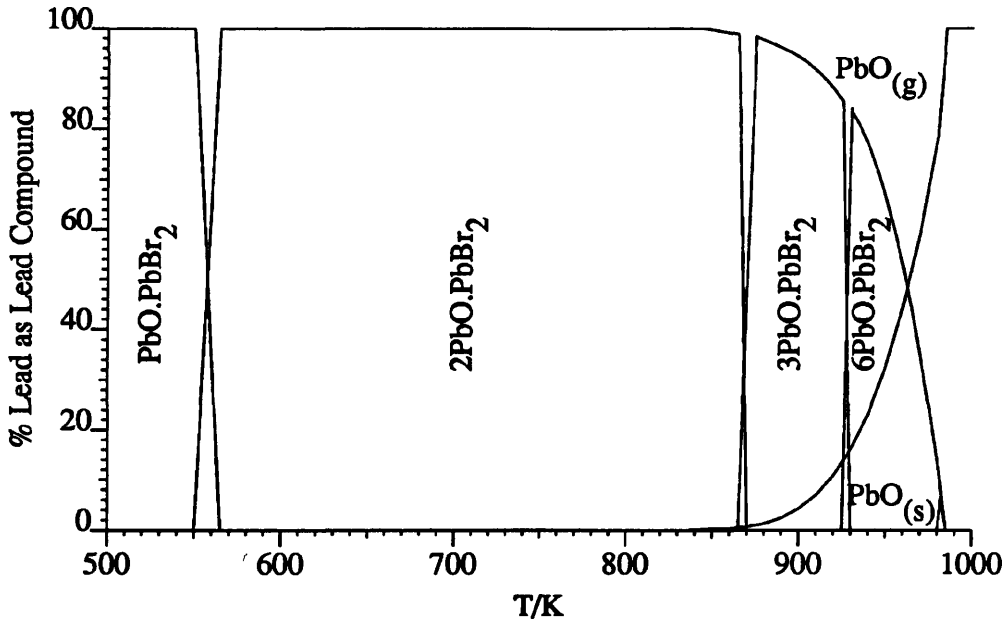

Figure 1.1: The change in lead species in the exhaust gas, fuel iso-octane, air/fuel ratio 15:1, 1 theory of dibromoethane and 0.4 g l^{-1} lead

filter were retained, when the engine load was increased however, the accompanying rise in the temperature of the filter led to the emission of a significant amount of the trapped lead. It was postulated, that at the lower exhaust temperatures associated with low engine loads (analogous to urban driving conditions) oxybromides rich in lead bromide were formed, i.e 1:1 or 2:1 lead oxybromide but, that these lead oxybromides become thermodynamically less stable with respect to those richer in lead oxide as the temperature is increased (see Figure 1.1). Thus, lead bromide was released as the ratio of lead oxide to lead bromide in the deposits increased. This free lead bromide then evaporated and was carried out of the exhaust by the stream of exhaust gas.

In order to gain a better understanding of the mechanism of lead retention in such a system it was necessary to obtain more data about the vapour / condensed phase equilibria between the lead compounds which could form under the relevant conditions and the exhaust gases. The priorities were identification of the species evaporating from lead oxybromides, the measurement of their vapour pressures and the determination of their relevant thermodynamic properties in the temperature range of interest.

1.2 The Determination of Vapour Pressure

The experimental methods for the determination of vapour pressure fall essentially into two categories, static and dynamic. When a vapour pressure is measured using a static

technique such as the boiling point method of Ramsay and Young [28], the isoteniscope of Smith and Menzies [39] and the numerous pressure balances [31, 13, 9, 2, 8], the amount of vapour or condensed phase does not change during the measurement. In contrast, dynamic techniques such as the evaporation methods attributed to Langmuir [24] and Knudsen [20] or the transpiration method devised by Renault [30] rely on a change in the amount of the condensed phase. Although the torsion effusion apparatus [42] is a form of pressure balance, it must be classed as a dynamic technique (see later). Each of the experimental methods which are commonly used to measure vapour pressure will be discussed in the following sections.

1.2.1 The Boiling Point Method

This technique provides the vapour pressure of a liquid under dynamic equilibrium conditions. At the boiling point the vapour pressure of a substance is assumed to be equal to the pressure in the vessel immediately above the surface of the liquid.

In general, the substance under test is enclosed in a vessel, the temperature and pressure of which can be accurately controlled and measured. Boiling is then induced by varying either the pressure or temperature, whilst the other is held constant. The temperature and pressure are then measured for the given conditions. The main sources of error in the determination of the boiling point are the actual measurement of the temperature and the ambiguous observation of the onset of boiling. The magnitude of the possible errors involved in the location of the boiling point when a poor means of indication is chosen can be illustrated by the work of Greenwood [12]. In his experiments he observed the boiling point as the point at which the surface of the liquid rippled and bubbles escaped; as much as 100 °C separated initial rippling and vigorous bubbling at the surface.

The precise identification of the boiling point has proved to be extremely difficult and a host of ingenious methods has been described. That of Smith and Menzies [38] involved submerging a small glass bulb with a fine capillary entry tube in a molten bath, the temperature of the bath was raised above the boiling point of the sample and then slowly lowered until the stream of bubbles emerging from the end of the capillary tube just ceased, at which point the vapour pressure of the sample was just equal to the pressure above the bath and the head of liquid above the mouth of the capillary tube.

Ruff and Bergdahl [32] used a metal spring balance to monitor the rate of weight loss of the sample as they raised the temperature of the apparatus at a constant rate and fixed pressure. The boiling point was then obtained from the position of the discontinuity in a plot of weight versus temperature. Unfortunately, this discontinuity is not always sharply

defined and, as the temperature is constantly rising it cannot be determined with any great precision. Fischer and Rahlfs [10] obtained a much more sharply defined boiling point from a plot of pressure against weight loss when they fixed the temperature and varied the pressure at a constant rate.

At elevated temperatures liquids can superheat and, under these conditions, a thermometer placed in the liquid gives a higher temperature than the "correct" value. Similarly, a thermometer suspended in the condensing vapour above the surface of the liquid can be affected by radiation (at low pressure) and convection from the heating section of the apparatus. In addition the vapour can superheat or supercool in a poorly designed apparatus.

These difficulties have led from the very simple early apparatus of Ramsay and Young [28] shown in Figure 1.2 to the sophisticated ebulliometers employed by the U.S. Bureau of Mines, Bartlesville and that used by the National Physical Laboratory, Teddington shown in Figure 1.3. The latter apparatus incorporates the following noteworthy features; the whole ebulliometer is surrounded by a heated jacket, the temperature of this jacket is held at between 1 and 5 K below that of the boiler and this reduces heat losses due to convection and radiation. There are four inverted bubble caps arranged such that they dip just below the surface of the liquid and, as the temperature is raised and the sample begins to boil, the steady stream of vapour bubbles emerging from the indentations in the caps promotes smooth boiling and helps prevent superheating. The drop counter, which is found at the bottom of the condenser is designed such that the drops of condensate do not fall directly into the liquid; instead they return via the sides of the boiler so that, the temperature of the boiling liquid is more homogeneous. Finally, a radiation shield is positioned around the condenser, although it has been suggested that this is of limited value. In practice, two of these ebulliometers are connected via condensers and cold traps, the boiling point of the sample and a reference compound are then measured simultaneously.

These ebullioscopic methods for the determination of the vapour pressure have been employed up to a temperature of 2000 K and down to a pressure of 2×10^{-2} mmHg. Below this pressure, the difficulties associated with the losses due to diffusion, coupled with radiation and superheating make the method unattractive in comparison with other methods. It is only applicable to liquids and as the lead oxyhalides studied in this work were solids, this precluded the use of an ebullioscopic method in the present work.

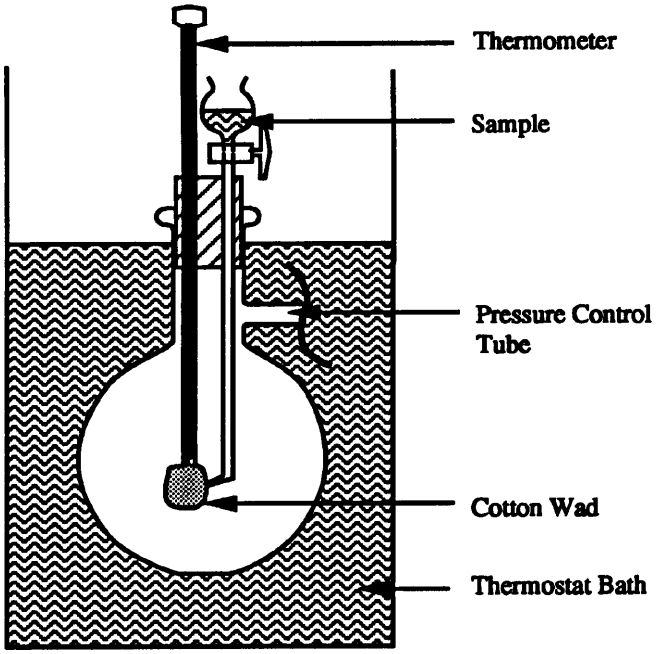

Figure 1.2: The boiling point apparatus of Ramsay and Young

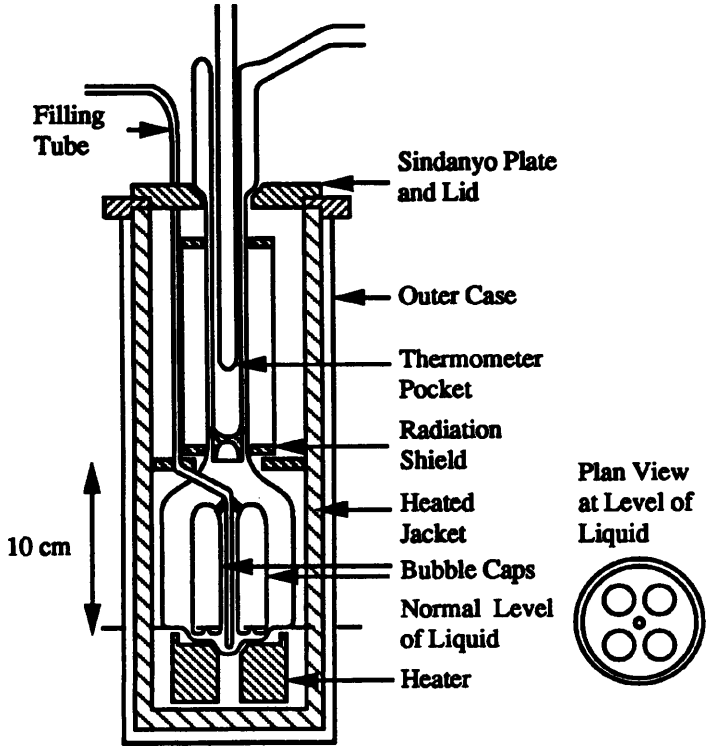

Figure 1.3: The boiling point apparatus used at the National Physical Laboratory

1.2.2 Manometer Measurements

The manometer technique for the measurement of vapour pressure is a static technique. In its simplest form it involves the use of two barometric tubes having a common cistern. The sample is introduced into a Torricelean vacuum in one tube and the depression in the level of the manometer fluid measured. The main inaccuracies of the method are due to dissolved gases which slowly diffuse into the vacuum and produce erroneously high vapour pressures.

This original technique has been improved considerably by subsequent workers. In general the apparatus consists of a sample chamber connected either directly or via a null instrument to a manometer. The residual gases are generally removed by boiling the sample. The main disadvantage of a system with a sample chamber connected directly to a manometer is that, in order to prevent distillation of the sample from one part of the apparatus to another, the complete system must be contained in a large thermostatic bath.

Probably the most famous static manometer apparatus is the isoteniscope of Smith and Menzies. In this apparatus the liquid itself was used as the null indicating manometer. This method can be applied to solids providing a suitable fluid is available for the U tube, but, the fluid must not be a solvent for the sample and it must be free from dissolved gases. The use of mercury is common when the vapour pressure is high, but this reduces the accuracy of the measurements when it is low.

In its simplest form, the manometer method is limited by the accuracy to which the level of the manometer fluid can be measured, and therefore a lower limit of approximately 1 mmHg exists. Rayleigh [29] sealed a small pointer into each leg of the manometer and measured the angle though which the apparatus had to be tilted in order to bring the meniscus of the fluid into contact with the tips of the pointers to obtain the pressure. Various elastic gauges such as a Bourdon [25] or sickle gauge have been used as null indicating devices in conjunction with a McLeod gauge to measure vapour pressures down to 10^{-5} mmHg. However, they also have associated problems such as variation of the null position and sensitivity with temperature. As the lead oxybromides are solids and were expected to have vapour pressure approaching the lower limit of the manometer method the technique was rejected for this work.

1.2.3 The Langmuir Free Evaporation and Knudsen Effusion Methods

The evaporation techniques first used by Langmuir [24] and Knudsen [20] are both dynamic techniques and are closely related. The vapour pressure of the sample is determined from the amount of material evaporating from a known area into a vacuum in a measured period of time. In the Langmuir free evaporation method the total surface area of the sample is considered, but in the Knudsen method the sample is contained in an effusion cell (Knudsen cell) which is essentially a box of approximately 2 cm dimensions with a small orifice in the top, and it is the area of this hole which is used. In the Langmuir technique it is imperative that an evaporated molecule does not condense on another part of the sample. Consequently, this technique is limited to samples in the form of smooth rods or foils and the surface area must be known accurately.

Originally the amount of material which had effused from a Knudsen cell was determined by weighing the cell before and after it had been placed in a vacuum for a known period of time. However, this led to errors due to the time taken for the outgassing of the cell and for equilibrium conditions within the cell to be reached. These problems were overcome by continuous weighing of the cell either with a vacuum balance [42, 7] or a quartz spring [41], but unfortunately this introduced new difficulties in maintaining thermal equilibrium within the cell, as it was suspended in a vacuum and heated by radiation.

Several workers [33, 21, 22] have applied the Knudsen effusion technique to the study of alloys. They used radioactive tracers to determine the amount of material effusing from the cell and chemical assay to determine its composition. In these cases the effused material was collected by condensation onto a cold target.

The dimensions of the orifice in the top of a Knudsen cell must be precisely determined if reliable vapour pressure measurements are to be obtained with this method. The area of this hole should be less than 1/100th of the internal surface area of the cell and have a diameter less than 1/10th of the mean free path of the gaseous species at the temperature and pressure concerned. The area of the orifice must be small in relation to the internal surface area of the cell so that the lost vapour, due to effusion through it, is rapidly replenished, maintaining equilibrium within the cell. The diameter of the hole must also be small to ensure that molecules pass through it without colliding with one another, as any reflected back into the cell by such collisions would lead to an erroneously low vapour pressure. If these requirements are fulfilled and the cell is constructed of a material which does not react with the sample, then the only major sources of error arise from temperature gradients within the cell and uncertainties in the molecular weight of the effusing species (see later).

The Knudsen effusion method is applied with a very low pressure of gas in the apparatus, under this condition, the mean free path of a molecule in the gas phase is sufficiently large to allow it to travel from the surface of the evaporating liquid or solid through the orifice in the cell lid and into the vacuum beyond before it collides with another molecule. The mean free path λ of a gaseous molecule is given by

$$\lambda = \frac{1}{\sqrt{2\pi n\sigma^2}} \tag{1.11}$$

where σ is the molecular diameter of the gas concerned and n is the number of molecules per unit volume. Providing all of the molecules arriving at the hole pass directly through to the other side, the amount passing through is controlled by the number of molecules arriving at it. This may be calculated from the kinetic theory of gases and the area of the hole, so that

$$\frac{dw}{dt} = \frac{1}{4}\rho\bar{C}A \tag{1.12}$$

where ρ is the gas density, $\bar{C}$ is the average velocity of the gas molecules and A is the area of the hole. Substituting for $\rho = p\bar{M}/RT$ and $\bar{C} = \sqrt{8RT/\pi\bar{M}}$ where p is the pressure of gas and $\bar{M}$ is the average molecular weight of the vapour, then

$$\frac{dw}{dt} = \frac{1}{4}\frac{p\bar{M}A}{RT}\sqrt{\frac{8RT}{\pi\bar{M}}} \tag{1.13}$$

Hence

$$p = \frac{1}{A}\frac{dw}{dt}\sqrt{\frac{2\pi RT}{\bar{M}}} \tag{1.14}$$

This is the basic equation used to calculate vapour pressure using the Langmuir method. In practice the effective area of the orifice in a Knudsen cell, which corresponds to A in the above equations, is smaller than the physical size because the cell wall has a finite thickness and some molecules strike the side of the hole and fail to escape. A correction factor which is related to the size and shape of the orifice must therefore be introduced, giving a final equation of the form

$$p = \frac{1}{KA}\frac{dw}{dt}\sqrt{\frac{2\pi RT}{\bar{M}}} \tag{1.15}$$

where K is the correction factor, often referred to as the Clausing factor (after Clausing [5], who first deduced its magnitude theoretically). The values for several shapes and sizes of orifice have since been calculated and tabulated by Searcy and Freeman [35]. Some typical values are given for circular holes in Table 1.1.

Equation 1.15 shows that the vapour pressure obtained using the evaporation techniques depends upon the molecular weight of the effusing species M. At elevated temperatures

Table 1.1: Typical values of Clausing factors for a circular orifice

Ratio of depth to radius	0.1	1.0	10.0
Clausing factor	0.952	0.672	0.191

the molecular weight of a gas is not necessarily the same as that of the solid as dimeric and polymeric species can be formed. Hence, the precise molecular weight of the vapour must be determined if reliable measurements are to be made.

These techniques have been applied to the study of many compounds with vapour pressures up to 1×10^{-3} mmHg, the lower practical limit of the Knudsen method is 5×10^{-5} mmHg but the Langmuir technique has been used down to 1×10^{-8} mmHg. Neither of these techniques were applicable to the present study, however, as the vapour pressure of the lead oxyhalides was expected to exceed the upper pressure limit.

1.2.4 Pressure Balances

In principle, the force exerted on a flat disc or plunger can be measured mechanically and any apparatus doing so is essentially a pressure balance.

Pressure balances of various forms have been used by several workers to measure vapour pressures in the range 2×10^{-4} to 0.5 mmHg at temperatures slightly above ambient. In the earliest designs, such as those of Rodebush and Coons [31], a flat disc was fitted over an orifice and the surfaces of both disc and orifice were ground to the finest possible tolerance. The pressure exerted by the vapour inside a chamber was measured from the force needed to just bring the disc into contact with the surface of the orifice, electromagnetic balances and quartz springs being used extensively for this purpose.

Another successful instrument which used this approach was the pendulum tensimeter which was designed by Hickman [13] and is shown in Figure 1.4. The sample was placed in compartment **B** and a vacuum applied to the opposite side of the duralmin disc **D** suspended on the long pendulum arm. The sample was then heated to the temperature at which the vapour pressure was to be measured and the vapour streaming past the disc was stopped by rotating the apparatus until the pendulum arm came into contact with the orifice. The magnitude of the rotation required to do so was related to the pressure. The pressure in the reference side of the apparatus **C** was held at 10^{-4} mmHg using a diffusion pump and measured with a pirani or similar gauge. The heating coil around the

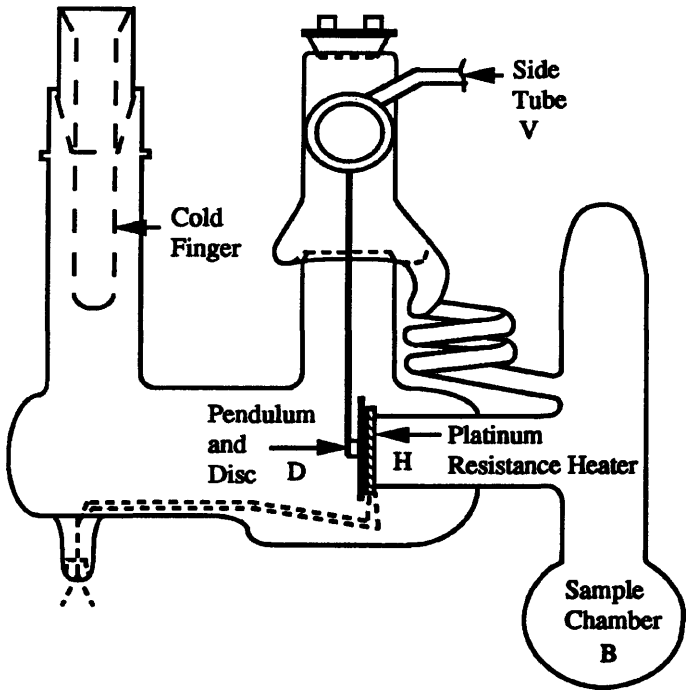

Figure 1.4: The Hickman pendulum tensimeter

orifice was used occasionally to remove any condensed solid from the surfaces of the disc and orifice. It was suggested by Hickman that the apparatus could be improved to extend its range considerably by lengthening and lightening the pendulum.

The more elegant apparatus of Ernsberger and Pitman [9] shown in Figure 1.5 incorporated a piston with an area of 10 cm^2 which fitted precisely into a cylinder. The piston slid vertically down into the cylinder and the force exerted by the vapour in the cylinder was measured using a quartz spring. The spring had a sensitivity of 0.8282 millimetre extension/mg of load, so that a measurement of an extension to $\pm$0.05mm enabled a pressure of 1×10^{-3} mmHg to be measured with 1 % accuracy. At this pressure the force is 1.33×10^{-1} N m^{-2} which is equivalent to 1.35×10^{-3} g mm^{-2}. The vapour pressure of mercury was measured in this apparatus in the range $4 \times 10^{-4} - 1.9 \times 10^{-2}$ mmHg.

Back and Betts [2] used an apparatus of similar design in their work with hydroxylamine between 8×10^{-2} and 0.5 mmHg, but they used a precision torque balance in place of the quartz spring. They reported that the effects of friction between the piston and the cylinder walls were minimised by "gentle thumping of the bench support". Finally a similar gauge has been described by Douslin and Osborn [8]. In this instance an inclined piston was used and the frictional effects were reduced by the use of an eccentrically

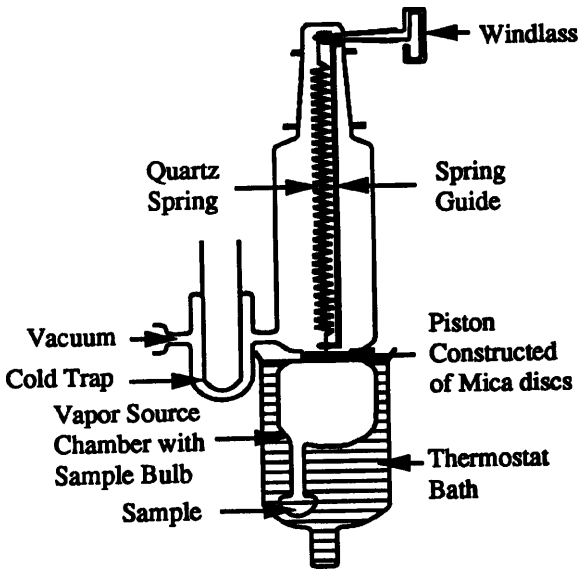

Figure 1.5: The pressure balance of Ernsberger and Pitman

weighted piston and rotating cylinder with the piston lubricated with oil. The angle of inclination necessary to just balance the pressure within the cylinder was related directly to the pressure.

The major problems associated with absolute pressure measurement in this way are in the degassing of the sample at the onset and in the reduction of back pressure effects on discs or pistons. These are caused by the leakage of vapour between cylinder and piston or orifice and disc. In addition, precautions must be taken to ensure that equilibrium conditions are maintained within the vessel during an experiment. Some authors have implied that the effective area of a piston may be determined to a greater accuracy than a disc, as it is not clear whether the internal or external diameter of the orifice should be used in the calculation of the pressure.

The back pressure from leaking vapours can be reduced to a minimum in many cases with the aid of a cold finger, which essentially condenses any vapours leaving the orifice. The problem of maintaining equilibrium conditions is usually overcome by making the surface area of the sample chamber large in comparison to the orifice and coating it with sample prior to a determination.

Pressure balances were considered to be inappropriate for the present study as the measurements were required at between 300 and 700 °C, as severe problems were anticipated in the construction and operation of an apparatus suitable for these conditions.

1.2.5 Torsion Knudsen Effusion

The torsion effusion technique, often referred to as TORKER (Torsion Knudsen Effusion Recoil), was first used by Volmer [42] and provides the vapour pressure of the sample directly. It is really a hybrid between a pressure balance and an effusion cell; two or more orifices are arranged in such a geometry that the recoil force produced by the beams of molecules effusing from them, twists the effusion cell in the same direction. Figure 1.6 shows a typical effusion cell. This is normally suspended from a fine torsion wire (usually made of quartz or tungsten) in a vacuum. The rotation of the cell caused by the recoil force of the effusing molecules is measured and related to the pressure by the equation

$$p = 2\omega\phi(A_1F_1d_1 + A_2F_2d_2) \tag{1.16}$$

where ω is the torsional constant of the support fibre, ϕ is the angular displacement of the cell, A_1 and A_2 are the areas of the orifices at distances d_1 and d_2 from the axis of rotation and F_1 and F_2 are factors related to the orifice geometry (analogous to the Clausing factor used in the Knudsen effusion equation). The torsion fibre is generally 10–30 cm in length and has a diameter of $2 \times 10^{-3} - 1 \times 10^{-2}$ cm. The bottom of the torsion wire is attached to the much thicker rod (shown in Figure 1.6) on which is mounted a small concave mirror and the effusion cell. The top of the torsion fibre is attached to the top of the apparatus and the angular displacement is measured from a beam of light reflecting off the mirror.

The effusion cells are generally rectangular boxes with dimensions of about $1.5 \times 1.5 \times 3.0$ cm, with two small orifices drilled into opposite faces 1 cm from the centre. Numerous materials have been used for the cell including graphite, platinum, tantalum [15], glass and brass [42]. Considerable controversy surrounds the use of cells made from some of these materials. This is particularly the case with graphite, as many forms of graphite have been used for the cell, with differing degrees of success.

This type of apparatus can be calibrated in two ways. In the most commonly used method, the torsional constant of the fibre is determined from the frequency of oscillation. For a cell of moment of inertia I the frequency of oscillation ν is related to the torsion constant ω by the equation

$$\nu = \frac{1}{2\pi}\left(\sqrt{\frac{\omega}{I}}\right) \tag{1.17}$$

Thus, if the period of oscillation ($r = 1/\nu$) is measured and the moment of inertia known

$$\omega = \frac{4\pi^2 I}{r^2} \tag{1.18}$$

In practice, the moment of inertia I is difficult to determine with any precision and the torsion constant is determined from measurement of the suspension system and cell alone,

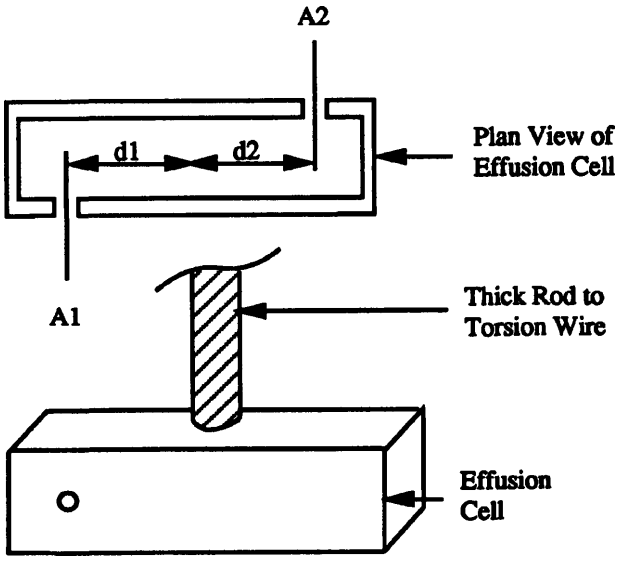

Figure 1.6: A typical TORKER effusion cell

and with an added mass which has a known moment of inertia I_s. The modified form of the previous equation is shown below

$$\omega = \frac{4\pi^2 I_s}{{r_s}^2 - {r_m}^2} \tag{1.19}$$

where r_m and r_s are the periods of oscillation for the suspension system alone and the system plus the additional moment of inertia respectively.

An alternative method of calibration was used by Hildenbrand and Hall [14] which involved the use of a standard substance (in this case gold), the vapour pressure of which is accurately known.

A different method of measuring the recoil force of a beam of molecules effusing from a cell similar to a Knudsen cell was that used by Klumb and Luckert [18]. The force was measured by the movement of a vane suspended from a torsion wire produced by the impact of the beam. Other workers have simultaneously monitored the weight loss from a torsion effusion cell and the recoil force of the effusing molecular beams [43]. They were then able to compare directly the results from the Knudsen effusion experiment with those from the torsion effusion and calculate the degree of polymerisation of the molecular species in the gas phase.

The torsion effusion method provides a direct measurement of the vapour pressure, but the effusion cell is suspended in a vacuum and the problems of temperature control described earlier in relation to the continuous weighing of a Knudsen effusion cell are also present here.

1.2.6 The Transpiration Method

The transpiration method, also known as the transport, entrainment or gas saturation method, was first applied by Renault [30] in 1845. As the vapour pressure of the sample is measured indirectly from the amount of material which has evaporated and been removed by a gas stream the method is classed as dynamic. In this technique it is assumed that at moderate pressures the presence of an non condensable gas does not affect the equilibrium between a condensed and vapour phase, and that the only effect of this gas is on the rate at which equilibrium is reached; for a gas flowing over a condensed phase at sufficiently low flow rate equilibrium conditions should be obtained. If these conditions are satisfied then a vapour pressure is given by

$$p_s = p_A \left(\frac{n_s}{n_s + n_c} \right) \tag{1.20}$$

where p_s is the partial pressure of the sample, n_s and n_c are the amounts of sample vapour and carrier gas respectively, and p_A is the total pressure of carrier gas and sample vapour in the apparatus.

The apparatus generally consists of a source of carrier gas (usually inert), a means by which the flow of this gas can be controlled and its amount either measured or calculated. There must also be a saturator, the temperature of which can be controlled and accurately measured, and a means by which the amount of evaporating material can be determined.

Initially the amount of carrier gas was determined by measurement of its volume, either by aspiration of a liquid from a suitable container or a gas meter. The main reason for this was the inability of the experimentalists to control the flow rate to an acceptable degree of accuracy. However, mass flow controllers which are used extensively in gas chromatography and the evolving semiconductor industry for the control of flow rates, now provide a more convenient means of determining the total volume of gas which has passed through the saturation chamber from the flow rate and time elapsed.

The amount of sample vapour removed by the carrier gas has been measured in a number of ways. Gilbert and Kitchener [11] in their measurements on cadmium, extracted the metal from the gas using dilute hydrochloric acid and determined the amount by electrolytic deposition. Bell and Tagami [3] used radioactive tracers to determine the amount of vapour

transported, and this provided a useful method of measuring the relative amounts of two transported compounds. Schmahl and Sienben [34] measured the amount of transported material by weighing the sample on a thermobalance. The latter method is especially useful in cases where the composition of the sample is suspected to change during an experiment as this often produces a detectable change in the rate of weight loss.

The geometry of the saturation chamber has been found to have a great effect on the accuracy of the vapour pressures obtained using the transpiration method. In particular, equilibrium conditions are obtained more easily when the surface of the evaporating sample is made to fill the cross section of the saturator as much as possible [1] and diffusion effects can be minimised by the use of constrictions at both the inlet and outlet of the chamber. The material of construction must also be inert with respect to both sample and carrier gas; platinum, glass and fused quartz have been used extensively. An indication of the quality of a saturation chamber can be obtained from a plot of apparent vapour pressure versus carrier gas flow rate. A satisfactory saturator, in which equilibrium conditions are being attained, will produce a region in which the apparent vapour pressure is independent of the flow rate of carrier gas. The plateau region can extend over a threefold range of flow rates and is typically found between 1 and 70 $cm^3\ min^{-1}$ at STP; the majority of workers endeavour to conduct their experiments in this range.

Providing adequate care is taken in the design of the apparatus, then the only significant error in the technique is introduced by the assumption that there is no polymerisation of the molecules in the gas phase. It has been shown that many metals form dimeric or polymeric species in the gas phase. For example, Kim and Cosgarea [17] found that bismuth vapour between 850 and 950 K contained approximately 65 % Bi_2 and 35 % Bi. Thus it is often necessary to determine the molecular weight of the vapour separately. Mass spectrometry has been used by several workers [16, 26] to establish the presence of dimeric and polymeric species in the vapour phase. Comparison of measurements made by pressure balance or Torker techniques with those of the transpiration method can also be used to give an indication of the extent of this polymerisation.

The method has been used to study the vapour pressures of many compounds (both liquid and solid) with vapour pressures above 10^{-3} mmHg at temperatures from a few hundred degrees to several thousand. The main limitation of the method is the time taken to obtain one measurement. In contrast to the majority of other techniques, which provide results in a few minutes or hours, the transpiration method can take several days and, in some cases, weeks. However, it is possible to reduce significantly the time taken to obtain a measurement by reducing the pressure of gas within the apparatus, as the associated increase in the partial pressure of the sample is accompanied by an increase in the rate of evaporation. For this reason the transpiration method is often used with a pressure in

the apparatus of down to 10 mmHg.

The transpiration method was chosen in this work because the apparatus is simple to construct and maintain. Perhaps more importantly, some very rough measurements of the vapour pressure of the lead oxybromides were made using a thermogravimetric balance, and the estimated vapour pressures measured in these experiments lay within the limits of the transpiration method. In these preliminary studies the sample was placed in a platinum crucible which was suspended in a stream of nitrogen flowing at approximately 10 cm^{-3} min^{-1} and heated by a small furnace. This apparatus was extremely crude, nevertheless, the results obtained provided valuable information and were remarkably accurate. The design and construction of the apparatus used in this work is described in Chapter 2.

1.2.7 The Present Study

In the present study samples of the 1:1 lead oxybromide ($PbO.PbBr_2$), 2:1 lead oxybromide ($2PbO.PbBr_2$), 3:1 lead oxybromide ($3PbO.PbBr_2$) and the 7:1 lead oxybromide ($7PbO.PbBr_2$) have been prepared from lead oxide and lead bromide of the highest purity, under carefully controlled conditions. It should be noted that an alternative stoichiometry has been proposed for many of these materials, but the values used here have been taken from the most recent study of the phase system [19] in which the authenticity of the materials used was confirmed by an X-ray powder diffraction study [23].

The temperature dependence of the materials formed when intimate mixtures of lead oxide and lead bromide were heated has been studied using both X-ray powder crystallography and Differential Thermal Analysis (DTA). The results from these experiments have been used to identify the causes for the differences in stoichiometry and in the nature of the phases which have been reported previously.

A transpiration apparatus has been constructed and used to measure the vapour pressure of a number of the compounds. The vapour pressure of pure lead bromide has been measured and the results used to verify the design of the vapour pressure apparatus. There are no reported experimental measurements of the vapour pressure of lead bromide at temperatures below the melting point and these results provide the only experimentally determined value for its enthalpy of sublimation.

The vapour pressure of the 1:1 lead oxybromide and the 2:1 lead oxybromide have been measured and the evaporating species identified. The thermodynamic implications of these results have been explored in detail and provide an explanation for behaviour observed

with the current lead filters.

References

[1] Alcock C.B. and Hooper G.W., *Thermodynamics of the Gaseous Oxides of the Platinum Group Metals*, Proc. Roy. Soc., 254, (1960), p. 551.

[2] Back R.A. and Betts J., *The Determination of the Vapour Pressure of Solid Hydroxylamine Using a Piston Gauge*, Canadian. J. Chem., 43, (1965), p. 2157.

[3] Bell W.E. and Tagami M., *High Temperature Chemistry of the Ruthenium-Oxygen System*, J. Phys. Chem., 67, (1963), p. 2432.

[4] Buck R.P. and Ryason P.R., *Lead Scavenging, A Quasithermodynamic Approach*, Am. Chem. Soc. Div. Petrol. Chem. Preprints, Vol. 10, part 2, (1965) p. 21.

[5] Clausing P., Ann. Phys. Lpz., 12, (1932), p. 1931.

[6] The Department of Health and Social Security, *Lead and Health*, The report of a DHSS Working Party on Lead in the Environment, HMSO, 1980. ISBN 0 11 320728 X.

[7] Dietz V., *The Vapour Pressure of Crystalline Benzene and Cyclohexane*, J. Am. Chem. Soc., 55, (1933) p. 472.

[8] Douslin D.R. and Osborn A., *Pressure Measurement in the 0.01-30 Torr Range With an Inclined Piston Gauge*, J. Sci. Instrum., 42, (1965), p. 369.

[9] Ernsberger F.M. and Pitman H.W., *New Absolute Manometer for the Measurement of Vapour Pressures in the Micron Range*, Rev. Sci. Instrum., 26, (1955), p. 584.

[10] Fischer W. and Rahlfs O., Z. Anorg. Allg. Chem., 1, (1932), p.205.

[11] Gilbert J.G.F. and Kitchener J.A., *The Dissociation Pressure of Cadmium Oxide*, J. Chem. Soc. London, (1956), p. 3919.

[12] Greenwood H.C., *Notiz über die Dampfdruckkurve und die Verdampfungswärme einiger schwerflüchtiger Metalle*, Z. Physik. Chem. (Leipzig), 76, (1911), p. 484.

[13] Hickman K.C.D., Hecker J.C. and Embree N.D., Ind. Eng. Chem. Anal. ed 9, (1937), p. 624.

[14] Hildenbrand D.L. and Hall W.F., *The Vapour Pressure and Heat of Sublimation of Gold*, J. Phys. Chem., 66, (1962), p. 754.

[15] Hildenbrand D.L. and Potter N.D., *The Vapour Pressure and Thermodynamics of Vaporisation of Calcium Chloride*, J. Phys. Chem., 67, (1963), p. 2231.

[16] Keneshea F.J. and Cubicciotti D., *Vapour Pressure of Zinc Chloride, Zinc Bromide and Their Gaseous Dimerization*, J. Chem. Phys., 40 (1964), p. 191.

[17] Kim J.H. and Cosgarea A., *Study of the Vapors of Liquid Lead and Bismuth*, J. Chem. Phys., 44, (1966), p. 806.

[18] Klumb K. and Luckert J., Vacuum Technology, 8, (1959), p. 52.

[19] Knowles L.M., *Thermal Analysis of the System $PbBr_2$-PbO*, J. Chem. Phys., 19, (1951), p. 1128.

[20] Knudsen M. Ann. Phys., Lpz., 29, (1909), p. 179.; 34, (1911), p. 593.

[21] Kubaschewski O. and Heymer G., *The Thermodynamics of the Iron-Chromium System*, Acta Metallurgica, 8, (1960), p. 416.

[22] Kubaschewski O., Heymer G. and Dench W.A., Z. Electrochem, 64, (1960), p. 801.

[23] Lamb F.W. and Niebylski L.M., *Phase Study of the PbO-$PbBr_2$ System by X-ray Diffraction*, J. Am. Chem. Soc., 75, (1953), p. 511.

[24] Langmuir I., *Chemical Reactions at Very Low Pressures*, J. Am. Chem. Soc., 35, (1913), p. 105.

[25] Machol R.T. and Westrum E.F., *Vapour Pressure of Liquid Tellurium*, J. Am. Chem. Soc., 80, (1958), p. 2950.

[26] Norman J.H. Gene H. Stanley Bell W.E., *Thermodynamics of Liquid In-Sb-Zn Solutions from Mass Spectrometry of Knudsen Cell Effusates*, J. Chem. Phys., 41 (1964), p. 60.

[27] Pease R.N. and Cook R.S., *Equilibrium in the Reaction $NiO+H_2 \rightleftharpoons Ni + H_2O$. The Free Energy of Nickelous Oxide*, J. Am. Chem. Soc., 48, (1926), p. 1199.

[28] Ramsay W. and Young S., *On a New Method of Determining the Vapour Pressure of Solids and Liquids, and on the Vapour Pressure of Acetic Acid*, J. Chem. Soc., 47, (1885), p. 42.

[29] Lord Rayleigh, *On a New Manometer, and on the Law of the Pressure of Gases between 1.5 and 0.01 millimetres of Mercury*, Phil. Trans., A196, (1901), p. 205.

[30] Renault H.V., Ann. Chem., 15, (1845) p. 129.

[31] Rodebush W.H. and Coons C.C., *A New Absolute Manometer for Low Pressures,* J. Am. Chem. Soc., 49, (1927), p. 1953.

[32] Ruff O. and Bergdahl B., Z. Anorg. Allg. Chem., 106, (1919), p. 76.

[33] Schadel H.M. and Birchenall C.E., *The Vapour Pressure of Silver*, J. Metals, 2, (1950), p. 1134.

[34] Schmahl N.G. and Sienben P., *The Physical Chemistry of Metallic Solutions and Intermetallic Compounds 1*, Paper 2K (1958)

[35] Searcy A.W. and Freeman R.D., The Effect of Channel Holes on the Force Exerted by Effusing Vapours, J. Chem. Phys., 22, (1954), p. 762.

[36] Simmons R.F. and Ting-Man Li, *A Theoretical Examination of the Distribution of Gaseous Lead Compounds in the Exhaust from a Petrol Engine*, Combustion and Flame, 56, (1984), p. 113.

[37] Simmons R.F. and Ting-Man Li, *The Mechanism of Lead Scavenging by Dibromoethane*, Nineteenth Symposium (International) on Combustion/The Combustion Institute, (1982), p. 1487.

[38] Smith A. and Menzies A.W.C., *Studies in Vapor Pressures: 1; A Method for Determining Under Constant Conditions the Boiling Points of Even Minute Quantities of Liquids and Non-Fusing Solids*, J. Am. Chem. Soc., 32, (1910), p. 897.

[39] Smith A. and Menzies A.W.C., *Studies in Vapor Pressures:...*, J. Am. Chem. Soc., 32, (1910), p. 1420.

[40] Ting-Man Li, personal communication.

[41] Ubbelohde A.R., *The Lattice Energy of Normal Paraffins*, Trans. Faraday Soc., 34, (1938), p. 282.

[42] Volmer M., Z. Physic. Chem. Bodenstein Festbond, (1931), p. 863.

[43] Wilson A.E., Kim J.H. and Cosgarea A., *Automatic Controlling-Recording Microbalance System for Torsion-Knudsen Effusion Recoil Studies*, Rev. Sci. Instrum., 36, (1965), p. 1428.

Chapter 2

Apparatus and Materials

2.1 Apparatus for the Measurement of Vapour Pressures Using the Transpiration Method

The apparatus used to measure the vapour pressures of lead bromide and the lead oxyhalides is shown in Figure 2.1. This may be divided into several sections, namely control and measurement of carrier gas flow rate, saturation of carrier gas with sample vapour, measurement and control of temperature of the saturation section and the determination of amount of material entering the gas phase. It is convenient therefore to discuss each of these sections separately.

2.1.1 Control of Carrier Gas Flow

The amount of carrier gas that had passed through the saturation chamber at any point during an experiment was calculated from the elapsed time and total flow rate. This is in sharp contrast to the techniques adopted by the majority of previous workers, who measured the quantity of gas using conventional gas meters. As the apparent vapour pressure of the sample depended upon the total volume of carrier gas passed through the saturation section of the apparatus, it was crucial that the flow be measured and controlled very accurately.

The apparatus was expected to operate with flow rates between 20 and 60 $cm^3\ min^{-1}$. Initial attempts at obtaining a steady flow rate using needle valves in conjunction with pressure regulators failed. The problem was eventually solved using a Porter Instrument Company mass flow controller model VCD1000A (See Figure 2.2) and two pressure regulators.

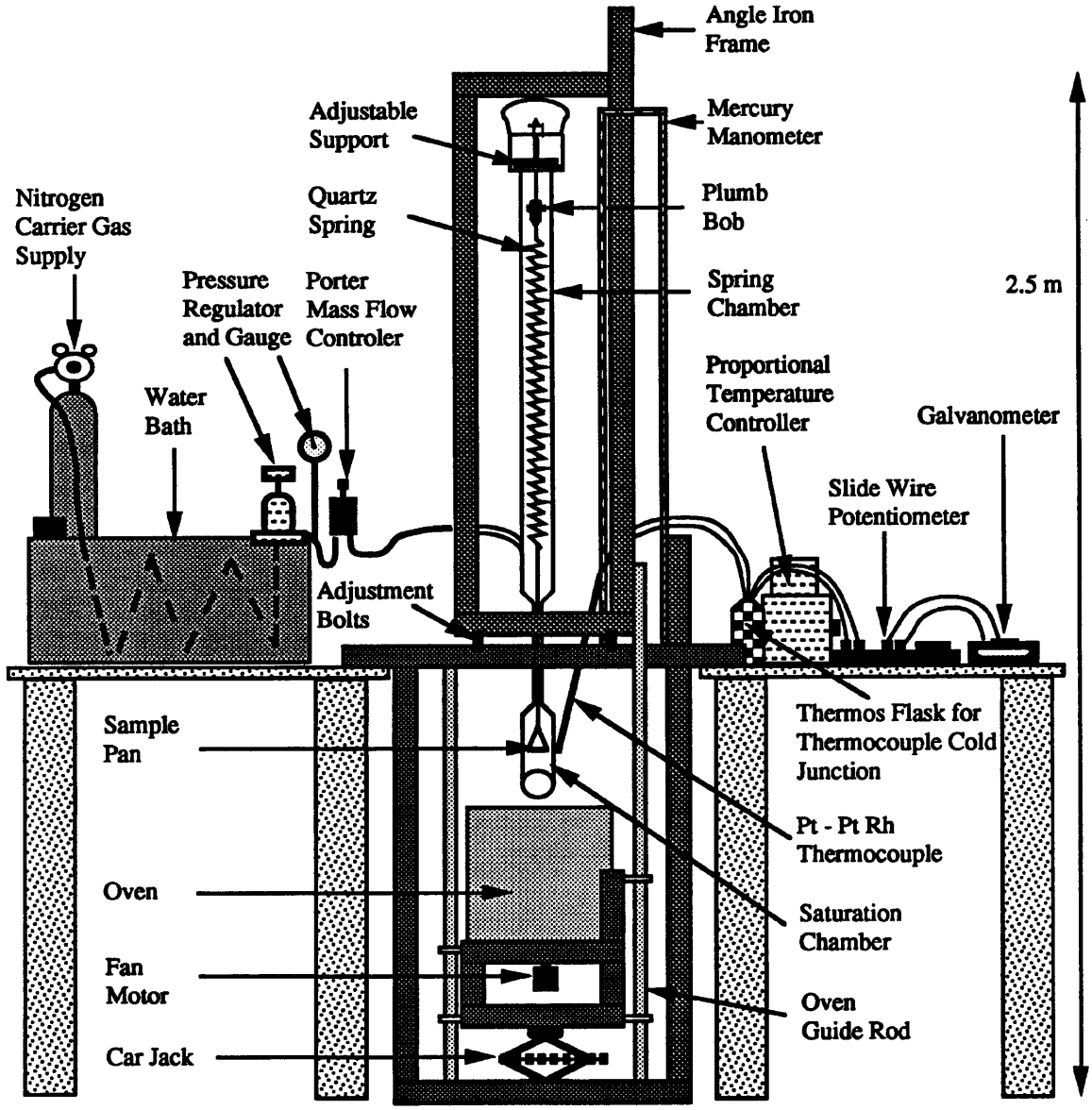

Figure 2.1: The transpiration apparatus

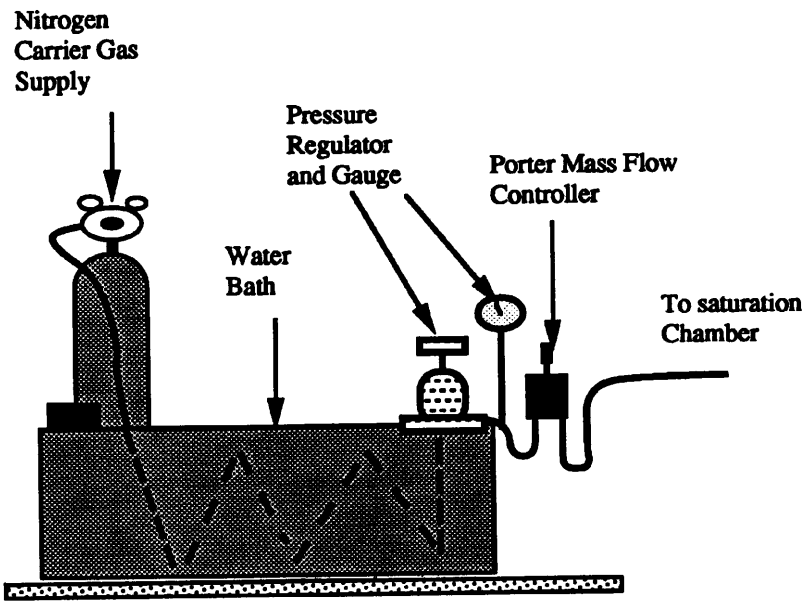

Figure 2.2: Flow control apparatus with Porter mass flow controller

The inert carrier gas (white spot nitrogen) was supplied through 6.35 mm o.d. copper tubing from a cylinder fitted with a standard gas regulator (0 – 70 PSIG outlet pressure). The outlet pressure of this cylinder was set at 50 PSIG and this was reduced to between 30 and 40 PSIG by a second pressure regulator. After leaving this second regulator the gas passed through a 2 m length of 6.35 mm o.d copper tubing submerged in a thermostat bath at 30 °C to the mass flow controller. This allowed a constant flow rate of up to 50 cm^3 min^{-1} at NTP to be set and the experimentally determined fluctuation over several days was less than 1 %.

2.1.2 Measurement of Carrier Gas Flow Rate

Traditional methods of flow measurement such as soap bubble meters require that the gas stream be saturated with water vapour before it enters a graduated tube. This is usually achieved by passing the gas through an air stone into a thermostatically controlled water bath, a procedure which produces appreciable back pressures. In the present apparatus these back pressures could not be tolerated, the ground glass joint at the base of the saturation chamber could not be greased because it would be subjected to temperatures of up to 600 °C, also the effects of the vapours from the grease on the vapour pressure measurements could not be predicted. Furthermore the effects of back pressure on the mass flow controller were unknown.

The carrier gas flow rate was measured using the apparatus shown in Figure 2.3. In this apparatus the time taken for the carrier gas to expel 100 cm^3 of decyl alcohol from an

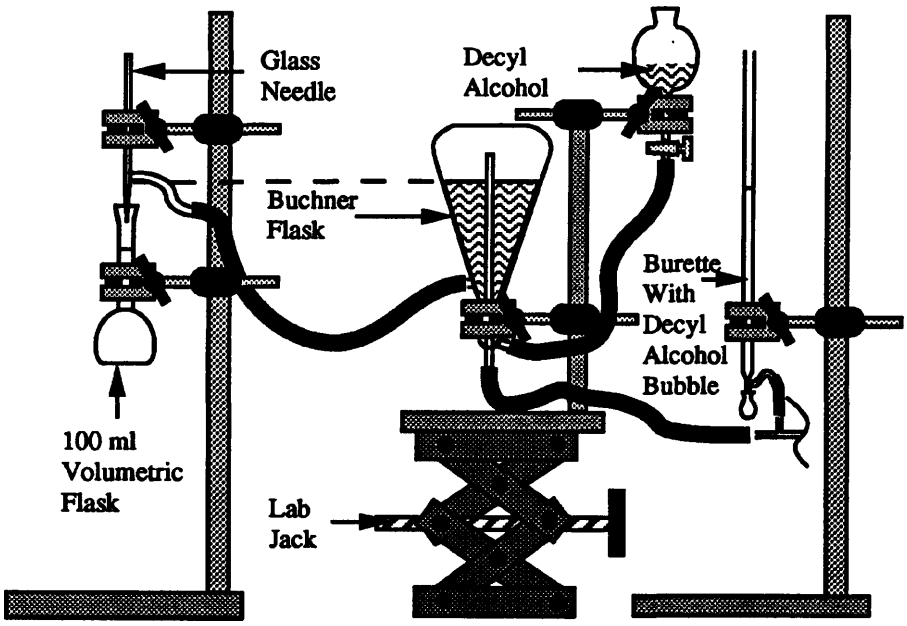

Figure 2.3: The apparatus used to measure the flow rate of carrier gas

inverted Buchner flask was measured. A 100 cm^3 volumetric flask was used to measure the volume of liquid exactly. During the measurement a decyl alcohol bubble was held at a fixed position within the burette, thus ensuring that the pressure within the apparatus exactly balanced the surrounding atmospheric pressure and that the volume of the apparatus was constant. The pressure inside the apparatus was controlled by adjusting the height of the head of liquid in the buchner flask relative to the siphon outlet.

Decyl alcohol was chosen as the liquid in the buchner flask because it has a low vapour pressure, density and viscosity at room temperature. Consequently, its flow rate changed rapidly with, and was very sensitive to, variations in the pressure of gas within the buchner flask. Mercury was also tested in the buchner flask, but the inertial effect on the siphon resulting from its greater density made the response to changes in flow and pressure unacceptable.

At the start of an experiment the desired flow rate of carrier gas was set using the mass flow controller and measured using the flow measurement apparatus without the gas flowing through the transpiration apparatus. This was done because small fluctuations in the laboratory temperature produced substantial changes in the effective volume of the gas contained in the saturation and spring chambers. However, during the vapour pressure experiments, the flow rate was periodically checked with the gas flowing through the complete apparatus and, providing the internal and external pressures were balanced, as described above, acceptably reproducible results could usually be obtained in a relatively short period of time.

2.1.3 The Saturation Chamber

The saturation chamber enclosed the sample and its design is shown in Figure 2.4. In previous work using the transpiration method, the carrier gas flowed horizontally through the chamber, but in the present study it flowed vertically downwards. This arrangement allowed a quartz fibre to connect the sample pan in the saturation chamber to a fine quartz spring housed in the spring chamber above. The two chambers were linked by a substantially long length of narrow bore glass tubing. This geometry allowed the mass of sample transported away by the stream of carrier gas to be determined directly from the change in extension of the spring. The size of the saturation chamber was chosen so that it was large enough to allow easy construction, but at the same time small enough for it to not require an unduly large amount of sample.

It has been shown by previous workers [3, 7, 9, 10, 11] that the design of the saturation chamber is a major factor in the success of vapour pressure determinations using the transpiration method. Particular attention must be paid to the entrance and exit of the chamber in order to prevent errors due to diffusion of sample vapour either with or against the flow of carrier gas. However, in the present apparatus the use of a quartz spring to weigh the sample made the use of conventional methods of diffusion control impractical. Figure 2.5 shows a typical arrangement used by previous workers.

The gas flows from left to right and as it lies outside the heated portion of the apparatus the ground glass joint **A** may be greased to prevent leaks should the apparatus be required to operate under reduced pressure. The obstruction **B** may be slid in and out of the tube to allow easy sample manipulation, but when in the position shown it provides an efficient barrier to diffusion of sample vapour against the flow of carrier gas. The sample is generally contained in a long crucible **C** and the constriction **D** provides the final barrier to diffusion of sample vapour with the flow of carrier gas. The transported material is generally collected by condensation or absorption and the amount determined quantitatively either by chemical assay or by weighing.

In the present apparatus a tube 5 mm i.d. $\times$ 10 cm long was used as the inlet constriction for the saturation chamber. Prior to entering this tube, the carrier gas was passed through a 1 m length of the same diameter tubing to allow it to reach thermal equilibrium. This arrangement allowed free suspension of the hangdown fibre and sample and the following calculation indicated that the rate of back diffusion of lead bromide could be neglected.

It has been shown [15, 16] that the downstream diffusion of vapour with a flow of carrier

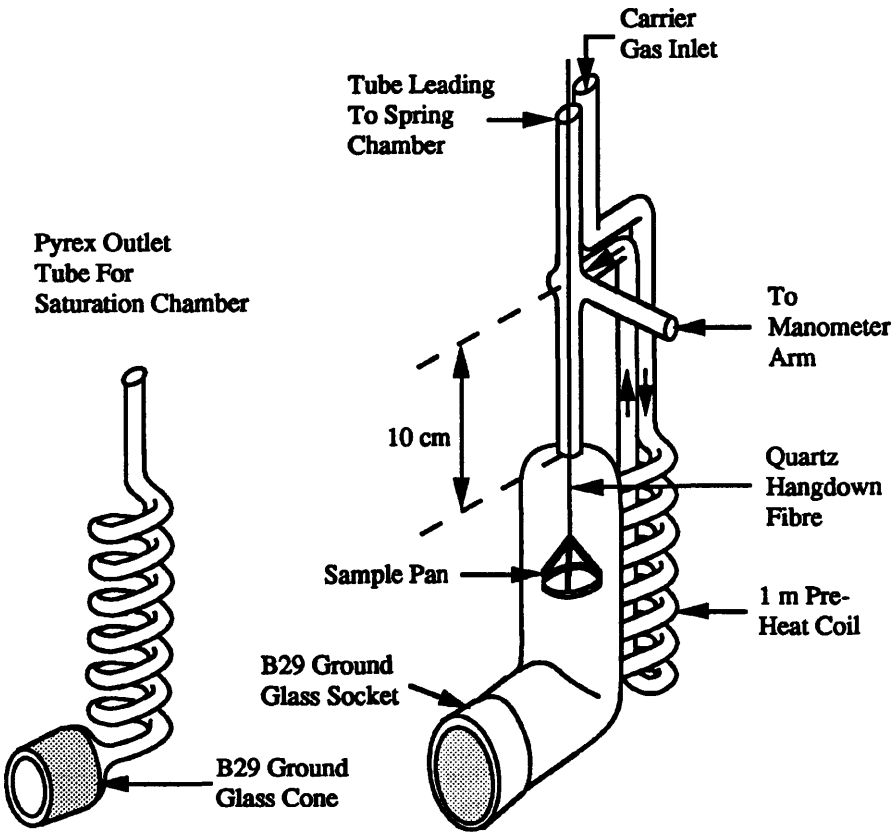

Figure 2.4: The saturation chamber used in the present work

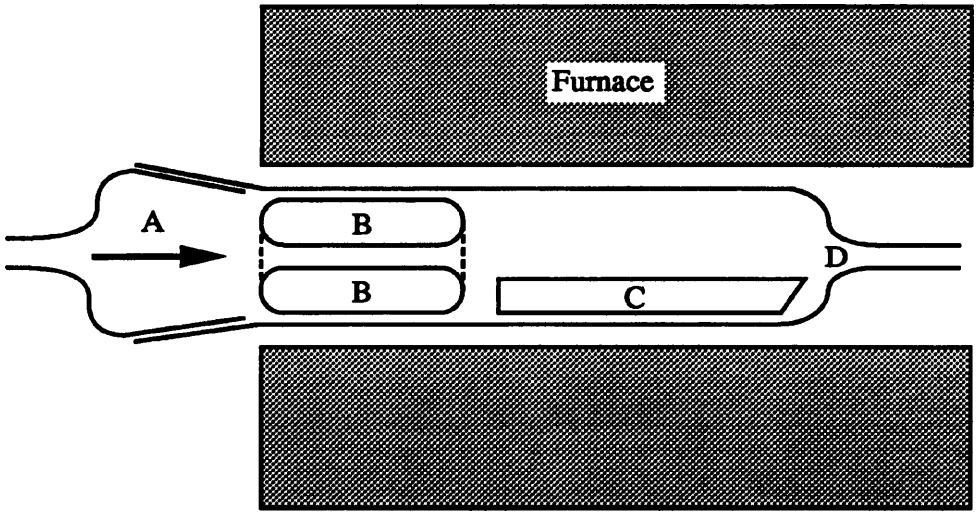

Figure 2.5: A typical saturation chamber

gas passing through an isothermal capillary can be expressed as

$$K = A\left(Vc_x - D\frac{dc}{dx}\right) \tag{2.1}$$

where A is the cross sectional area of the capillary, K is the mass flow rate of the vapour, V the velocity of the gas mixture, D the coefficient of diffusion, x the distance along the capillary and c is the vapour density at any point x. This equation comprises two terms, a mass flow term Vc_x, and a diffusion term $D\frac{dc}{dx}$. Rearrangement of Equation 2.1 provides a definition for the diffusion of vapour against the flow of carrier gas. Thus, for the present apparatus, where gas flows through a narrow tube into a region where the concentration of the vapour corresponds to the vapour pressure of the sample, back diffusion can be neglected when the back diffusion just balances the forward mass flux, i.e.

$$Vc_x = D\frac{dc}{dx} \tag{2.2}$$

Under these conditions, the decrease in concentration along the tube is given by

$$\frac{Vx}{D} = \ln\left(\frac{c_o}{c}\right) \tag{2.3}$$

where c_o is the initial concentration and c is the final concentration.

Table 2.1: The radii of lead and bromine

Species	Ionic radius	Covalent radius
	m	m
Lead	0.120×10^{-10}	1.47×10^{-10}
Bromine	0.195×10^{-10}	1.14×10^{-10}

In order to evaluate the magnitude of diffusion through the tube a value for D is required for lead bromide in nitrogen (the carrier gas used here). The interdiffusion coefficient for a trace species diffusing into a second is given by the kinetic theory of gases [12] as

$$D_{12} = \frac{2}{3\pi(N_1 + N_2)\sigma_{12}^2}\sqrt{\frac{2kT}{\pi}\left(\frac{1}{m_1} + \frac{1}{m_2}\right)} \tag{2.4}$$

where k is the Boltzmann constant, N is the number of gas molecules per unit volume, σ_{12} is the average collision diameter of the two species (1 and 2) and m_1, m_2 are the masses of one molecule of each of the two species involved.

The collision diameter for nitrogen [1] is 3.1×10^{-10} m and that for lead bromide has been estimated using the atomic radii for lead and bromine shown in Table 2.1 [13]. The Br-Pb-Br bond angle and the Pb-Br bond length are believed to be 95° and 2.6×10^{-10} m respectively [4]. The maximum possible rate of diffusion and hence the most unfavourable result in the present case, occurs when the smallest radii are used to calculate a value of D. Simple trigonometry and the smallest of the tabulated atomic radii, along with the above bond angle and length, predicts the minimum molecular diameter of lead bromide to be about 6.1×10^{-10} m.

Substituting the above parameters along with an estimate of the number of gas molecules per unit volume into equation 2.4 gives

$$D_{PbBr_2,PbO} = 0.459 \text{ cm}^2 \text{ sec}^{-1} \text{ at } 550 \text{ °C} \text{ and } 0.502 \text{ cm}^2 \text{ sec}^{-1} \text{ at } 600 \text{ °C} \tag{2.5}$$

These temperatures were chosen to be within the expected range of the measurements to be conducted on the lead oxybromides.

Using typical conditions of temperature 600 °C, pressure 760 mmHg, flow of nitrogen 20 $\text{cm}^3 \text{ min}^{-1}$, initial concentration of lead bromide vapour c_o of 7.96×10^{16} molecules cm^{-3} (vapour pressure of lead bromide at 600 °C) and capillary length 10 cm, Equation 2.3

gives the concentration of lead bromide vapour at the upstream end of the capillary as 166 molecules cm^{-3}.

The rate of effusion of lead bromide from the end of the tube (assuming that it is condensed immediately) is given by the product of the diffusion coefficient, concentration gradient and the cross sectional area of the tube. Under the above conditions, this gives a rate of effusion of 55.2 molecules sec^{-1}, which corresponds to 9.4×10^5 years for the loss of 1 μg of sample. Even if the error in the estimation of the diffusion coefficient is 50 %, it does not change the conclusion that back diffusion can be neglected.

These calculations are supported by the fact that during the measurements (in which flow rates as low as 8 cm^3 min^{-1} were employed) there was no noticeable deposition of sample on the walls of the inlet tube or hangdown fibre.

In the course of the vapour pressure measurements several saturation chambers were used. The only major differences were in the materials of construction and the diameter and shape of the outlet tube. The basic design is shown in Figure 2.4. The manometer line shown in this figure was omitted from later saturation chambers as initial measurements indicated that the pressure difference between the inside of saturation chamber and the surrounding atmospheric pressure was insignificant. Furthermore its presence served to weaken the already delicate glassware.

The saturation chambers were constructed either from Pyrex or quartz glass, the latter being used for measurements at temperatures in excess of 540 °C. In saturation chambers constructed from quartz, the inlet and outlet tubes were redesigned to allow easier construction, although the length of tube remained the same. The quartz inlet and outlet tubes were no longer wound into a coil as shown in Figure 2.4, instead they were constructed in a series of straight sections linked by bends as shown in Figure 2.6.

2.1.4 The Sample Holder

In the present work the sample was contained in a basket which was suspended from a quartz spring and the quantity of material entering the gas phase was determined by monitoring regularly the extension of the spring. The main requirement for the support fibre (hangdown fibre (the fibre which connected the sample pan to the spring)) and sample pan was that they be as light as possible, because the spring could support a maximum load of only 1 g.

Initially the sample container was made from a single 2.5 × 2.5 cm square sheet of 0.0125

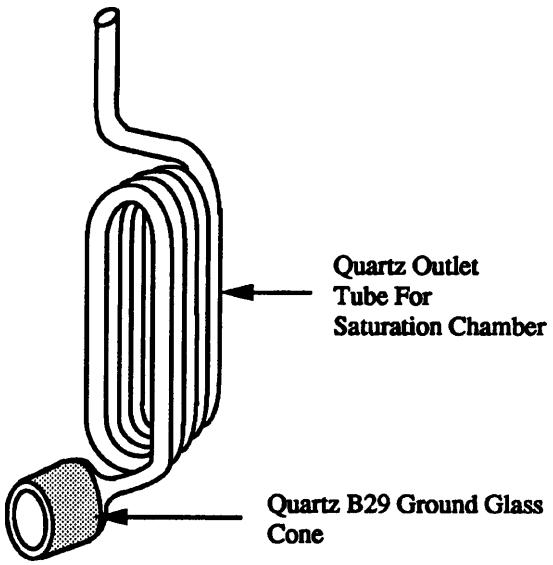

Figure 2.6: The modified saturation chamber outlet

mm thick platinum foil which was formed into a circular pan 2 cm in diameter with an upstanding edge of approximately 1 mm. This was accomplished by pressing a small plastic stopper into a cardboard tube [14], after the platinum foil had been carefully positioned between the top of the tube and the stopper. This dish was then mounted in a support made from a 13 cm length of 0.25 mm diameter platinum wire, see Figure 2.7. The dish was secured to the mounting by wrapping the corners of the original square of foil around the circular body of the support.

This first sample pan weighed 0.3017 g and was used successfully in the determination of the vapour pressure of lead bromide. However, subsequent experiments using a 1:1 lead oxybromide showed that the carrier gas could be saturated at greater flow rates if two pans were used. This lead to the construction of two new pans along similar lines to the original. The second of the pans hung below the first. In order to reduce the combined mass of the sample pans the supports had to be modified. Each pan was made from two lengths of 0.25 mm diameter platinum wire and a 25 x 25 x 0.0125 mm sheet of platinum, as shown in Figure 2.8. Initially the joint labelled **A** was welded on a small arc welder, unfortunately this made the wire very brittle and caused it to deform and eventually break when placed in the oven at temperatures in excess of 500 °C. The method found to be most suitable was one in which one of the two lengths of wire was simply wrapped around the second and then the two crimped together. In order to keep the weight to a minimum, 0.013 mm tungsten wire was used for the support wire **B** shown in Figure 2.8. This arrangement provided a reliable and relatively sturdy sample holder with a total combined weight of 0.4689 g (0.2479 g upper pan, 0.2210 g lower pan).

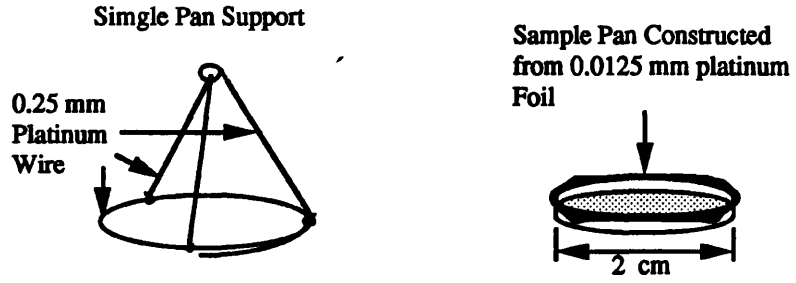

Figure 2.7: The single sample pan and support

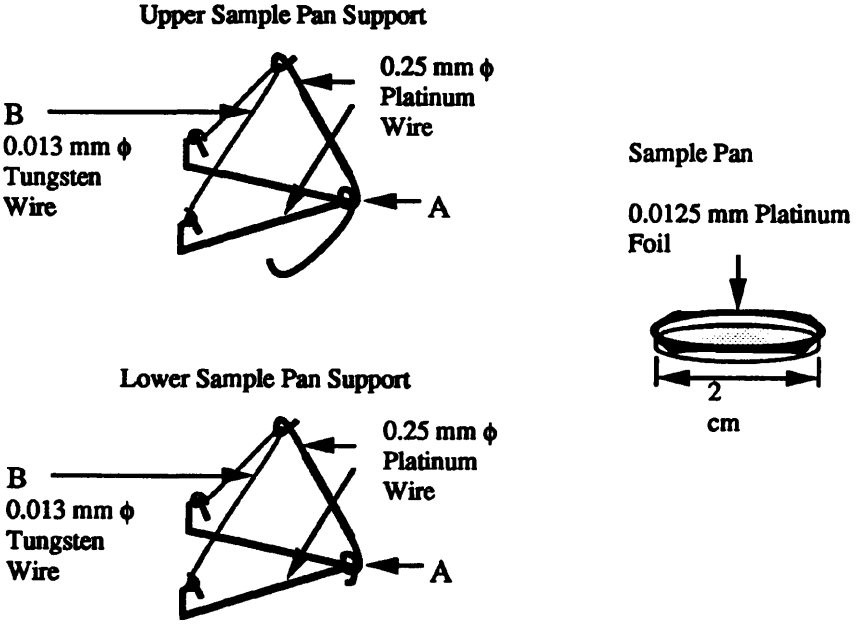

Figure 2.8: The twin sample pans and supports

2.1.5 The Sample Support

The hangdown fibre connected the spring to the sample baskets (see Figure 2.1). Initially, it was intended to make the hangdown fibre from 0.013 mm diameter tungsten wire, but this could not be straightened sufficiently to allow it to hang freely through the long narrow tube leading from the spring chamber to the saturation chamber. Thus a quartz fibre was prepared and this provided a very light but durable hangdown, although at temperatures above 600 °C the lower region of the fibre thinned drastically and became brittle. This may have been because the already thin fibre softened and stretched under load. The mass of the hangdown fibres varied between 0.02 g and 0.1 g.

2.1.6 Temperature Control

The saturation chamber design and construction allowed it to fit neatly into an existing fan oven. The oven was made from a double layer of 2.54 cm thick "Marinite" and had internal dimensions of 30 × 30 × 30 cm. The top was split into two halves, each half had holes strategically positioned to accommodate the protruding limbs of the apparatus. When the lid was in position the space between the glassware and the sides of the holes was insulated with quartz wool. The fan, which was mounted on the base of the oven, and the motor assembly were taken from a Pye Unicam Series 104 Gas Chromatograph. The oven was resistively heated by four elements each of which formed a square on separate walls of the oven. These elements were wired into two parallel circuits and were powered by a CNS Instruments proportional temperature controller, which used a platinum resistance thermometer as a temperature sensor.

The temperature profile through the oven was measured using a calibrated Pt - Pt 13 % Rh thermocouple. The results showed a uniform temperature in all but the upper and lower 2 cm of the oven, in addition temperature measurements throughout the vapour pressure determinations indicated that the fluctuation in oven temperature over several days was less than 0.3 °C.

2.1.7 Temperature Measurement

The temperature of the oven was measured using a Pt - Pt 13 % Rh thermocouple which had been calibrated in the normal way against boiling water and the melting points of the metals lead, zinc and tin, all of which were supplied with a purity $\geq$ 99.999 %. The E.M.F. produced by the thermocouple was measured using a Cambridge slide wire potentiometer

reading to ±0.002 mV. As a rough guide 0.002 mV corresponds to an uncertainty of 0.2 °C in the temperature at 500 °C.

The thermocouple was positioned as near as possible to the saturation chamber wall at roughly the same height as the sample pan. The temperatures quoted in the vapour pressure results were those obtained with this thermocouple.

2.1.8 The Adjustable Spring Support

In the present work the mass of sample evaporating into the carrier gas stream was calculated from measurements of the extension of a quartz spring. The spring was suspended from a wire support which was attached to a nylon cord. The nylon cord permitted the spring to be raised and lowered to allow the sample pans to be added or removed as required. When the spring was at the desired height the nylon cord was clamped in the pin vice shown in Figure 2.9, the adjustable support which held the pin vice provided the lateral adjustment necessary to enable the quartz support fibre to hang freely through the narrow tube leading to the saturation chamber. When all the adjustments were complete the locking screws on the adjustable support were tightened, the excess nylon cord coiled neatly around the stem of the pin vice and the greased ground glass stopper inserted to seal the upper section of the apparatus. The entire arrangement is shown in Figure 2.10. The adjustable support was held in position by three rubber supports, which also absorbed a considerable amount of the vibrations set up in the framework by the fan oven and other external sources. The plumb bob on the end of the nylon cord also increased stability to vibration and without it the nylon cord was not held taut.

2.1.9 The Spring Support

The wire support which connected the spring to the nylon cord was made from tungsten wire 0.013 mm in diameter. It was found that the shape of this support wire had a marked effect on the reproducibility of measurements of the spring extension. The various stages of the design are shown in Figure 2.11 by diagrams **A** to **E**. **B** and **C** show the source of the error which resulted from the slipping of the helix on the wire support. The support wire was bent in attempt to trap the spring in the V shaped notch (See Diagram **C**), subsequently the bottom 3 mm of the support wire were completely closed together and the spring forced between them (Diagram **D**). Some slipping still occurred, however, and the problem was eventually solved by modifying the shape of the top of the spring as shown in diagram **E**, together with the shape of support shown in diagram **D**. The lower end

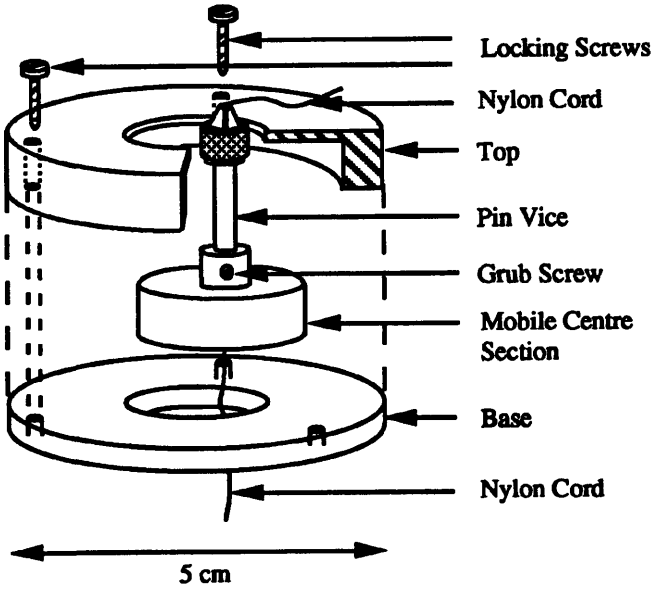

Figure 2.9: The adjustable spring support

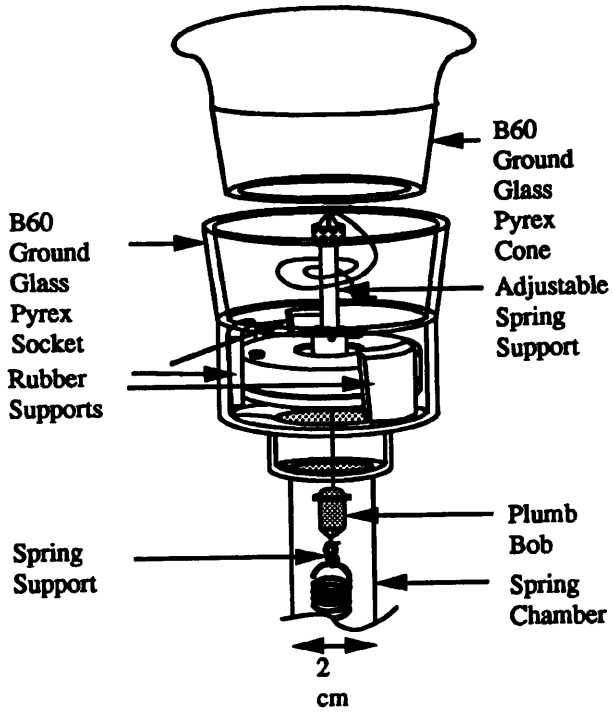

Figure 2.10: The adjustable spring support in position at the top of the spring chamber

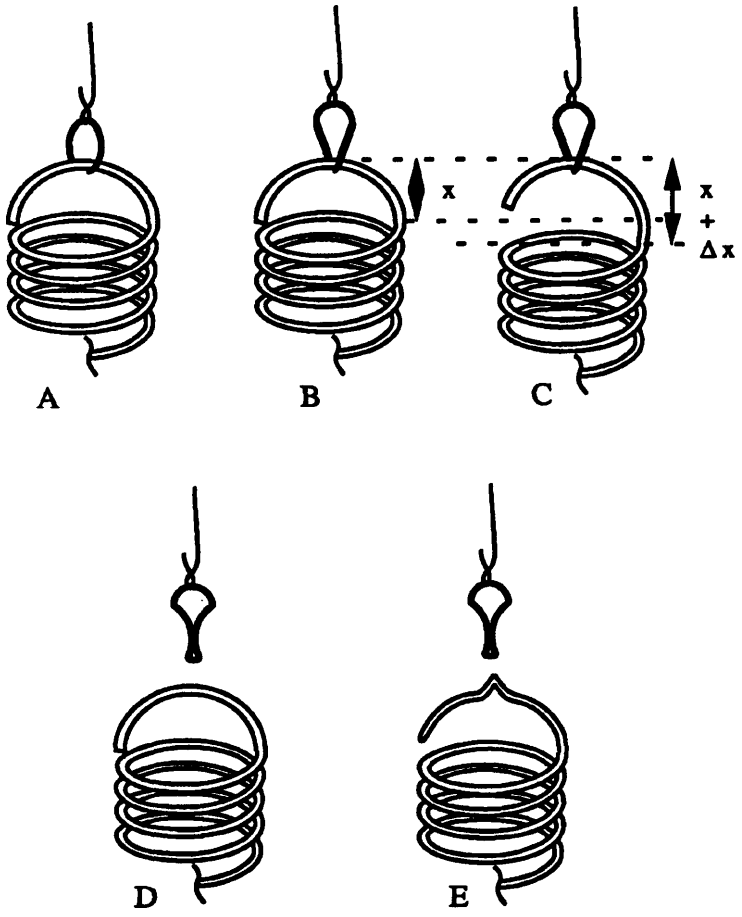

Figure 2.11: The development of the spring support

of the spring was also modified in a similar fashion to prevent the hook of the hangdown fibre slipping and resulting in further errors.

2.1.10 The Spring

The quartz spring had a maximum load of 1 g and a sensitivity of 51 cm g^{-1}. The helix had 68 turns, each 15.5 mm in diameter and when unloaded it was 9.7 cm long. The total mass of the spring was 0.2092 g.

Before it could be used as a balance the spring had to be calibrated. The calibration was done with the spring in the normal operating position in the apparatus using a series of standard weights, which had been thoroughly cleaned and checked to six decimal places on a Mettler analytical balance. The calibration was confirmed following a small earthquake, which had broken the manometer arm on the saturation chamber. At this point

the manometer arm was removed as experience had shown that the pressure inside the saturation chamber was equal to atmospheric pressure even at high flow rates.

Unfortunately the spring was later broken when the three mounting points of the saturation chamber sheared and it dropped to the laboratory floor. The oven motor bearings had become worn in the previous experiment which resulted in violent vibrations throughout the apparatus and a considerable amount of stress in the glassware. When the glassware cooled it cracked, the sample pan was still in position and jammed in the narrow entrance of the saturation chamber. The falling saturation chamber dragged the spring downwards until the lower loop hit the bottom of the spring chamber and fractured. After this the spring was repaired and recalibrated; the over extension had no measurable detrimental effect on the linearity of extension with load.

2.1.11 Results of the Spring Calibration

The calibration weights were placed in a single sample pan and the extension of the spring measured using a 1 m cathetometer which was fitted with a magnifying lens and mounted on a substantial steel support. Using this arrangement measurements were reproducible to better than ± 0.05 mm. The cross hairs of the cathetometer were aligned with the upper edge of the spring where it passed over the wire support and the lower edge of the spring where it passed under the hook of the quartz hangdown fibre.

The results of the calibrations are shown in Tables 2.2 to 2.6 and are shown graphically in Figures 2.12 to 2.18.

Least squares linear regression analysis of these data yielded a spring constant of 0.002053 g mm^{-1} for Table 2.2, 0.002057 g mm^{-1} for Table 2.3 and 0.002054 g mm^{-1} for the combined data with an estimated error of $\pm 1 \times 10^{-6}$ g mm^{-1}.

Table 2.4 shows the results of a similar calibration carried out six months later. Similar treatment of these results yielded a spring constant of $0.002062 \pm 1 \times 10^{-6}$ g mm^{-1}. The combination of data from Tables 2.2, 2.3 and 2.4 in the mass range 0.7 – 0.95 g provides a spring constant of **0.002065 g mm^{-1}** which was the value used in the calculation of most of the vapour pressures throughout this work. Figure 2.15 provides a graphical comparison of all the data. The results in this mass range were chosen as the majority of the experimental measurements were made in this region.

Figure 2.16 contains the combined data of Tables 2.2 to 2.4. The error bars representing the experimental points correspond to 0.05 mm in length of the spring. This graph shows

Table 2.2: The initial calibration of the spring over the full mass range 0.3–0.9 g

Mass / g	Extension / mm	
	Increasing	Decreasing
0.000000	118.63	118.87
"	118.67	118.80
0.301785	266.38	266.44
"	266.46	266.47
0.331755	281.05	281.14
"	281.05	281.13
0.432790	330.45	330.49
"	330.41	330.48
0.531605	378.57	378.67
"	378.58	378.65
0.631595	427.30	427.30
"	427.28	427.33
0.732630	476.39	476.40
"	476.37	476.38
0.831690	524.33	524.32
"	524.29	524.34
0.932725	573.22	573.22
"	573.22	573.22

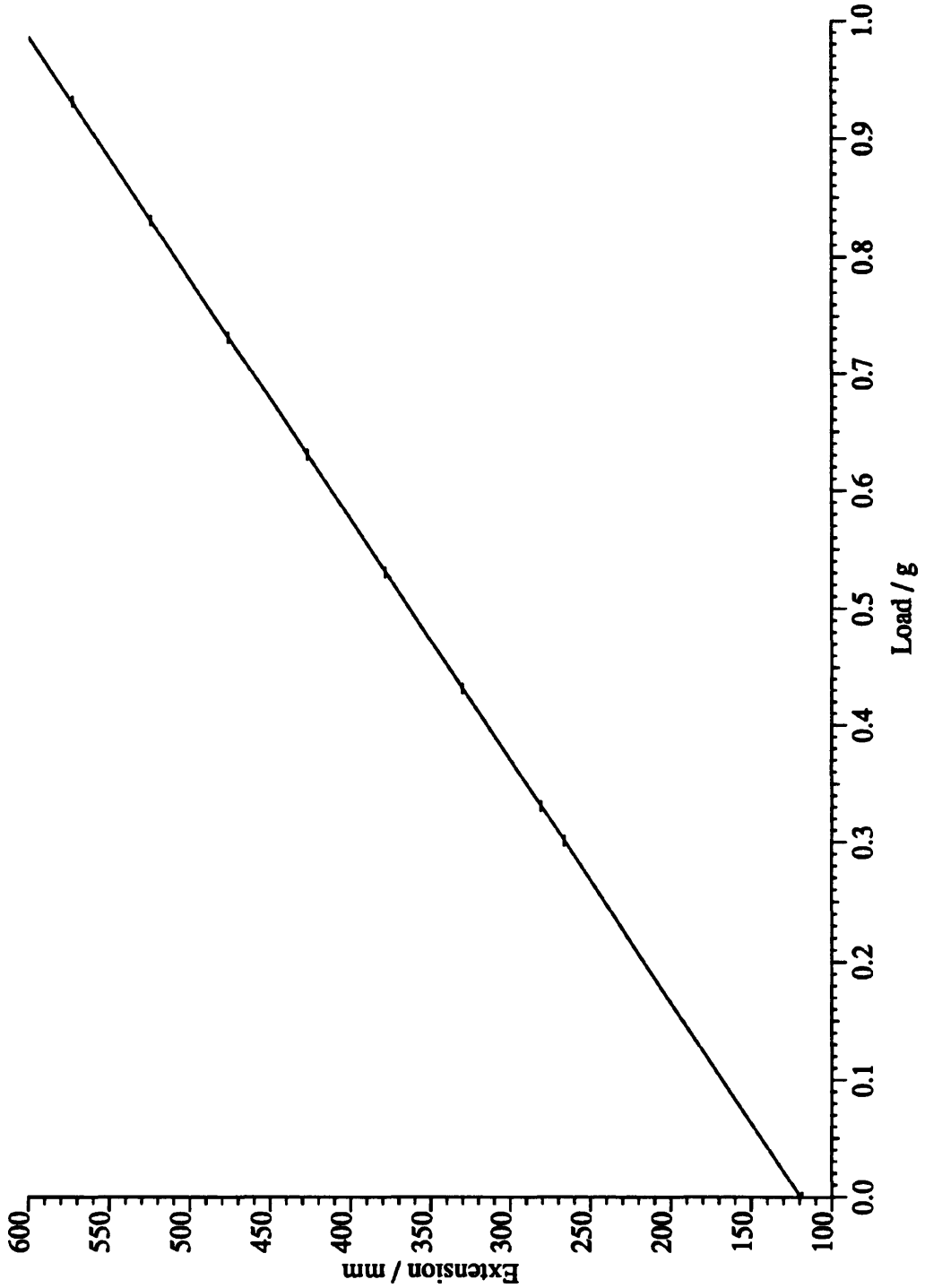

Figure 2.12: The initial calibration of the spring over the full mass range

Table 2.3: The initial calibration of the spring over a limited mass range 0.8–0.9 g

Mass / g	Extension / mm	
	Increasing	Decreasing
0.301785	266.50	
0.801720	509.80	509.78
0.811690	514.63	514.67
0.821710	519.47	519.45
0.831690	524.29	524.30
0.841660	529.12	529.13
0.851755	533.93	533.96
0.861725	538.79	538.79
0.871745	543.63	543.66
0.881725	548.47	548.50
0.932725	573.22	573.22

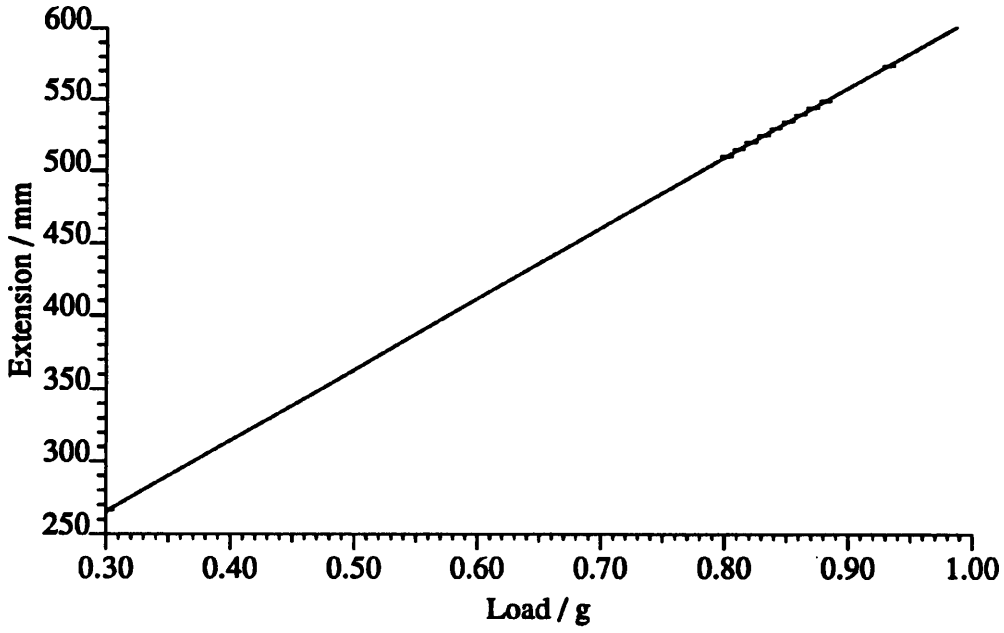

Figure 2.13: The initial calibration of the spring over a limited mass range

Table 2.4: The confirmation of the calibration of the spring over the full mass range

Mass / g	Extension / mm	
	Increasing	Decreasing
0.301600	266.62	266.60
0.401640	316.50	316.50
0.502715	364.80	364.81
0.801580	509.82	509.81
0.901620	558.23	558.27
0.911620	563.04	563.10
0.921630	567.94	567.94
0.931670	572.80	572.82
0.941610	577.62	577.62
0.951600	582.46	582.44
0.961600	587.05	587.05

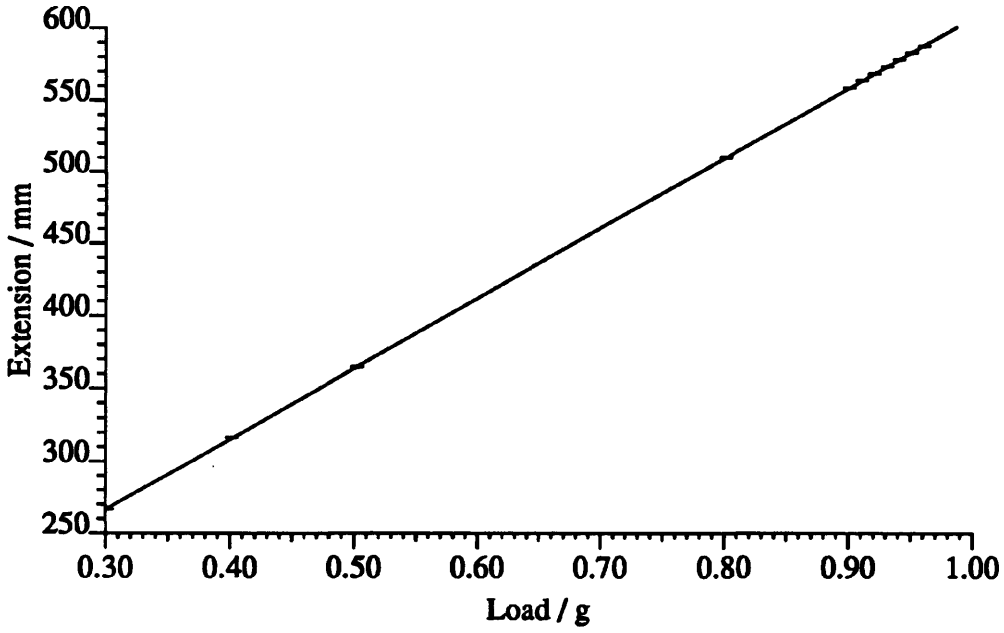

Figure 2.14: The confirmation of the calibration of the spring over the full mass range

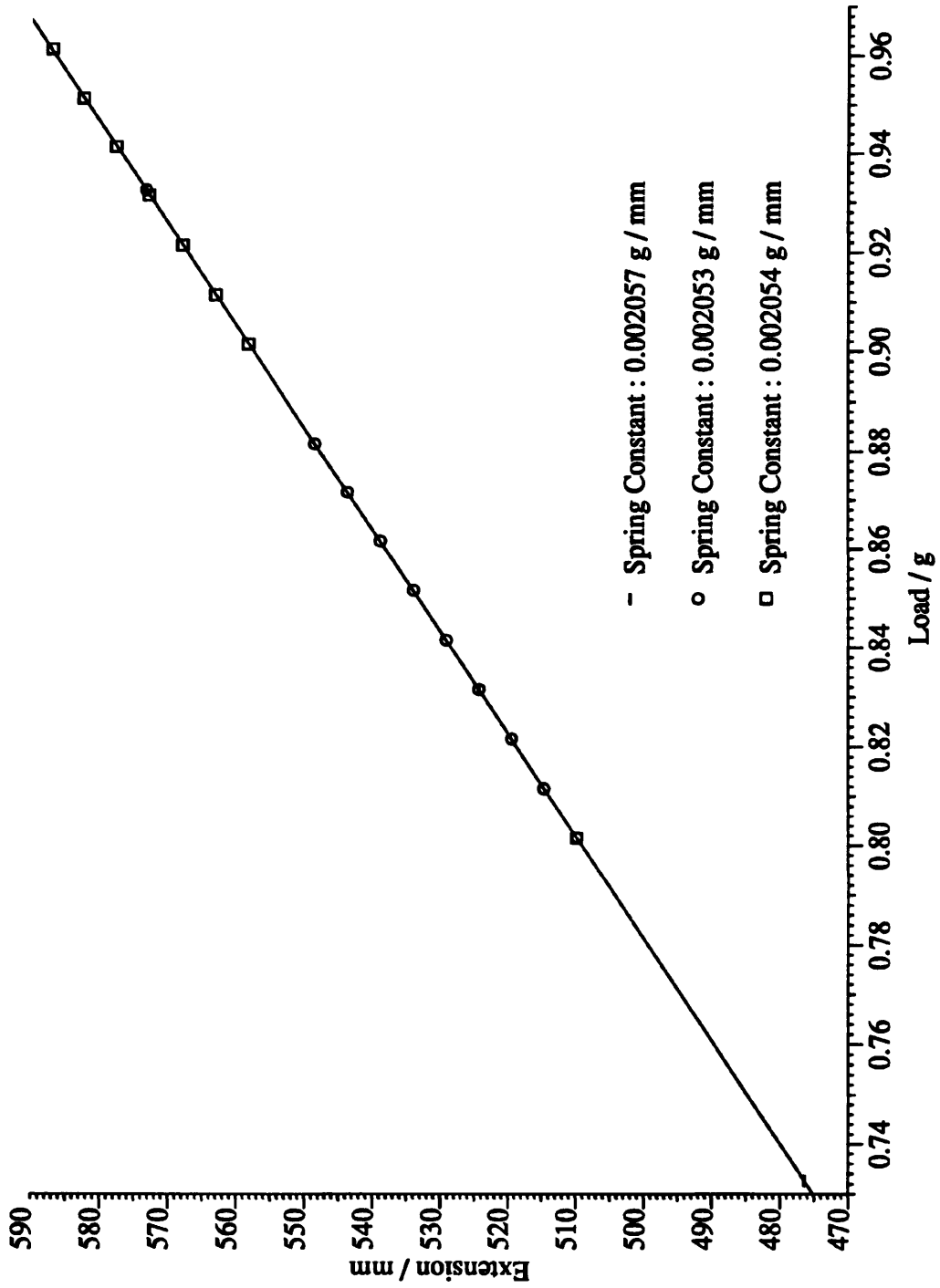

Figure 2.15: The combined data for a limited mass range used to calculate the spring constant

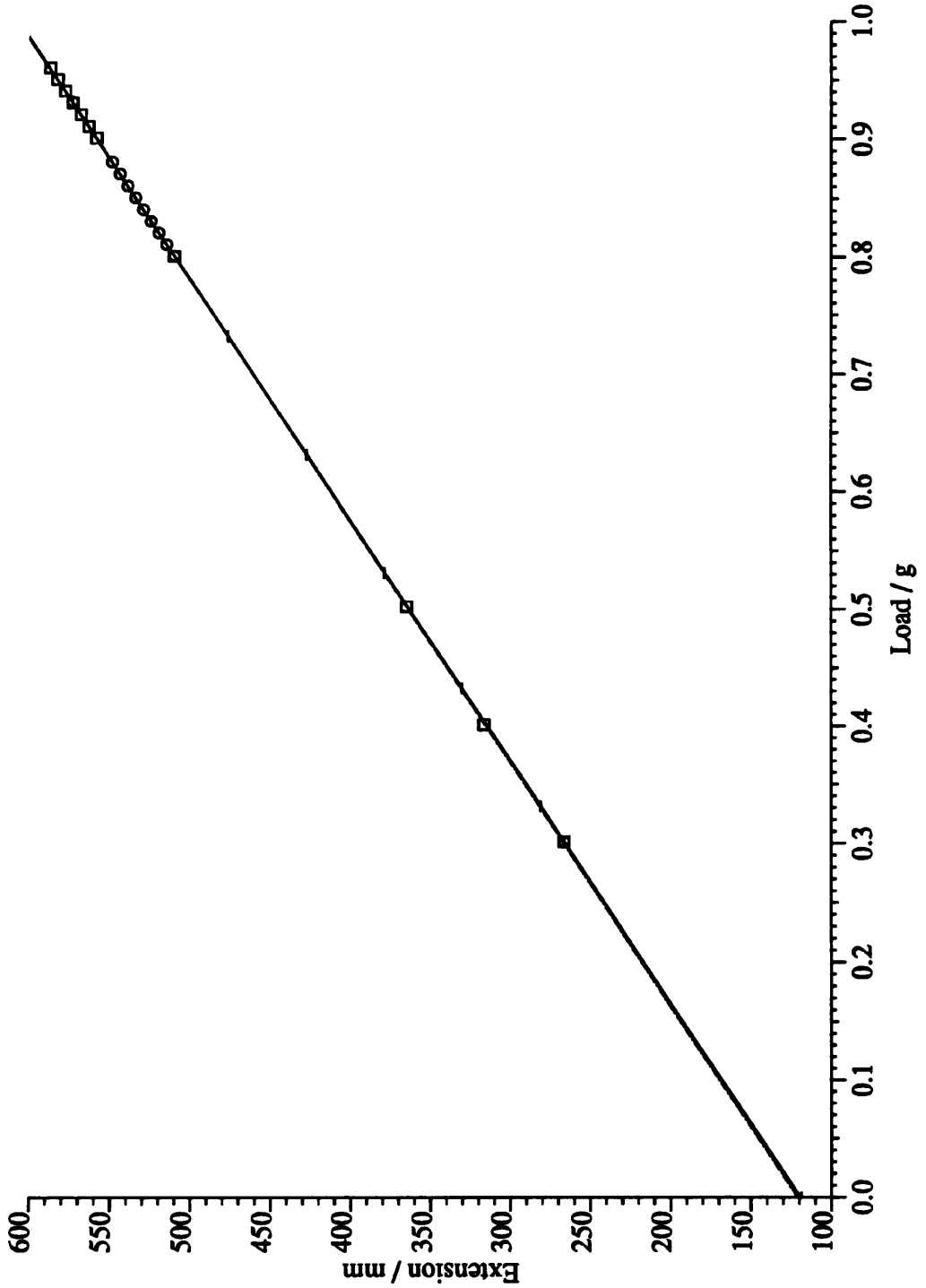

Figure 2.16: The combined data of the initial calibration results

Table 2.5: The calibration of the repaired spring over the full mass range

Mass / g	Extension / mm	
	Increasing	Decreasing
0.301414	321.11	321.12
0.402514	370.96	370.98
0.503014	418.37	418.35
0.703024	514.61	514.58
0.803014	562.61	562.60
0.902529	610.41	610.36
0.902529	610.42	610.44

the remarkable linearity of the change in length of the spring with respect to load. The lines drawn which represent each of the calculated spring constants are virtually inseparable on a graph of this scale. An error in the measurement of the extension of 0.05 mm corresponds to a mass of 0.0001 g, which is of a similar order to the common analytical laboratory balance!

The repairs carried out on the spring after it was broken resulted in the loss of approximately one turn of the helix and led to the need for a subsequent recalibration. The results of this calibration are tabulated in Table 2.5 and Table 2.6 and shown graphically in Figure 2.17 and Figure 2.18. The linear regression analysis of these results showed that although the spring had been extended beyond the recommended limit prior to its fracture, this had no visible detrimental effect on its linearity. The new spring constant of **0.002083 g mm^{-1}** was used in the remainder of the work.

2.2 Sample Loading and Experimental Technique

The following section describes the procedure adopted when loading the samples into the transpiration apparatus.

The spring and hangdown fibre were positioned such that the lower hook of the hangdown fibre was just visible at the top of the B29 socket at the base of the saturation chamber. The previously weighed sample was then balanced on the end of a standard 12" hacksaw blade, carefully placed inside the base of the saturation chamber and manipulated until the upper support wire of the basket was hooked over the lower hook of the hangdown

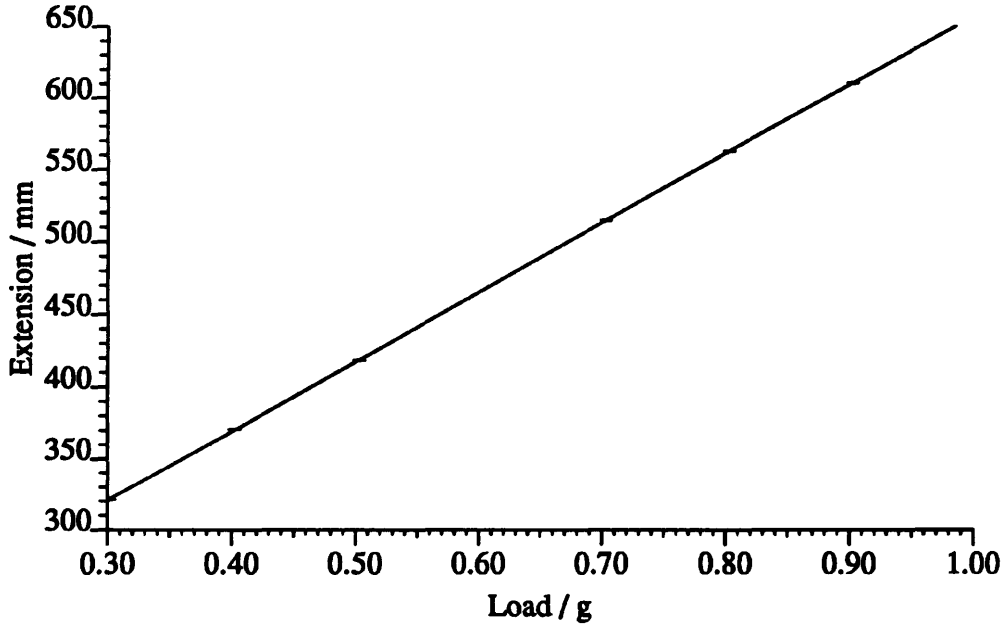

Figure 2.17: The calibration of the repaired spring over the full mass range

Table 2.6: The calibration of the repaired spring over a limited mass range

Mass / g	Extension / mm	
	Increasing	Decreasing
0.803014	562.45	562.50
0.813039	567.26	567.28
0.833074	576.80	576.80
0.843039	581.66	581.66
0.853049	586.52	586.50
0.863024	591.30	591.26
0.873049	596.16	596.12
0.883059	600.86	600.83
0.893084	605.53	605.57

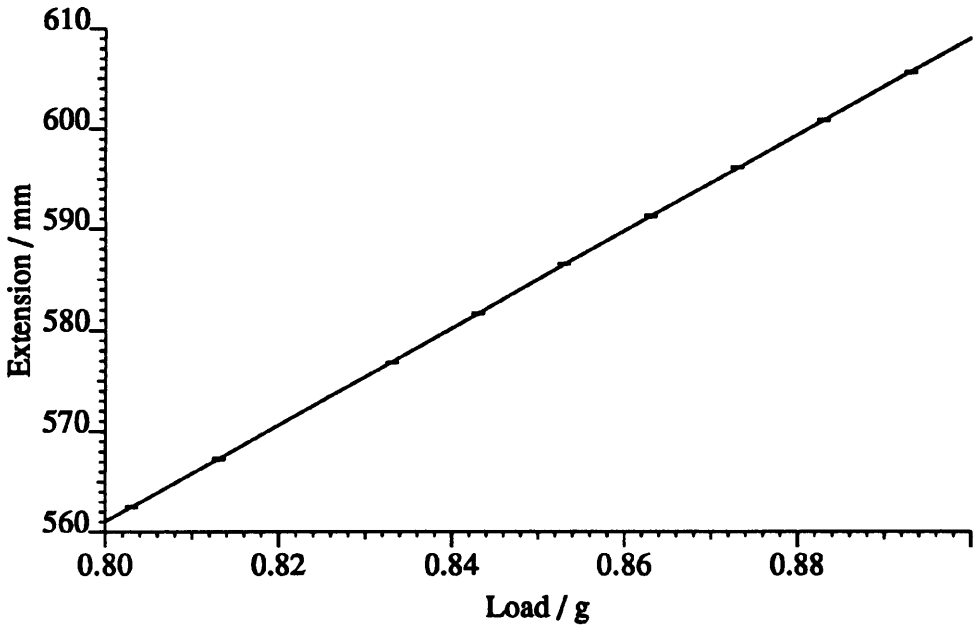

Figure 2.18: The calibration of the repaired spring over a limited mass range

fibre. The hacksaw blade was then supported by a piece of plastic which held it level whilst the spring was tensioned from the top of the apparatus. The nylon cord which supported the spring was slowly pulled up until the basket lifted off the hacksaw blade and, when the basket was at a suitable starting position for the experiment, the cord was clamped in the pin vice. This position was such that the bottom of the basket was about 2 cm above the B29 aperture at the base of the saturation chamber. The hacksaw blade was then removed and the hangdown fibre inspected to see if it was hanging freely.

Static electricity often caused the fibre to stick to the walls of the capillary inlet. This effect could be reduced with the aid of an antistatic spray although generally the static dissipated sufficiently over a 5 to 10 minute period without the spray. When the fibre was hanging freely its position was adjusted via the adjustable support so that it hung through the centre of the inlet tube. The tower which supported the spring chamber was mounted on four bolts which could be used to tilt the whole assembly slightly to give more adjustment if necessary. The adjustable support was then clamped using the three clamping screws, the loose nylon cord coiled around then pin vice and the spring chamber sealed with the greased B60 ground glass stopper. The outlet tube was then fitted to the saturation chamber and held in place by two small steel springs.

Finally the fan oven was replaced around the saturation chamber. The split lid was removed and the jack used to raise the oven to its normal operating position. Once in the correct position the split lid of the oven was carefully replaced, the holes plugged with quartz wool and the power restored. The whole procedure of positioning the oven took approximately 2 minutes and the operating temperature was reached and stabilised within

half an hour.

Between experiments the oven temperature was maintained at the level at which the next experiment was to be conducted; heat losses during this period were reduced by covering the access holes with a thin sheet of Marinite.

In the later experiments, where the single sample pan was replaced by two which hung one below the other (see Section 2.1.4), the sample was introduced in two stages as there were added complications. The hook which hung below the first basket prevented it from sitting on the hacksaw blade whilst the nylon cord was adjusted to lift it to a height at which the second pan could be added. Instead, the first basket was hooked over the bottom of the hangdown wire, then balanced on its lower hook and propped up against the side of the saturation chamber. The hacksaw blade was then removed !! (if the sample pan toppled over at this stage, the sample spilt into the saturation chamber and forced a painstaking clean-up operation). The basket was then raised until the lower hangdown support was in a suitable position for the second basket to be added. The second basket was then added in the same manner as described previously when a single basket was being used.

2.3 Sample Preparation and Materials

High purity (99.999 %) lead bromide and lead chloride were obtained from Johnson Matthey Chemicals, lead oxide (yellow) of the same high quality was obtained from Koch Light Chemicals. A sample of the lead bromide was tested using a differential scanning calorimeter and found to have a melting point of 370.3 °C which agrees well with the currently accepted melting point of 370 $\pm$ 0.2 °C [6].

The lead oxyhalides used throughout this work were prepared from these high purity lead bromide, lead chloride and lead oxide. Stoichiometric quantities of oxide and halide were mixed and subjected to a specific treatment in a specially constructed gas-tight vessel. In all cases the total mass of lead oxide and lead halide was approximately 5 g.

The crucible shown in Figure 2.19 was made from platinum foil 0.25 mm thick which fitted snugly into a stainless steel outer case. When the steel lid of this outer case was secured using the clamp, the platinum top of the inner liner was pressed firmly against the shoulder of its lower counterpart, thus furnishing an inert sealed container. It was important for this container to be gas-tight in order to prevent changes in the overall composition of the mixture due to evaporation of lead halide during the prolonged heat treatment (often in excess of 12 hours).

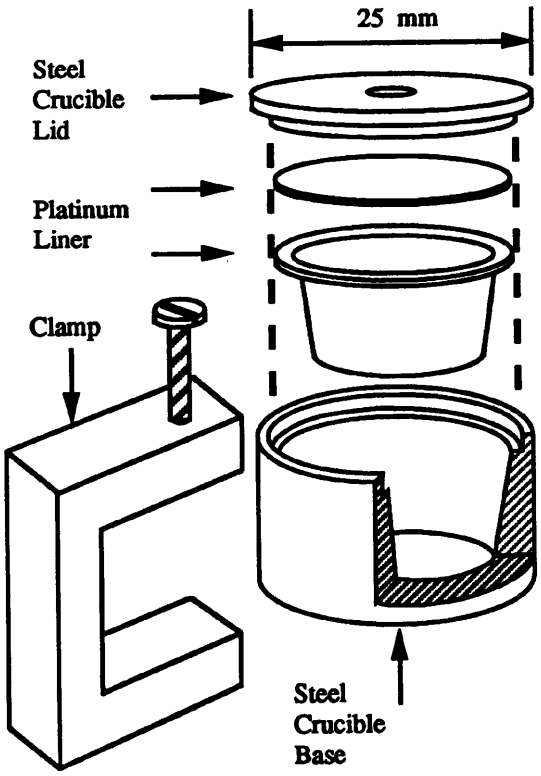

Figure 2.19: The crucible used in sample preparation

Table 2.7: The temperature cycle during production of lead oxybromide

Temperature °C	Isothermal Time Hours	Rate of Cooling
700	3	Unhindered
600	2	Unhindered
500	12	Gradual over 5 hours
400	0	Oven Power removed

Platinum was chosen as the material of construction as it was known to be sufficiently impervious to lead oxyhalides. Other materials reported to be suitable are gold and magnesia [6]. Previously a small sample of stainless steel was tested for its resistance to the lead oxyhalides, as it was hoped that crucibles of this material could be used for measurements of the thermal properties of the oxyhalides by differential scanning calorimetry. The sample was badly corroded and became ferromagnetic, in addition the lead oxyhalide was found to contain significant amounts of iron.

A simple tube furnace equipped with a CNS Instruments proportional temperature controller was used to heat the sample mixtures and the thermocouple used to measure the temperature of the fan oven during the vapour pressure measurements was used to measure the temperature at regular intervals during sample preparation. Following the heat treatment the samples of lead oxyhalide were crushed to a powder with an agate mortar and pestle and stored in the dark in capped Pyrex tubes.

2.3.1 Preparation of 1:1 Lead Oxybromide

The 1:1 lead oxybromide has, as its name implies, a stoichiometric amount of one mole of lead bromide per mole of lead oxide. It was the most difficult of the oxybromides studied in this work to prepare as it is formed in a peritectic reaction occurring at 497 °C [6], the rate of temperature decrease was carefully controlled around this point in an attempt to maintain phase equilibrium for as long as possible. Table 2.7 summarises the heat treatment employed in the generation of the 1:1 lead oxybromide.

In his early work Knowles indicated that $PbO.PbBr_2$ existed in three polymorphic forms. He suggested that the form produced depended upon the heat treatment of the sample. These findings were based upon the X-ray crystallographic work of Lamb and Niebylski [8], but the existence of the various crystallographic modifications is a subject of controversy.

Davies, Garner and Caddock [2] proposed the existence of two compounds, $4PbO.5PbBr_2$ and $6PbO.7PbBr_2$, which correspond to two of the three polymorphic forms, and Julien and Ogilvie [5] maintained that there is only one stable form of the 1:1 lead oxybromide.

The nature of the pale yellow $PbO.PbBr_2$ formed in this work was determined by X-ray powder crystallography, the results of which are discussed in greater detail in Chapter 3. However, the X-ray results did show that the samples of $PbO.PbBr_2$ produced by the heat treatment were consistent in crystal structure, and that the vapour pressure measurements were obtained with consistent samples.

2.3.2 Preparation of 2:1 Lead Oxybromide

The 2:1 lead oxybromide has a stoichiometry of 2 moles of lead oxide per mole of lead bromide. Samples were prepared by intimately mixing the exact proportions of halide and oxide and then heating the mixture in the crucible shown in Figure 2.19 to approximately 730 °C for 2 to 3 hours. The oven was allowed to cool naturally to room temperature before the samples were removed.

The individual batches of the 2:1 lead oxybromide produced were analysed using X-ray powder crystallography to ensure that they were consistent in crystal structure. These X-ray powder photographs are discussed in greater detail in Chapter 3. The 2:1 lead oxybromide was a slightly brighter yellow than the 1:1 oxybromide but could still be described as a pale yellow compound.

2.3.3 Preparation of 3:1 and 7:1 Lead Oxybromide

The 3:1 and 7:1 lead oxybromide were prepared from stoichiometric mixtures of lead oxide and lead bromide. The appropriate mixture was placed in the sealed crucible and heated to a temperature in excess of the melting point of the particular lead oxybromide. The temperature was then reduced slowly to approximately 100 °C below the melting point and the oven was then turned off and allowed to cool naturally.

2.3.4 Preparation of 1:1 and 2:1 Lead Oxychlorides

Samples of both 1:1 and 2:1 lead oxychloride were prepared by fusing intimately mixed stoichiometric quantities of lead chloride and lead oxide. The mixtures were heated to approximately 730 °C in the same gas-tight crucible used during the preparation of the

lead oxybromides, and they were then allowed to cool slowly to room temperature before being removed from the oven.

X-ray powder photographs were obtained for the two oxychlorides and the results are presented in Chapter 3. These oxychlorides were a pale yellow/green colour.

References

[1] CRC press. *Handbook of Chemistry and Physics,* 64^{th} *Edition* CRC press, 1983-1984.

[2] Davies P.T., Garner E.V. and Caddock B.D., *An X-ray Study of the Lead Bromide Rich Region of the Lead Oxide-Lead Bromide System*, Acta. Cryst., 7, (1954), p. 640.

[3] I.U.P.A.C., *Thermodynamics of Non Reacting Fluids*, Experimental Thermodynamics Vol II: Experimental Thermodynamics of Non-reacting Fluids, Butterworths, (1975). ISBN 0 408 70566 3.

[4] JANAF, *Thermochemical Tables*, 2nd Ed. US Dept. of Commerce, National Bureau of Standards, 1971.

[5] Julien H.P. and Ogilvie R.E., *High Temperature X-Ray Study of Lead Halides and Oxyhalides*, Anal. Chem., 82, (1960), p. 293.

[6] Knowles L.M., *Thermal Analysis of the System* $PbBr_2$*-PbO,* J. Chem. Phys., 19 (1951), p. 1128.

[7] Kubaschewski O. and Alcock C.B., *Metallurgical Thermochemistry*, 5th edition. Pergamon Press. ISBN 0 08 020897 5.

[8] Lamb F.W. and Niebylski L.M., *Phase Study of the PbO-*$PbBr_2$ *System by X-Ray Diffraction*, Anal. Chem., 75, (1953), p. 511.

[9] Margrave J.L., *The Characterisation of High Temperature Vapours*, J. Wiley and Sons Inc.

[10] Merten A.J., *Diffusion Effects in the Transpiration Method of Vapour Pressure Measurement*, Phys., Chem., 63, (1959), p. 445.

[11] Nesmeyanov N., *Vapour Pressures of the Chemical Elements*, Elsevier, N. York, (1963).

[12] Partington J.R., *Advanced Treatise on Physical Chemistry*, Vol.1, Longmans, (1949);

[13] Tables of Periodic Properties of the Elements, Sergant Welch Sci. Co.

[14] *The Tube from a Packet of Smarties*, Rowntree Macintosh.

[15] Storms E.K., High Temp. Sci., 1, (1969), p. 456.

[16] Ward J.W., Mulford R.N.R. and Bivins R.L., *Study of Some of the Parameters Affecting Knudsen Effusion. II A Monte Carlo Computer Analysis of Parameters Deduced from Experiment*, J. Chem. Phys., 47, (1967), p. 1718.

Chapter 3

X-ray and Thermal Analysis of the Lead Oxybromides

3.1 X-ray Powder Diffraction

3.1.1 The X-ray Powder Diffraction Patterns of the Lead Oxyhalides

Samples of the lead oxyhalides used in the course of this work were characterised by X-ray Powder Crystallography. The lead oxyhalide was crushed to a powder with an agate pestle and mortar and then sprinkled onto a strip of Sellotape which covered the bottom of a round hole in the centre of the thin disc which was used as a sample holder. The excess sample was removed by gently tapping the inverted sample holder. When the disc was in the camera it was turned continuously by a small electric motor. The powder photographs were taken with a Guinier camera and it was found that an exposure time of 1 hour with the X-ray source operating at 40 kV and 35 mA gave satisfactory results. The camera and sample holder are shown in Figure 3.1.

The copper source in the X-ray generator emitted $K\alpha_1$ and $K\alpha_2$ radiation with wavelengths of 0.154050 nm and 0.154434 nm respectively, but in the powder photographs the individual lines produced by these two wavelengths were not resolved and the intensity weighted average wavelength of 0.154178 nm was used in all calculations. When the X-ray powder photographs were processed the side of the film which had been outermost in the camera was covered with Sellotape whilst it was in the photographic developer, but the Sellotape was removed before the film was transferred to the fixer. Thus, the diffraction pattern appeared on only one side of the film; this prevented parallax errors in measurement of the line positions.

The distinctive fingerprint powder patterns of successive batches of each lead oxyhalide

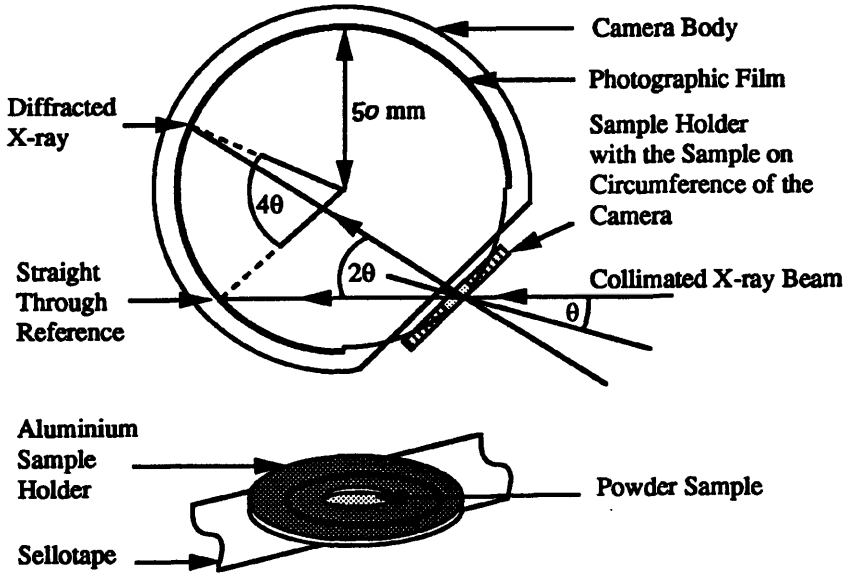

Figure 3.1: The Guinier camera and sample holder

were compared qualitatively by eye to ensure that they were consistent. In addition a selection of power photographs from each of the different phases was digitised with a microdensitometer. The microdensitometer took 238 intensity measurements per centimetre along the length of the photograph. The digitised data were then processed as described below and Figure 3.2 shows a typical set of data at each stage of processing.

The very high spatial resolution of the microdensitometer led to slightly noisy raw data, but the quality could be improved greatly by simple "box car" style smoothing. There were between six and eight intensity samples per diffraction line and a box width of 8 points gave the best results.

The position of the centre and intensity of each peak in the smoothed data was measured and tabulated. This operation was accomplished using the peak detection facilities of a high resolution mass spectrometer data processing system. The positions were then used to calculate θ, 2θ and d spacing values and the results for each of the phases studied are discussed below.

A computerised copy of the JCPDS (Joint Committee on Powder Diffraction Standards) [3] X-ray powder diffraction pattern library was searched for entries which resembled the digitised diffraction patterns obtained in this work. Matching entries were then retrieved and printed. In addition a computerised literature search provided a list of publications which contained X-ray diffraction patterns of compounds containing the elements lead,

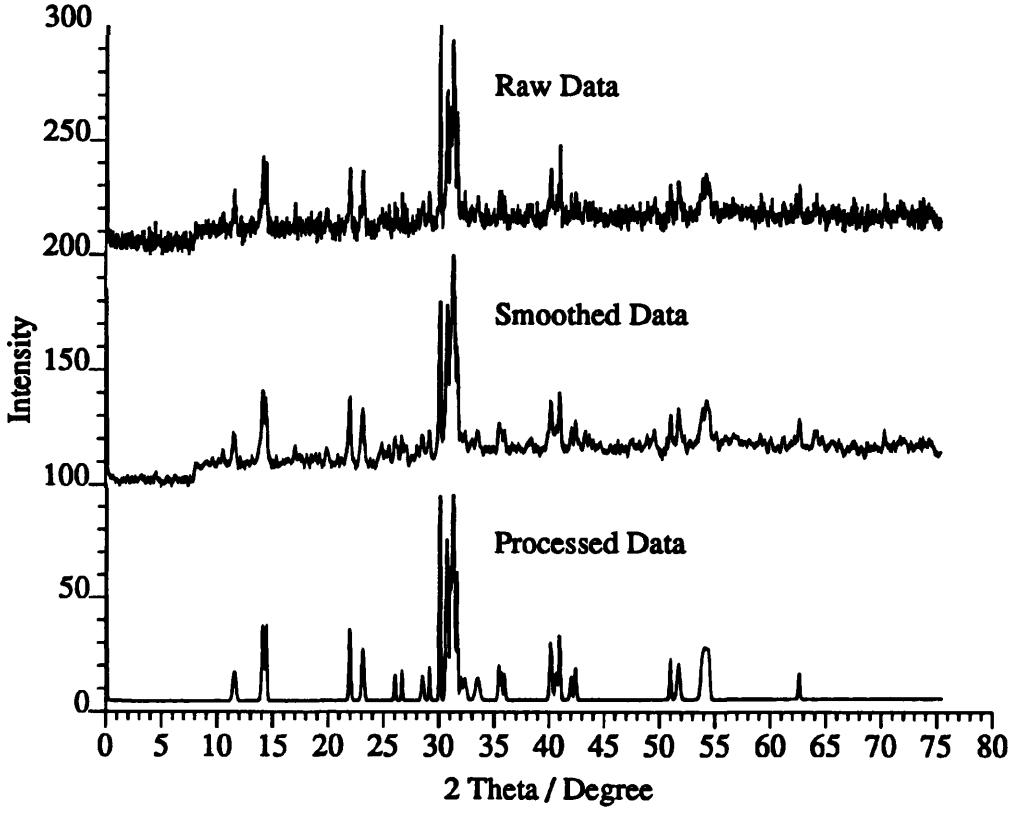

Figure 3.2: Comparison of a typical set of X-ray data at each stage of processing

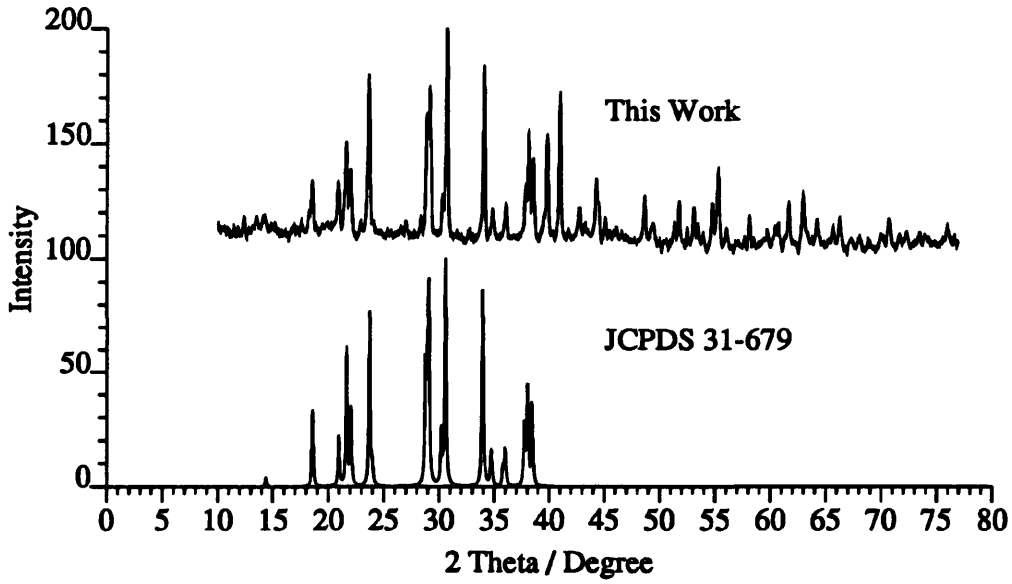

Figure 3.3: The X-ray powder diffraction pattern of lead bromide

oxygen and bromine.

3.1.2 The X-ray Powder Diffraction Pattern of Lead Bromide

The X-ray powder diffraction pattern of the lead bromide used in the present work is shown in Figure 3.3 along with the most recent of the JCPDS library patterns. Unfortunately the library entry which created the data for this figure did not include the reflections above 2θ values of approximately 39 degrees. The complete set of 2θ, intensity and d spacing values (as reported by the National Bureau of Standards) is shown, along with the data obtained in the present work, in Table 3.1.

The correlation between the present results and the library data is excellent. The small discrepancy in the data for the low angle reflection at a 2θ value of approximately 14 degrees is due to the width and fuzziness of the reflection. The line produced on the photographic film was at least ten times wider than the other lines in the diffraction pattern and did not have a distinct border. Three possible sources of this uncharacteristic poorly defined reflection were identified, namely the Sellotape on which the samples were mounted, defects in the crystal lattice and the presence of an amorphous impurity.

The X-ray diffraction pattern of Sellotape contains two reflections with low 2θ angles, but they occur at 12 and 20 degrees and it is therefore unlikely that the Sellotape was the source of the curious reflection. Figure 3.4 shows the diffraction pattern of Sellotape.

Table 3.1: The X-ray powder diffraction data for lead bromide

This Work			JCPDS		This Work			JCPDS	
2θ (deg)	I/I_o	d (Å)	d (Å)	I/I_o	2θ (deg)	I/I_o	d (Å)	d (Å)	I/I_o
13.48	0.06	6.56			not	visible		1.8843	0.06
14.16	0.06	6.25	6.16	0.03	48.61	0.21	1.87	1.8773	0.12
18.63	0.23	4.76	4.774	0.30	49.42	0.07	1.84	1.8483	0.06
20.99	0.22	4.23	4.239	0.20	51.33	0.07	1.78	1.7834	0.07
21.67	0.53	4.10	4.105	0.56	51.73	0.18	1.77	1.7702	0.12
22.10	0.30	4.02	4.032	0.31	52.45	0.05	1.74	1.7459	0.02
23.76	0.76	3.74	3.751	0.73	53.08	0.15	1.73	1.7291	0.14
24.05	0.05	3.70	3.711	0.08	53.43	0.05	1.71	1.7242	0.10
28.30	0.07	3.15	3.102	0.50	53.89	0.03	1.70		
28.86	0.50	3.09	3.081	0.55	54.71	0.20	1.68		
29.12	0.72	3.06	3.071	0.56	55.27	0.36	1.66		
30.30	0.18	2.94	2.958	0.23	56.04	0.06	1.64		
30.66	1.00	2.92	2.924	1.00	58.08	0.13	1.59		
34.03	0.83	2.63	2.641	0.90	59.69	0.06	1.55		
34.68	not	visible	2.586	0.10	60.44	0.07	1.59		
34.80	0.13	2.58	2.580	0.09	60.72	0.07	1.59		
35.79	very faint	doublet	2.509	0.08	61.62	0.21	1.51		
36.05	0.14	2.49	2.495	0.16	62.94	0.24	1.48		
37.81	0.24	2.38	2.385	0.28	64.24	0.13	1.45		
38.09	0.50	2.36	2.367	0.45	65.63	0.06	1.42		
38.53	0.36	2.34	2.341	0.38	66.23	0.13	1.41		
39.24	0.11	2.29	2.286	0.14	67.26	0.03	1.39		
39.80	0.47	2.26	2.271	0.42	68.03	0.04	1.37		
40.96	0.67	2.20	2.208	0.55	69.92	0.06	1.35		
42.76	0.13	2.11	2.122	0.05	70.73	0.13	1.33		
43.24	0.05	2.09	2.099	0.04	71.59	0.03	1.32		
44.01	0.20	2.06	2.052	0.18	72.15	0.03	1.31		
44.25	0.15	2.04	2.042	0.12	73.38	0.03	1.29		
45.02	0.07	2.01	2.016	0.08	73.91	0.03	1.28		
45.41	not	visible	1.997	0.02	75.83	0.12	1.25		
45.89	0.05	1.97	1.972	0.04					

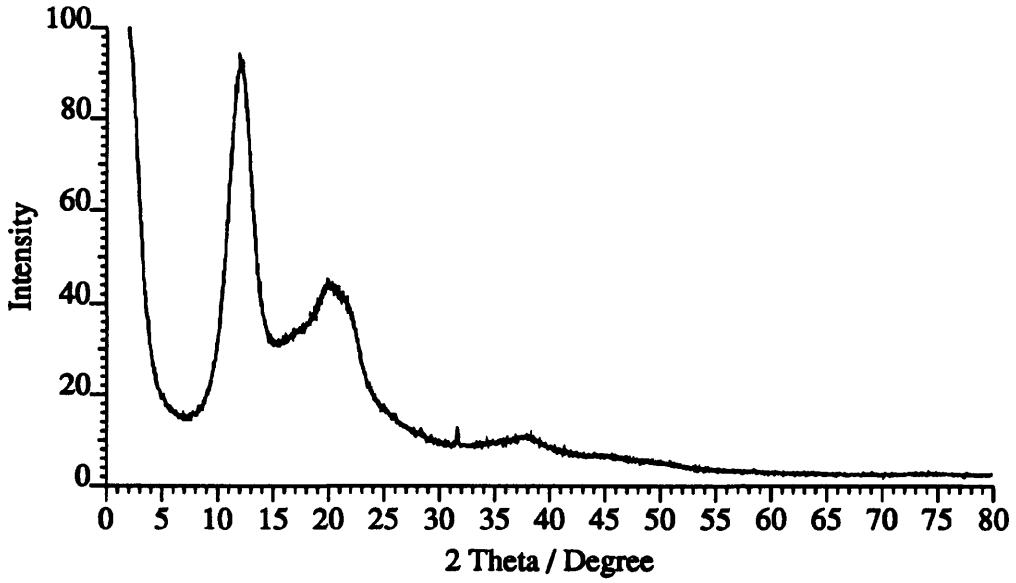

Figure 3.4: The X-ray powder diffraction pattern of Sellotape

The powder photographs obtained in this work appear to show that the relative intensity of the reflection at a 2θ angle of 14 degrees is greater in the samples which had been held at elevated temperatures for several days. As these samples had effectively been annealed it seems unlikely that the reflection was due to defects in the crystal lattice.

It was observed that over a period of time the surface layer of samples of white lead bromide, stored in clear glass bottles and exposed to daylight darkened (the dark layer appeared to be finely divided particles of metallic lead). It seems reasonable to assume that this decomposition would proceed more rapidly at elevated temperatures and the resulting amorphous impurity provides a plausible explanation for the existence of the curious reflection.

3.1.3 The X-ray Powder Diffraction Pattern of Lead Oxide

The X-ray powder diffraction pattern of the yellow (massicot) lead oxide used in this work is compared with the JCPDS library pattern in Figure 3.5 and Table 3.2 shows the corresponding 2θ, intensity and d spacing values. The correlation of relative intensities and positions for all of the reflections is excellent apart from the single most intense line. The difference in the intensity of the most intense reflection is difficult to explain, the diffraction pattern of lead oxide was measured many times in this work and in all cases the pattern was consistent.

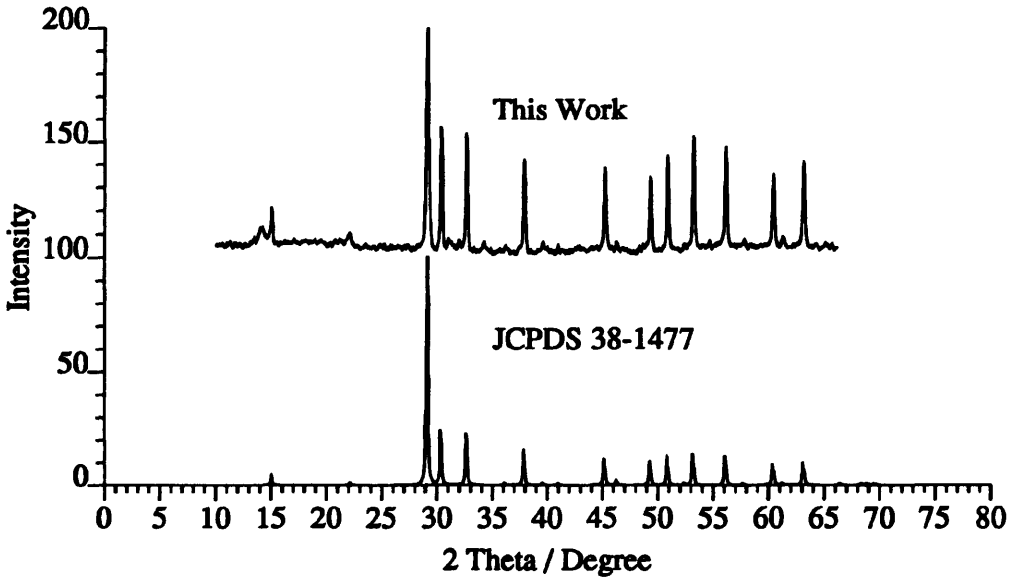

Figure 3.5: The X-ray powder diffraction pattern of lead oxide

Table 3.2: The X-ray powder diffraction data for lead oxide

This Work			JCPDS	
2θ (deg)	I/I_o	d (Å)	d (Å)	I/I_o
15.03	0.18	5.89	5.89	0.05
22.02	0.05	4.03	4.02	0.01
29.10	1.00	3.06	3.07	1.00
30.35	0.71	2.94	2.95	0.24
32.63	0.66	2.74	2.74	0.22
34.22	0.05	2.62		
36.17	0.03	2.48	2.49	0.01
37.90	0.52	2.37	2.38	0.16
39.63	0.05	2.27	2.28	0.10
41.00	0.05	2.20	2.20	0.09
45.19	0.43	2.00	2.01	0.11
46.29	0.05	1.96	1.96	0.02
49.30	0.39	1.84	1.85	0.11
50.86	0.50	1.79	1.80	0.12
52.42	0.03	1.75	1.75	0.01
53.19	0.58	1.72	1.72	0.14
55.09	0.05	1.67		
56.10	0.52	1.63	1.64	0.13
57.84	0.04	1.59	1.60	0.09
60.38	0.36	1.53	1.53	0.09
61.33	0.05	1.51	1.51	0.06
63.13	0.42	1.47	1.47	0.10

3.1.4 The X-ray Powder Diffraction Pattern of 1:1 Lead Oxybromide

X-ray crystallography was used extensively in this work as a means of investigating the nature and crystal structure of the "compounds" which were formed when lead oxide and lead bromide were intimately mixed in equal molar amounts and subjected to specific heat treatment.

The X-ray powder diffraction patterns of the 1:1 lead oxybromides prepared in this work are shown in Figure 3.6 along with several patterns taken from the JCPDS library. It is evident that previous workers [1, 4, 6, 7, 9] produced a number of different crystallographic phases with equimolar amounts of lead oxide and lead bromide which they labelled as the L, N and R forms.

The X-ray powder diffraction pattern of the 1:1 lead oxybromide used in the vapour pressure experiments was not a perfect match for any of the previously reported patterns. However, this was not at all surprising; as other workers have reported different X-ray powder diffraction patterns for supposedly equivalent 1:1 lead oxybromides. Fortunately, the powder diffraction patterns of the individual phases contain characteristic features which can be used for identification.

The X-ray powder diffraction pattern of the N form of the 1:1 lead oxybromide has a single group of intense reflections at 2θ angles between 30 and 32 degrees, there are also two pairs of reflections one with components at 2θ angles of 22 and 23 degrees and the other with components at 40 and 41 degrees. In comparison the pattern of the R form of the 1:1 lead oxybromide contains a much wider band which encompasses two very striking reflections at 2θ angles of 27 and 28 degrees and a group of reflections between 30 and 32 degrees which are similar to those found in the corresponding region of the N form of the 1:1 lead oxybromide. The only other notable differences between the patterns of the N and R form of the 1:1 lead oxybromide are a doublet at 33 and 34 degrees and a triplet at 36, 37 and 38 degrees which are found exclusively in the R form.

The presence of a group of prominent reflections concentrated between 2θ angles of 30 and 32 degrees coupled with the absence of a strong doublet at 2θ angles of 27 and 28 degrees, a doublet at 33 and 34 degrees and a triplet at 36, 37 and 38 degrees indicated that the 1:1 lead oxybromide used in the vapour pressure measurements was the N form of the 1:1 lead oxybromide. Table 3.3 contains the 2θ, intensity and d spacing data obtained in this work along with the published data for the N form of the 1:1 lead oxybromide.

The precise experimental details which led to the preferential production of the N form of the 1:1 lead oxybromide in this work are given in Chapter 2. This involved the slow cooling

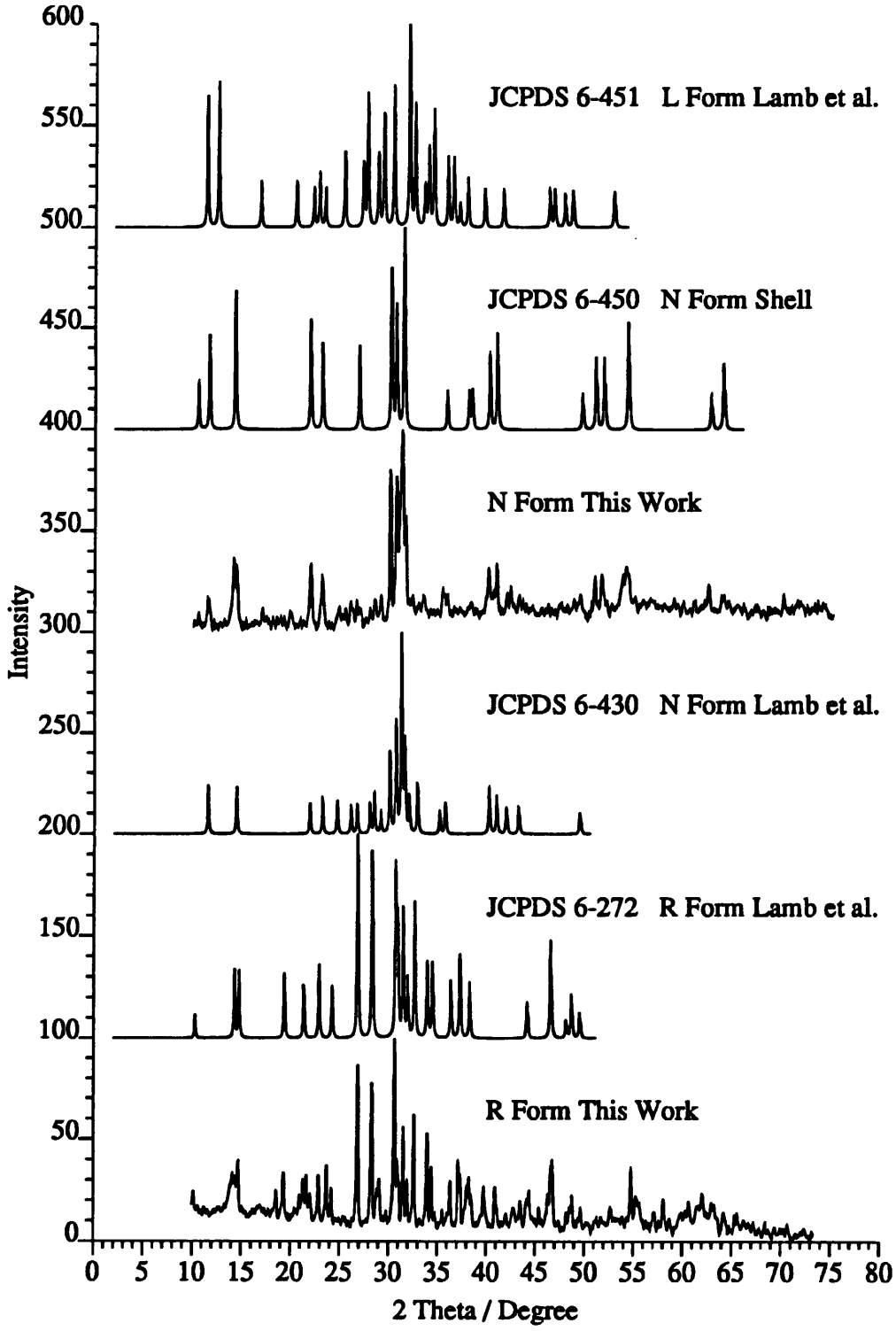

Figure 3.6: The X-ray powder diffraction pattern of 1:1 lead oxybromide

Table 3.3: The X-ray powder diffraction data for 1:1 lead oxybromide, N form

This Work			Lamb & Niebylski		Shell	
2θ (deg)	I/I_o	d (Å)	d (Å)	I/I_o	d (Å)	I/I_o
10.58	0.08	8.35			8.40	0.20
11.54	0.14	7.66	7.65	0.20	7.60	0.40
14.14	0.35	6.26			6.20	0.60
14.45	0.35	6.12	6.12	0.20		
21.98	0.34	4.04	4.05	0.14	4.05	0.50
23.13	0.24	3.84	3.83	0.16	3.84	0.40
24.72			3.60	0.15		
26.04	0.11	3.42	3.41	0.11		
26.67	0.12	3.34	3.33	0.13	3.31	0.40
28.06			3.18	0.15		
28.52	0.11	3.12	3.13	0.20		
29.14	0.15	3.06	3.06	0.10		
30.11	0.99	2.96	2.97	0.40	2.96	0.80
30.73	0.78	2.90	2.91	0.55	2.91	0.60
31.04	0.54	2.88				
31.31	1.00	2.85	2.86	1.00		
31.67	0.61	2.82	2.83	0.43	2.84	1.00
31.98	0.10	2.79	2.79	0.18		
32.34	0.10	2.76	2.72	0.25		
33.50	0.10	2.67				
35.44	0.15	2.53	2.55	0.10		
35.69	0.13	2.51	2.51	0.15	2.50	0.20
35.95	0.12	2.49				
38.13					2.36	0.20
38.47					2.34	0.20
40.18	0.27	2.24	2.24	0.25	2.24	0.40
40.42	0.08	2.23				
40.66	0.13	2.21				
41.00	0.30	2.20	2.20	0.20	2.20	0.50
42.01	0.10	2.15	2.15	0.13		
42.42	0.15	2.13				
43.29			2.09	0.13		
49.54			1.84	0.12	1.833	0.20
50.98	0.18	1.79			1.79	0.40
51.73	0.17	1.76			1.76	0.40
53.87	0.19	1.70				
54.18	0.22	1.69				
54.44	0.17	1.68			1.686	0.60
62.60	0.12	1.48			1.478	0.20
64.13					1.452	0.12

of a melt (above 497 °C) of an equimolar mixture of lead bromide and lead oxide. The R form of the 1:1 lead oxybromide was also prepared in this work when a 1:1 mixture of lead bromide and lead oxide was heated to 400 °C and then cooled slowly. This temperature dependence of the R and N forms of the 1:1 lead oxybromide has been confirmed by Differential Thermal Analysis, See Section 3.2.3. Table 3.4 compares the 2θ, relative intensity and d spacing data for the R form of the 1:1 lead oxybromide prepared here, with that of previous workers. The intensity data from the laboratories at Shell was not available in absolute form, so the visual estimates are presented instead.

The N form and the R form of the 1:1 lead oxybromide were the only phases produced in the course of the present study. The powder diffraction patterns of the phases resulting from other thermal treatments were found to be mixtures of the N and R form of the 1:1 lead oxybromide and the 2:1 lead oxybromide (discussed later). The results from the Differential Thermal Analysis and X-ray powder diffraction studies show just how sensitive the system is to variations in sample preparation and explain why, up until now, the published discussions of this phase system are confusing.

In the present work the phases were prepared in a sealed container which prevented loss of lead bromide by evaporation and rendered the atmospheric oxidation of the reactants insignificant. Previous workers appear to have prepared their phases in open vessels in the presence of an unlimited supply of air; the high temperatures and long reaction times undoubtedly led to considerable changes in the composition of their samples through the evaporation and oxidation of lead bromide. Hyde [2] has stressed the likelihood of considerable oxidation of lead bromide in air at temperatures around 327 °C, while, Julien and Ogilvie [4] observed considerable changes in sample composition due to evaporation, when studying the lead oxyhalides at elevated temperatures. They were unable to obtain reproducible results under such conditions and this serves to further underline the importance of using sealed reaction vessels to prepare the lead oxyhalides.

The earliest comprehensive description of the system was provided by Lamb and Niebylski [7]. This work was carried out in conjunction with a thermal analysis study of the phase system by Knowles [5]. The L form of the 1:1 lead oxybromide was produced by the thermal decomposition / dehydration of $PbO.PbBr_2.H_2O$, which had been precipitated from an aqueous solution of lead bromide with ammonium hydroxide.

Lamb and Niebylski reported that heating the hydrate at temperatures between 125 and 210 °C resulted in the formation of the L form of the 1:1 lead oxybromide and its X-ray diffraction pattern is shown in Figure 3.6. The L form was reported to convert to the N form at temperatures between 210 and 260 °C which in turn was converted to the R form at temperatures between 260 and 450 °C. Finally, the R form was reputed to return to

Table 3.4: The X-ray powder diffraction data for 1:1 lead oxybromide, R form

This Work			Shell		Lamb & Niebylski	
2θ (deg)	I/I_o	d (Å)	d (Å)	I/I_o	d (Å)	I/I_o
10.19	0.24	8.67	8.70	m	8.61	0.10
10.66			8.30	vw		
14.20	0.23	6.23			6.20	0.30
14.40			6.15	w		
14.76			6.00	ms	6.00	0.30
18.67	0.24	4.75				
19.42	0.34	4.57	4.58	ms	4.58	0.30
20.39	0.16	4.35	4.33	vw		
21.08	0.22	4.21				
21.37	0.30	4.16	4.16	m	4.16	0.25
21.71	0.31	4.09				
22.05	0.23	4.02				
22.91	0.32	3.88	3.88	ms	3.88	0.35
23.60	0.36	3.76				
24.17	0.25	3.68	3.67	m	3.67	0.26
26.98	0.86	3.30	3.31	vs(1)	3.32	1.00
28.36	0.77	3.14	3.15	vs(2)	3.15	0.95
28.87	0.25	3.09				
29.16	0.30	3.06				
29.79	0.14	2.99				
30.82	1.00	2.90	2.92	s (3)	2.91	0.87
31.00	0.39	2.88	2.88	m	2.89	0.55
31.57	0.56	2.83	2.84	ms	2.84	0.65
32.08	0.30	2.79	2.80	m	2.80	0.31
32.71	0.62	2.74	2.74	s	2.74	0.68
33.97	0.52	2.64	2.65	ms	2.64	0.38
34.43	0.36	2.60	2.60	ms	2.60	0.42
35.58	0.15	2.52	2.53	vw		
36.38	0.29	2.47	2.472	m	2.47	0.30
37.18	0.38	2.42	2.42	m		
37.29	0.31	2.41			2.41	0.46
38.10	0.27	2.36	2.355	m		
38.33	0.31	2.34				
38.50	0.22	2.33			2.35	0.29
39.82	0.26	2.26				
40.90	0.26	2.20				
42.74	0.16	2.11				
43.43	0.19	2.08				
44.40	0.24	2.03	2.04	w	2.05	0.22
45.32	0.16	2.00				
46.29	0.23	1.96				
46.52	0.36	1.95	1.948	m	1.95	0.56
46.86	0.39	1.93				
48.12	0.13	1.89			1.89	0.10
48.41	0.16	1.88				
48.75	0.22	1.86	1.870	mw	1.87	0.24
49.56	0.15	1.83			1.84	0.15
54.77	0.35	1.67	1.676	m		
55.23	0.22	1.66	1.656	mw		

the N form at temperatures above 450 °C.

Julien and Ogilvie [4] claimed that the R form of the 1:1 lead oxybromide is its ONLY stable form and attributed the other phases reported by Lamb and Niebylski to differing quantities of water of hydration! In the present work, the N form of the 1:1 lead oxybromide was prepared from dried starting materials in a sealed crucible and an inert atmosphere; clearly the N form is not a hydrated R form. Julien and Ogilvie fail to give precise experimental details and it is conceivable that they did not heat the samples to temperatures in excess of the melting point of the 1:1 lead oxybromide (497 °C). In the present work such constraints led to the preferential formation of the R form of the 1:1 lead oxybromide.

Shell [9] reported that the N form was produced by "fusion" of stoichiometric quantities of lead oxide and lead bromide, whereas the R form was produced by heating stoichiometric quantities of lead oxide and lead bromide at 300 °C for 16 hours. This relationship between temperature and the nature of the product agrees with the findings of the present work.

There has been considerable disagreement over the exact stoichiometry of the N and R forms of the 1:1 lead oxybromide, indeed Davies, Garner and Caddock [1] clearly had great difficulty in settling upon a single value for either form. The variations were probably due to changes in sample composition, which are to be expected when the phases are prepared in open vessels in the presence of air. The use of a sealed reaction vessel and the added precaution of an inert atmosphere in the present work prevented compositional changes in the samples, so that the precise amount of lead oxide and lead bromide in the product is known.

The present study did not provide any evidence to suggest that the actual stoichiometry of the N form of the 1:1 lead oxybromide is anything other than 1:1. The X-ray powder diffraction patterns did not indicate the presence of free lead oxide or lead bromide in the products, and the severe difficulties encountered in the accurate determination of the concentrations of lead oxide and lead bromide in "known mixtures" by Quantitative Micro Analysis showed that such data cannot be used to obtain the exact stoichiometry. The safest option is to assign a simple stoichiometry of 1:1 to the N form of this lead oxybromide.

In contrast, the X-ray powder diffraction pattern of the R form of the 1:1 lead oxybromide prepared here undoubtedly contains a subset of reflections which suggest that the sample contains free lead bromide. This is shown by Figure 3.7 which gives the two diffraction patterns. The subset of reflections is an excellent match for those of pure lead bromide in both intensity and position, but there is no evidence of free lead oxide in the sample. Thus,

N Form of the 1:1 Lead Oxybromide

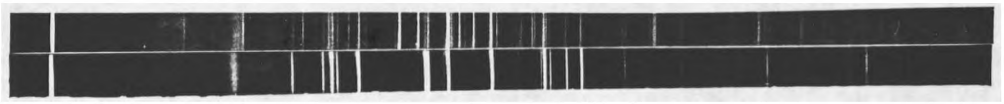

Lead Bromide

Figure 3.7: The X-ray powder diffraction pattern of lead bromide and the R form of 1:1 lead oxybromide

assuming that all of the lead oxide has been used up, and given that the starting material contained equimolar quantities of lead oxide and lead bromide, free lead bromide can only be present in the product if it contains less lead bromide (per mole) than it does lead oxide. This is the opposite conclusion to that of Davies *et al.* who proposed $4PbO.5PbBr_2$, but, they prepared their samples in open crucibles using reaction time in excess of 16 hours. In order to compensate for the evaporation losses during this period an initial excess of lead bromide would have been required and this may explain the discrepancy.

The level of confusion surrounding the 1:1 lead oxybromide and the various crystallographic modifications is typified by the JCPDS library pattern for the N form of the 1:1 lead oxybromide. The reported diffraction pattern is identical to that in the Shell publication but has the associated chemical formula $Pb_5O_2Br_2$! this is clearly an error. There is another error in the computerised crystallographic database at the Daresbury laboratory where one of the entries refers to data published by Julien and Ogilvie [4] for the 1:1 lead oxybromide, but this relates to their 2:1 lead oxybromide.

An X-ray powder diffraction pattern of a sample of the N form of the 1:1 lead oxybromide prepared in the early stages of this work was obtained also several years later using an advanced diffractometer (Scintag XDS2000). The intensity of the broad low angle reflection discussed earlier in this section was greatly reduced and the resulting pattern contained a few reflections which were not present in the pattern obtained with the Guinier camera, although much of the original pattern was still visible (see Figure 3.8). The new reflections did not correspond to those of any of the other phases prepared in this work, or to any found in the library patterns indicating that the sample had undergone some changes, although their precise nature is not clear.

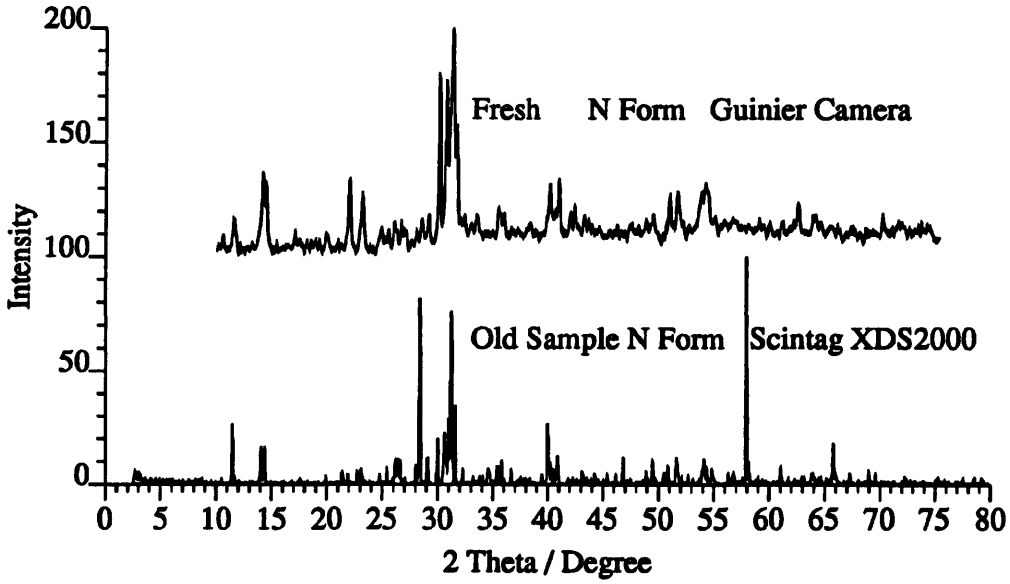

Figure 3.8: The X-ray diffraction pattern of the N form of 1:1 lead oxybromide, Guinier camera (fresh sample) and (old sample) Scintag XDS2000 diffractometer

3.1.5 The X-ray Powder Diffraction Pattern of 2:1 Lead Oxybromide

The X-ray powder diffraction pattern of the 2:1 lead oxybromide which was used in the vapour pressure measurements was taken using the Guinier camera described earlier. The pattern for a sample prepared in this work was obtained several years later with the XDS2000 diffractometer described in Section 3.1.4 and the results were remarkably similar. The only notable differences were a slight increase in the intensity of the reflection corresponding to a 2θ angle of approximately 28 degrees and the absence of the broad reflection discussed in Section 3.1.2 at a 2θ angle of approximately 14 degrees. The disappearance of this enigmatic reflection suggests that it was an artifact of the Guinier camera or sample holder, although it is possible (but seems unlikely) that the sample had altered.

The X-ray powder diffraction patterns of the 2:1 lead oxybromide obtained here are shown in Figure 3.9 along with several patterns taken from the JCPDS library. It is evident from this figure that previous workers [1, 4, 6, 7, 9] obtained essentially similar diffraction patterns. There are several prominent features which are visible in all of the patterns and it appears that the 2:1 lead oxybromide occurs predominantly in one crystalline form irrespective of the conditions under which it is prepared.

The patterns obtained in this work are in best agreement with that published by the National Bureau of Standards, although the pattern obtained on the Scintag diffractometer

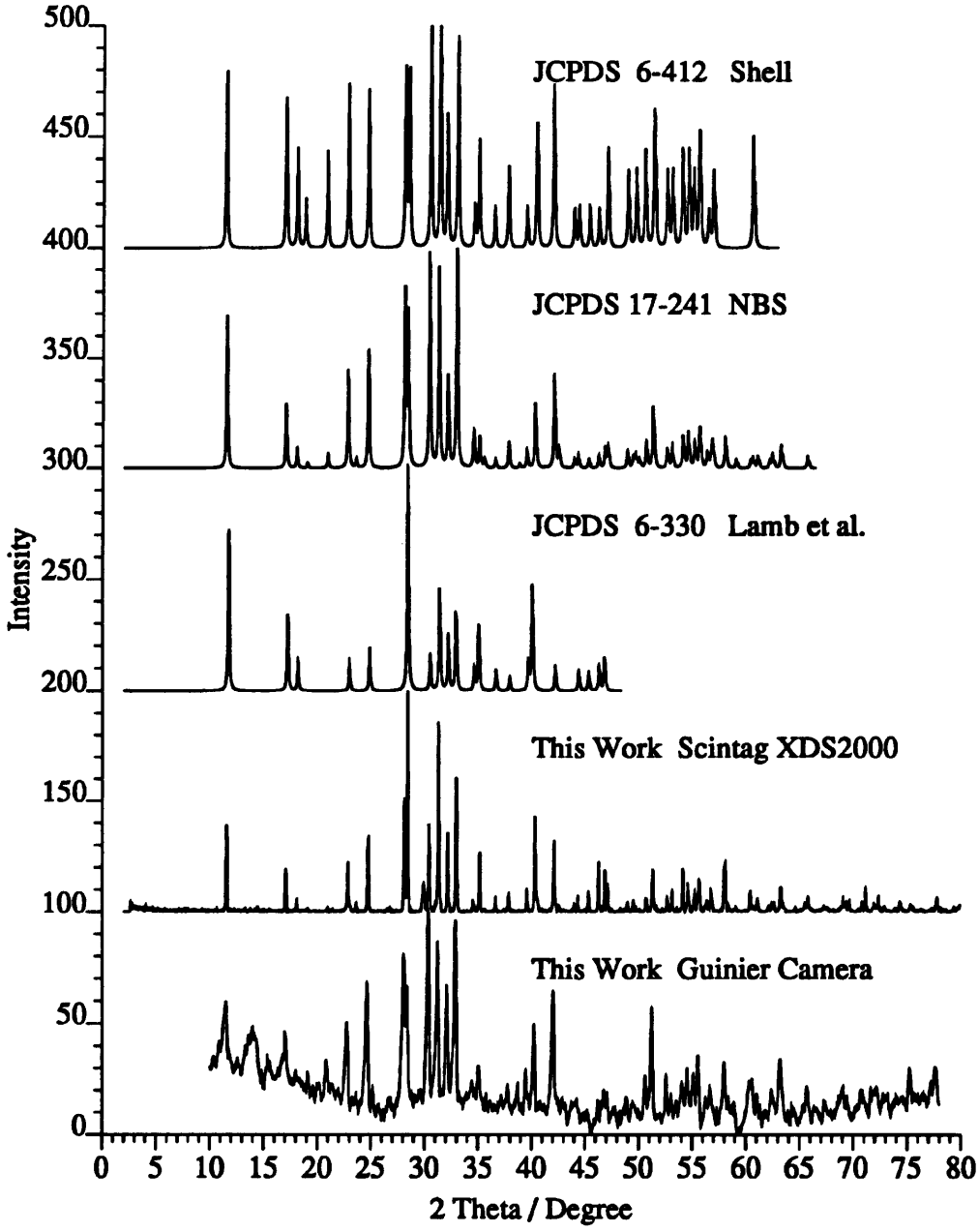

Figure 3.9: The X-ray powder diffraction pattern of 2:1 lead oxybromide

Table 3.5: The X-ray powder diffraction data for 2:1 lead oxybromide

This Work			Shell		Lamb & Niebylski		NBS	
2θ (deg)	I/I_o	d (Å)	d (Å)	I/I_o	d (Å)	I/I_o	d (Å)	I/I_o
11.47	0.60	7.71	7.70	0.70	7.55	0.59	7.67	0.55
13.90	0.48	6.37						
14.31	0.43	6.19						
17.03	0.45	5.21	5.20	0.60	5.15	0.30	5.20	0.25
18.10			4.90	0.40	4.88	0.12	4.91	0.08
18.88			4.70	0.20			4.66	0.02
20.83	0.33	4.26	4.25	0.40			4.241	0.06
22.73	0.51	3.91	3.89	0.70	3.87	0.11	3.895	0.40
23.59							3.771	0.04
24.60	0.68	3.62	3.60	0.70	3.58	0.17	3.600	0.50
28.04	0.80	3.18	3.17	0.80	3.14	1.00	3.172	0.75
28.36	0.67	3.15	3.13	0.80			3.139	0.65
30.33	1.00	2.95	2.93	1.00	2.93	0.16	2.937	0.95
31.19	0.87	2.87	2.85	1.00	2.85	0.45	2.857	0.90
32.06	0.67	2.79	2.79	0.60	2.78	0.24	2.783	0.40
32.88	0.96	2.72	2.71	1.00	2.72	0.35	2.715	1.00
34.42	0.23	2.61	2.59	0.20	2.59	0.10	2.597	0.10
34.61							2.591	0.10
35.06	0.32	2.56	2.56	0.50	2.56	0.29	2.554	0.14
34.88							2.572	0.04
36.52			2.46	0.20	2.45	0.10	2.454	0.04
37.76	0.22	2.38	2.38	0.40	2.37	0.06	2.376	0.12
38.72	0.23	2.33	2.28	0.20			2.317	0.02
39.47	0.30	2.28			2.27	0.14	2.278	0.08
40.24	0.50	2.24	2.23	0.80	2.25	0.47	2.236	0.30
42.02	0.64	2.15	2.15	0.80	2.14	0.11	2.145	0.45
42.91	0.16	2.11					2.124	0.08
43.70	0.13	2.07	2.06	0.20			2.058	0.04
44.01	0.14	2.06	2.04	0.20	2.04	0.09	2.042	0.06
45.14	0.10	2.01	1.998	0.20	2.00	0.08	2.000	0.04
46.20	0.16	1.96	1.963	0.20	1.96	0.12	1.962	0.06
46.54	0.18	1.95			1.94	0.15	1.938	0.10
46.78	0.20	1.94	1.931	0.50			1.927	0.10
47.04	0.21	1.93	1.861	0.40			1.861	0.08
47.64	0.10	1.91					1.842	0.06
48.87	0.17	1.86	1.834	0.40			1.833	0.06
49.45	0.15	1.84					1.822	0.04
50.60	0.26	1.80	1.806	0.50			1.800	0.12
51.23	0.58	1.78	1.778	0.70			1.779	0.30
52.55	0.26	1.74	1.740	0.40			1.738	0.10
53.51	0.16	1.71	1.725	0.40			1.724	0.10
54.02	0.24	1.70	1.698	0.50			1.694	0.16
54.52	0.30	1.68	1.681	0.50			1.680	0.18
55.10	0.28	1.67	1.667	0.40			1.663	0.14
55.53	0.36	1.65	1.653	0.60			1.650	0.20
56.25	0.18	1.64	1.630	0.20			1.631	0.08
56.69	0.21	1.62					1.621	0.08
57.98	0.33	1.59					1.5878	0.16
58.92	0.15	1.57					1.5637	0.04
60.32	0.22	1.53					1.5314	0.04
61.02	0.18	1.52	1.528	0.60			1.5265	0.04
62.47	0.18	1.49					1.5167	0.06
63.18	0.34	1.47					1.4921	0.04
64.43	0.12	1.45					1.4865	0.06
65.34	0.13	1.43					1.4694	0.12
65.64	0.12	1.42					1.4200	0.06

is in many ways similar to that of Lamb and Niebylski. The later pattern does not contain any reflections above a 2θ angle of approximately 47 degrees, but this data may simply have been omitted because of the number and faintness of the lines.

In the present work the 2:1 lead oxybromide was prepared by the slow cooling of a molten mixture of lead oxide and lead bromide from approximately 750 °C. When a 2:1 mixture of lead oxide and lead bromide was heated to a temperature below 350 °C a phase was produced which was not the 2:1 lead oxybromide. Examination of the diffraction pattern revealed the presence of the R form of the 1:1 lead oxybromide and lead oxide, the patterns are shown in Figure 3.10 along with the pattern for lead bromide. The diffraction pattern of lead bromide is included in the figure because in this work the R form of the 1:1 lead oxybromide was not prepared free from lead bromide impurity; this must be taken into account when comparisons are drawn between the patterns.

3.1.6 The X-ray Powder Diffraction Pattern of 3:1 Lead Oxybromide

The vapour pressures of the 3:1 and 7:1 lead oxybromides were not measured in this study, but the X-ray powder diffraction patterns were used to characterise the contents of the baskets at the end of the vapour pressure experiments.

The X-ray powder diffraction pattern of the 3:1 lead oxybromide prepared in this work is shown in Figure 3.11 along with related entries from the JCPDS library. The 3:1 lead oxybromide also exists in more than one crystalline form, previously designated D and E by Lamb and Niebylski and α and δ by Shell. An ϵ form has been reported by Shell but attempts to prepare samples in the laboratory have failed, and the only evidence for its existence comes from the analysis of the deposits from an automobile engine. Although the published diffraction patterns of each of these phases agree to some extent, it would be audacious to suggest that they are consistent. Thus, it is not surprising that the diffraction pattern obtained in this work does not match any of them exactly. Nevertheless, it clearly resembles the E (or δ) form and the D (or α) form was not prepared in this work. It is possible that it is a composite of the two forms, but this is difficult to establish due to the variation which exists in the published patterns.

The description of the temperature dependence of each phase provided by Lamb and Niebylski explains the present results. In this study the product was formed by allowing the molten sample to cool slowly to room temperature. Lamb and Niebylski found that the E form of the 3:1 lead oxybromide was produced when a molten sample was cooled slowly to below 695 °C and quenched. In contrast quenching the molten mixture gave the D form. They also found that the D form was produced upon quenching a molten sample

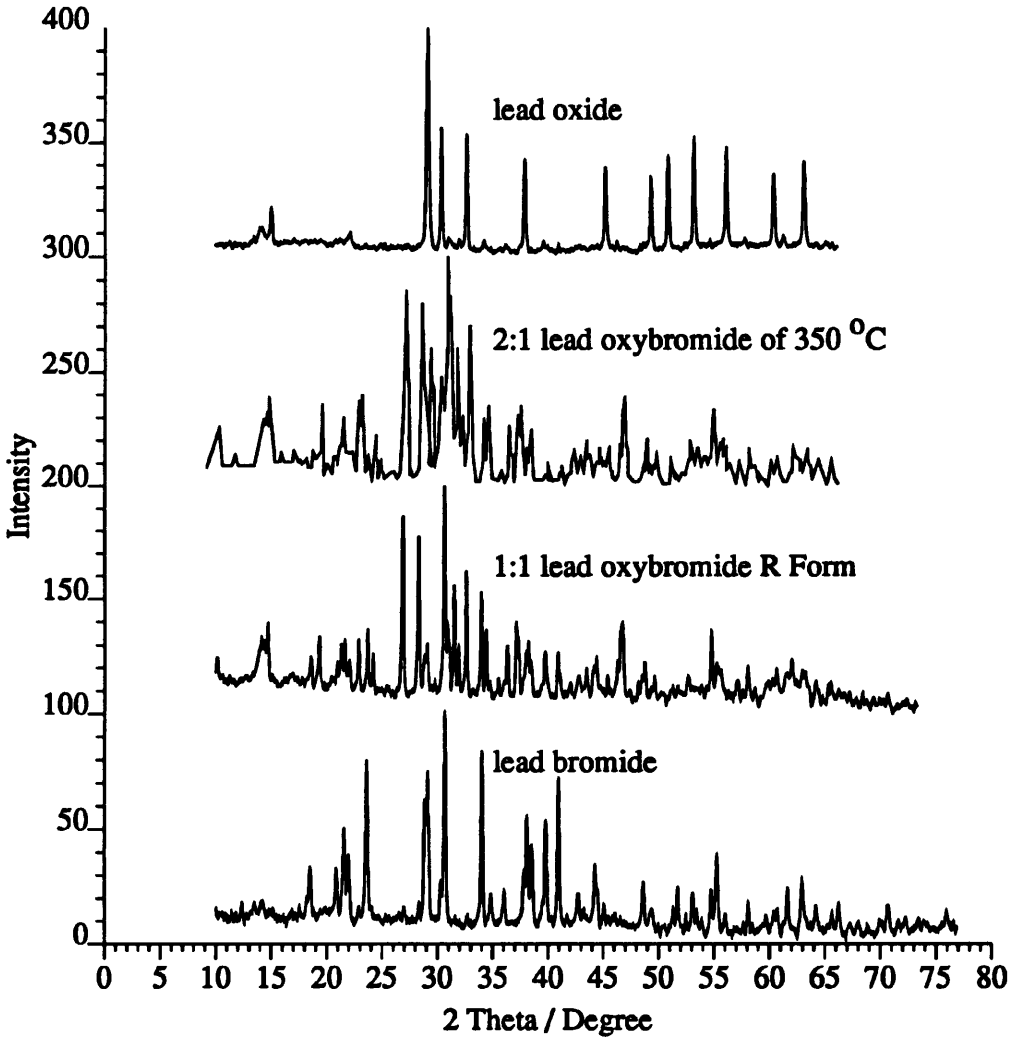

Figure 3.10: The X-ray powder diffraction pattern of 2:1 lead oxybromide formed at temperatures below 350 °C

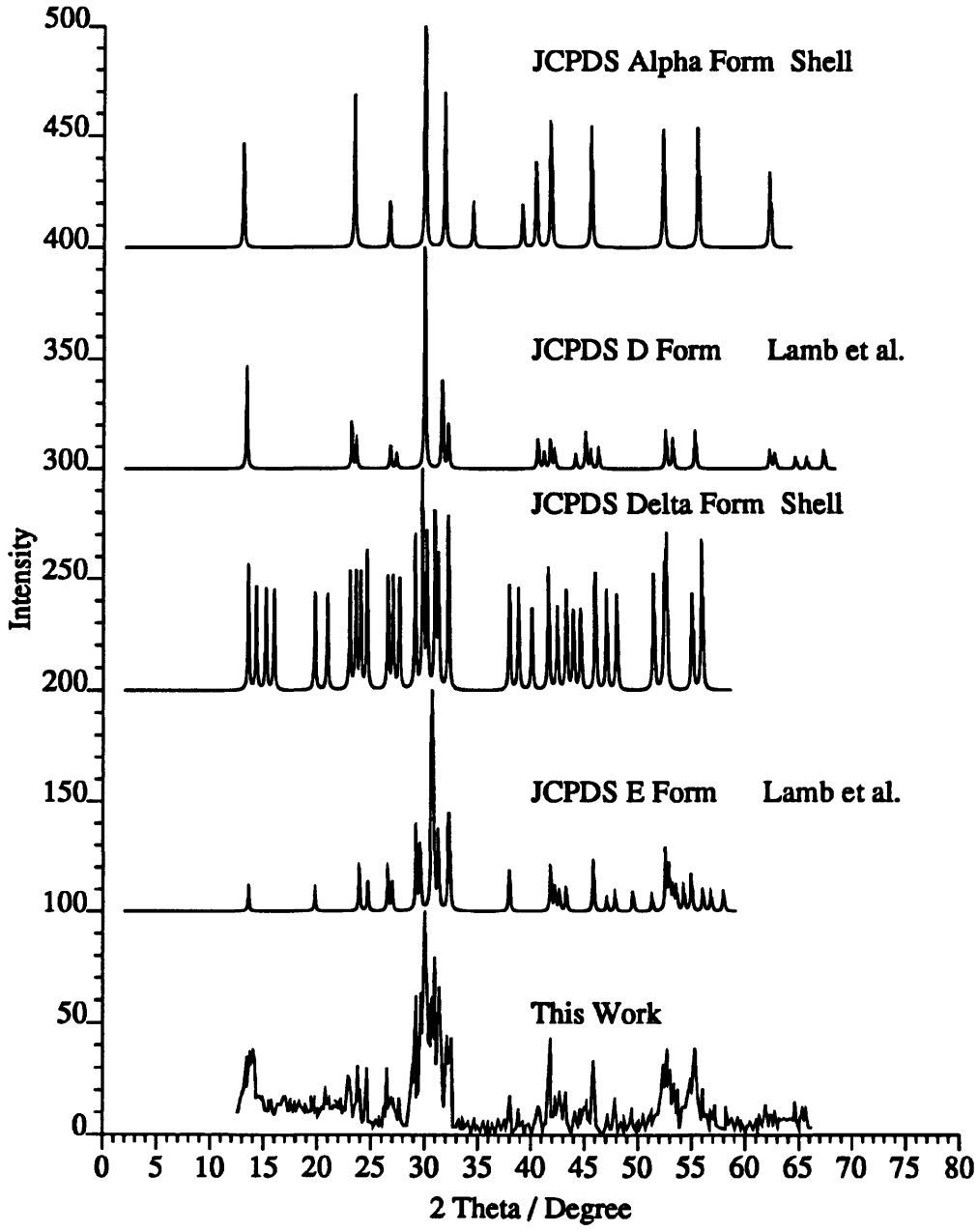

Figure 3.11: The X-ray powder diffraction pattern of 3:1 lead oxybromide

containing 72 mole % lead oxide.

The experimental details regarding the preparation of the α and δ forms of the 3:1 lead oxybromide, which appear in the Shell publication, are confusing. It is suggested that the α form may be produced either by heating $3PbO.PbBr_2$ hydrate to 250 °C or alternatively by rapidly cooling a fused mixture of lead bromide and lead oxide, although the latter method may produce a mixture of the lead oxybromides. Sadly, the recommended method of producing the δ form is the same as the latter method for producing the α form! It is suggested that if a mixture of the 3:1 lead oxybromides results, then the individual crystals of each be separated by virtue of the variation in colour!

3.1.7 The X-ray Powder Diffraction Pattern of 7:1 Lead Oxybromide

Of the lead oxybromides studied in this work the X-ray powder diffraction pattern of the 7:1 lead oxybromide had the most pleasing appearance, it contained relatively few lines and they were nicely distributed. Apart from this aesthetic quality the X-ray powder diffraction pattern of the 7:1 lead oxybromide was of little significance to this work.

The stoichiometry of 7:1 proposed by Lamb and Niebylski is disputed and the authors of the Shell publication prefer the ratio 6:1. However, both parties agree that two forms of this lead oxybromide exist. Lamb and Niebylski christened them the Q and T forms and Shell refer to them as α and β. The phase produced in this work with a stoichiometry of 7:1 was clearly the T or β form. Table 3.6 contains the 2θ, d spacing and intensity data obtained in this work and that of other workers.

3.1.8 The X-ray Powder Diffraction Pattern of Lead Chloride

The 2θ, d spacing and intensity data for the lead chloride used in this work are compared with the published data in Table 3.7 and the agreement is excellent.

3.1.9 The X-ray Powder Diffraction Pattern of 1:1 Lead Oxychloride

The 1:1 lead oxychloride is known to exist in a number of polymorphic forms [6]. Two of these (L and N) are isomorphous with the L and N forms of the 1:1 lead oxybromide but the remaining M form has no corresponding phase. The alternative formula $2PbO.3PbCl_2$ has been reported for the N form of the 1:1 lead oxychloride [9]. Which of the two stoichiometries is most accurate is difficult to ascertain as the samples were prepared in

Table 3.6: The X-ray powder diffraction data for 7:1 lead oxybromide

This Work			7:1 T Form, Lamb & Niebylski		6:1 β Form, Shell	
2θ (deg)	I/I_o	d (Å)	d (Å)	I/I_o	d (Å)	I/I_o
8.32					10.63	0.06
8.54	0.20	10.36	10.4	0.20	10.35	0.07
8.71					10.15	0.08
14.76			6.00	0.20	6.08	0.06
14.90	0.15	5.95	6.00	0.20	5.97	0.06
20.05	0.08	4.43	4.45	0.20		
20.91	0.14	4.25	4.24	0.40		
22.63	0.15	3.93	3.90	0.40	3.91	0.17
24.92	0.12	3.57	3.56	0.20		
27.97			3.19	0.10		
29.22	0.99	3.06	3.06	0.80	3.06	0.17
29.91	1.0	2.99	2.99	1.00	2.99	0.22
31.17	0.98	2.87	2.87	0.80	2.87	1.00
31.80	0.22	2.81	2.79	0.40		
33.40	0.09	2.68				
35.29	0.07	2.54				
37.93	0.08	2.37			2.37	0.06
39.76	0.45	2.27	2.268	0.60		
40.64			2.220	0.20		
42.28	0.10	2.14	2.132	0.10		
43.66	0.28	2.07	2.071	0.60	2.07	0.24
45.49	0.29	1.99	1.993	0.40	1.99	0.24
46.29	0.11	1.96	1.963	0.20	1.96	0.03
48.82	0.06	1.86			1.86	0.02
50.53	0.05	1.81				0.03
51.34	0.52	1.78	1.778	0.70	1.73	0.15
53.74	0.54	1.71	1.705	0.70	1.71	0.15
55.06	0.51	1.67	1.669	0.70	1.67	0.13
55.96			1.643	0.60		
58.49			1.578	0.10	1.58	0.04
60.62	0.06	1.53	1.531	0.20		
61.99	0.08	1.50	1.498	0.40		
65.03	0.07	1.43	1.439	0.40	1.44	0.20
72.10					1.31	0.10
74.75					1.27	0.15

Table 3.7: The X-ray powder diffraction data for lead chloride

This Work			Shell	
2θ (deg)	I/I_o	d (Å)	d (Å)	I/I_o
19.71	0.25	4.50	4.52	m
22.00	0.51	4.04	4.04	ms
22.92	0.82	3.88	3.88	s(2)
23.38	0.48	3.80	3.80	ms
24.92	1.00	3.57	3.57	vs(1)
30.42	0.18	2.94	2.92	mw
30.80	0.48	2.90		
32.37	0.81	2.77	2.77	s(3)
35.87	0.79	2.50	2.50	ms
37.87	0.16	2.38		
39.88	0.47	2.26	2.262	ms
40.91	0.45	2.21	2.212	ms
41.83	0.18	2.16		
42.11	0.90	2.15	2.151	ms
43.32	0.80	2.09	2.096	ms
44.92	0.20	2.02		
46.47	0.45	1.95	1.953	s
46.75	0.44	1.94		
47.90	0.15	1.90	1.910	w
51.22	0.23	1.78	1.789	w
54.49	0.19	1.68	1.684	vw
56.15	0.33	1.64	1.641	m
57.70	0.19	1.60		
58.33	0.37	1.58	1.584	m
59.01	0.20	1.57		
61.02	0.20	1.52	1.516	w
61.42	0.12	1.51		
62.91	0.13	1.48		
63.48	0.14	1.47		
63.71	0.15	1.46	1.457	w
64.46	0.12	1.45		
65.32	0.27	1.43	1.424	mw
66.58	0.35	1.40	1.401	m

the same manner as the 1:1 lead oxybromide (see Section 3.1.4) and are subject to the same sources of error.

The correlation between the X-ray powder diffraction pattern of the 1:1 lead oxychloride prepared for use in vapour pressure experiments and the reported data for the N form of the 1:1 lead oxychloride was excellent. The 2θ, intensity and d spacing values are presented in Table 3.8 along with two sets of previously published values.

3.1.10 The X-ray Powder Diffraction Pattern of 2:1 Lead Oxychloride

The X-ray powder diffraction pattern of the 2:1 lead oxychloride prepared for use in vapour pressure experiments was very surprising, as each line on the photograph was a doublet! Closer inspection revealed that the spacing between the two lines of each reflection increased with 2θ. In addition the two lines in each doublet were of different intensities, with the line to the higher values of 2θ the less intense. There are two known causes of such a pattern, namely line doubling due to absorption and line doubling due to resolution of multiple frequency incident radiation.

The former is most likely with longer wavelength radiation and occurs when a very thick or heavily absorbing sample is used. The X-ray beam is absorbed in the region in which the sample is thickest and in some cases the centre of the diffraction line is removed. The splitting of the lines is also most pronounced at low 2θ angles where the X-ray beam passes the greatest distance through the sample, so that the splitting decreases with increasing glancing angle. Thus, this explanation does not account for the present observation.

The second cause of line doubling is a direct result of using non-monochromatic radiation. As described in Section 3.1.1, X-ray generators used in X-ray powder diffraction studies often produce a collimated beam of radiation containing two slightly different wavelengths and normally these two wavelengths are unresolved. However, in certain cases with almost perfect crystalline material these two wavelengths can be resolved. The line spacing of each doublet increases with increasing 2θ angle, precisely the effect observed here.

In the powder diffraction pattern of the 2:1 lead oxychloride the intensity of the lower angle reflection of each doublet was more intense than its counterpart. The $K\alpha_1$ and $K\alpha_2$ frequency radiation are produced with unequal intensities from a single X-ray source and the ratio of the intensities and the magnitude of the line splitting observed here were of the expected order. This reinforced the conclusion that the line splitting resulted from resolved $K\alpha_1$ and $K\alpha_2$ radiation.

Table 3.8: The X-ray powder diffraction data for 1:1 lead oxychloride

This Work			1:1 N form, Lamb & Niebylski		Shell	
2θ (deg)	I/I_o	d (Å)	d (Å)	I/I_o	d (Å)	I/I_o
10.17					8.7	vvw
11.06					8.0	w
11.97	0.33	7.39	7.40	0.80	7.41	w
14.90	0.54	5.95	6.00	0.40	5.96	ms
20.40	0.30	4.35			4.30	w
22.69	0.56	3.92	3.94	0.30	3.93	m
23.43	0.32	3.80	3.74	0.40	3.74	s
23.89	0.58	3.72			3.58	vw
25.38	0.33	3.51	3.52	0.25		
25.90	0.33	3.44	3.46	0.20	3.45	vw
26.87	0.38	3.32	3.33	0.25	3.33	w
27.56	0.27	3.24	3.24	0.30	3.21	w
27.96	0.23	3.19	3.10	0.25		
28.99	0.31	3.08	3.04	0.50		
29.45	0.24	3.03				
30.02	0.24	2.98	2.98	0.20		
30.65	0.93	2.92	2.92	0.35	2.91	s
31.86	0.80	2.81	2.81	0.60		
32.20	1.00	2.78	2.79	1.00	2.79	vs
32.77	0.72	2.73	2.74	0.60	2.74	vs
33.00	0.27	2.71	2.71	0.30		
33.86	0.31	2.65	2.65	0.30		
36.78	0.29	2.44	2.43	0.30	2.445	vw
41.25	0.27	2.19			2.188	mw
41.65	0.36	2.17	2.17	0.25		
42.28	0.37	2.14	2.14	0.25	2.134	mw
43.14	0.34	2.10	2.10	0.20		
43.54	0.29	2.08			2.085	m
45.21	0.28	2.01	2.02	0.25	2.008	m
46.32					1.961	w
49.56	0.18	1.84				
50.13	0.25	1.82	1.82	0.15		
50.76	0.30	1.80			1.802	w
51.80	0.16	1.76				
53.29	0.28	1.72			1.728	m
54.42					1.686	vw
55.58	0.48	1.65			1.652	m
57.12	0.28	1.61				

In the course of this work the 2:1 lead oxychloride was the only sample which produced this surprising effect and the method used to determine the 2θ and d spacing values of the other samples was inappropriate in this case. Instead the position of the most intense line of each doublet was recorded and the wavelength of $K\alpha_1$ radiation was used in the calculations. The results are compared in Table 3.9 with the previously published data and the correlation with the results from Shell is clearly very good. In contrast, the agreement with the results of Lamb and Niebylski is poor, the experimental conditions appear to be the same in all cases and there is no obvious explanation for the discrepancy.

3.2 Thermal Analysis

The thermal behaviour of mixtures of lead oxide and lead bromide has been studied by Differential Thermal Analysis. The aim of the thermal analysis was to ensure that formation of the lead oxybromides used in the vapour pressure experiments was complete. It has also been used along with the X-ray crystallographic data, to provide a clear picture of the behaviour of the lead oxide / lead bromide system.

The melting point and enthalpy of fusion of lead bromide was determined by Differential Scanning Calorimetry (DSC), while the temperatures at which the mixed lead oxide and lead bromide samples underwent visible changes were determined with a hot stage microscope.

3.2.1 The Thermal Analysis of Lead Bromide

The purity of the lead bromide used in this work was confirmed by Differential Scanning Calorimetry (DSC), the instrument used was a Dupont 1090. The sample was contained in a sealed aluminium crucible and heated to 440 °C at 10 °C min^{-1}. The melting point was found to be 370.3 °C which agrees with the accepted value of 370.2 °C. The enthalpy of fusion was estimated to be 10.6 kJ mol^{-1} which was somewhat lower than the most recent experimentally determined value [8] of 16.4 kJ mol^{-1}. The aluminium crucible which contained the sample during the experiment was not attacked by the lead bromide in the relatively short duration of the experiment.

Table 3.9: The X-ray powder diffraction data for 2:1 lead oxychloride

This Work			2:1 Lamb & Niebylski		2:1 Shell	
2θ (deg)	I/I_o	d (Å)	d (Å)	I/I_o	d (Å)	I/I_o
11.90	0.50	7.43			7.41	ms
12.11			7.31	0.81		
17.62	0.27	5.03	4.97	0.27	5.02	m
18.69	0.12	4.74	4.70	0.12	4.76	w
19.43	0.19	4.56			4.57	w
21.45	0.41	4.14			4.13	m
23.38	0.63	3.80	3.77	0.18	3.80	ms
25.42	0.90	3.50	3.48	0.25	3.50	s
28.86	0.80	3.09	3.08	0.28	3.10	ms
29.34	0.82	3.04	3.05	1.0	3.03	ms
30.83	1.00	2.90	2.89	0.25	2.90	s
32.20	0.84	2.78	2.78	0.75	2.78	s
33.08	0.65	2.71	2.70	0.27	2.71	m
33.92	0.94	2.64	2.64	0.48	2.64	s
35.66	0.29	2.52	2.51	0.11	2.52	w
36.33	0.36	2.47	2.48	0.26	2.465	w
37.87	0.27	2.37	2.37	0.20	2.380	w
38.98	0.27	2.31			2.309	w
39.68	0.23	2.27	2.21	0.14	2.206	w
41.71	0.51	2.16	2.17	0.71	2.163	m
43.13	0.97	2.10			2.099	s
44.63	0.18	2.03	2.10	0.31	2.012	mw
46.12	0.26	1.97	1.98	0.15	1.975	mw
46.96	0.29	1.93	1.94	0.09	1.937	w
47.18	0.23	1.92				
47.93	0.27	1.90				
48.55	0.39	1.87	1.88	0.34	1.875	m
49.79	0.30	1.83			1.838	w
50.62	0.50	1.80			1.806	mw
51.73	0.39	1.77			1.771	w
52.81	0.65	1.73			1.737	ms
53.70	0.44	1.71			1.711	w
55.05	0.26	1.67			1.671	vw
55.86	0.44	1.64			1.645	ms
56.09	0.61	1.64				
56.28	0.50	1.63				
57.16	0.55	1.61			1.616	ms
57.40	0.37	1.60				
60.14	0.56	1.54				

3.2.2 The Thermal Analysis of the Lead Oxyhalides

The study of lead oxide / lead bromide mixtures by DSC proved impossible as an inert crucible could not be made which satisfied the requirements of the method. Instead, the differential thermal analysis (DTA) was conducted in a Differential Thermal Analyser, Stanton Redcroft model 673-4, which had an upper operational temperature limit of approximately 850 °C. The advantage of this instrument was that open top ceramic crucibles (which were sufficiently resilient to attack by lead oxybromide) were readily available.

The experiments were conducted in an inert nitrogen atmosphere which prevented oxidation of the sample, but the open crucibles undoubtedly resulted in some change in sample composition at higher temperatures; this was unavoidable. Throughout this work alumina was used as a reference material.

The following procedure was employed for all samples, and independent experiments were conducted at heating rates of 10 and 20 °C min^{-1}. First of all the sample was heated from ambient to the highest temperature of interest. It was then cooled and reheated. The two thermograms showed which of the transitions were reversible and the temperatures at which reaction occurred. A fresh sample was then heated to a temperature just above that at which the first thermal process had been observed in the previous experiment, allowed to cool and reheated. This temperature cycling was continued until there was no significant change in the thermogram. The temperature of this sample was then raised to the next point of interest and the thermal process examined using the temperature cycling method described above. Thus, a detailed picture of the behaviour of each sample was obtained.

The oven of the differential thermal analyser had a large thermal mass, which made the temperature ramp nonlinear for several minutes after heating began and it also prevented a sharp *cut off* at a precise temperatures. Thus, when two or more transitions were found in fairly close proximity a linear temperature ramp could not be obtained through any individual transition. It follows that individual traces had different temperature profiles and the absolute intensities of each thermal process varied from trace to trace.

The main features of the thermograms of the lead oxide / lead bromide mixtures are reproduced in Figure 3.12, exothermic processes are identified by positive peaks, whereas endothermic processes are represented by negative peaks. The data in the figure have been scaled and transformed onto a linear temperature axis to allow direct comparisons to be made.

The results show that slight changes in sample preparation (degree of mixing or level of

grinding) lead to dramatic changes in the appearance of the thermograms. However, these effects are limited to processes which ultimately disappear when the sample is heated to higher temperatures. Upon reheating a sample which has previously melted, each specific lead oxybromide gives a characteristic thermogram. This indicates that in order to ensure that a mixture of lead oxide and lead bromide has been completely converted to the corresponding lead oxybromide it is necessary to heat the sample to a temperature in excess of the melting point.

The thermograms obtained with samples of the lead oxybromides prepared for use in the vapour pressure experiments showed that in all cases the formation of the particular lead oxybromide was complete.

The following sections provide a detailed discussion of the behaviour observed for each phase and show how this behaviour correlates with the results of the X-ray powder crystallography.

3.2.3 The Thermal Analysis of the 1:1 Lead Oxybromide

The thermograms of 1:1 lead oxide / lead bromide mixtures show three temperatures at which endothermic or exothermic transitions take place, trace A in Figure 3.12 depicts a typical thermogram. The first starts as an endothermic process, but appears to be closely followed by an exothermic reaction. It is typically found at temperatures between 340 and 365 °C depending upon heating rate, sample size and preparation. The endotherm presumably indicates the onset of melting of the lead bromide (depressed by the lead oxide impurity) and the molten lead bromide then combines with the lead oxide in an exothermic reaction. The reaction is relatively slow and several minutes elapse before the thermogram attains a consistent baseline. When the samples are cooled and reheated the thermogram is completely flat in this region, indicating that the reaction between the lead bromide and lead oxide is irreversible. The X-ray powder diffraction pattern of the product formed in this reaction shows that it is the R form of 1:1 lead oxybromide.

The next feature in the thermogram begins between 460 and 480 °C and it can be either exothermic or endothermic. In experiments where fresh sample is heated from ambient conditions in a single pass, the peak in the thermogram represents an exothermic process. However, if the sample has been heated to above of 370 °C and cooled, the thermogram contains a peak which indicates an endothermic process. The temperature at which this second process is observed coincides with the temperature at which the R form of 1:1 lead oxybromide is transformed to the N form [6, 7]. When the samples are cooled and reheated the thermogram is level in this region, indicating that this process is also irreversible. The

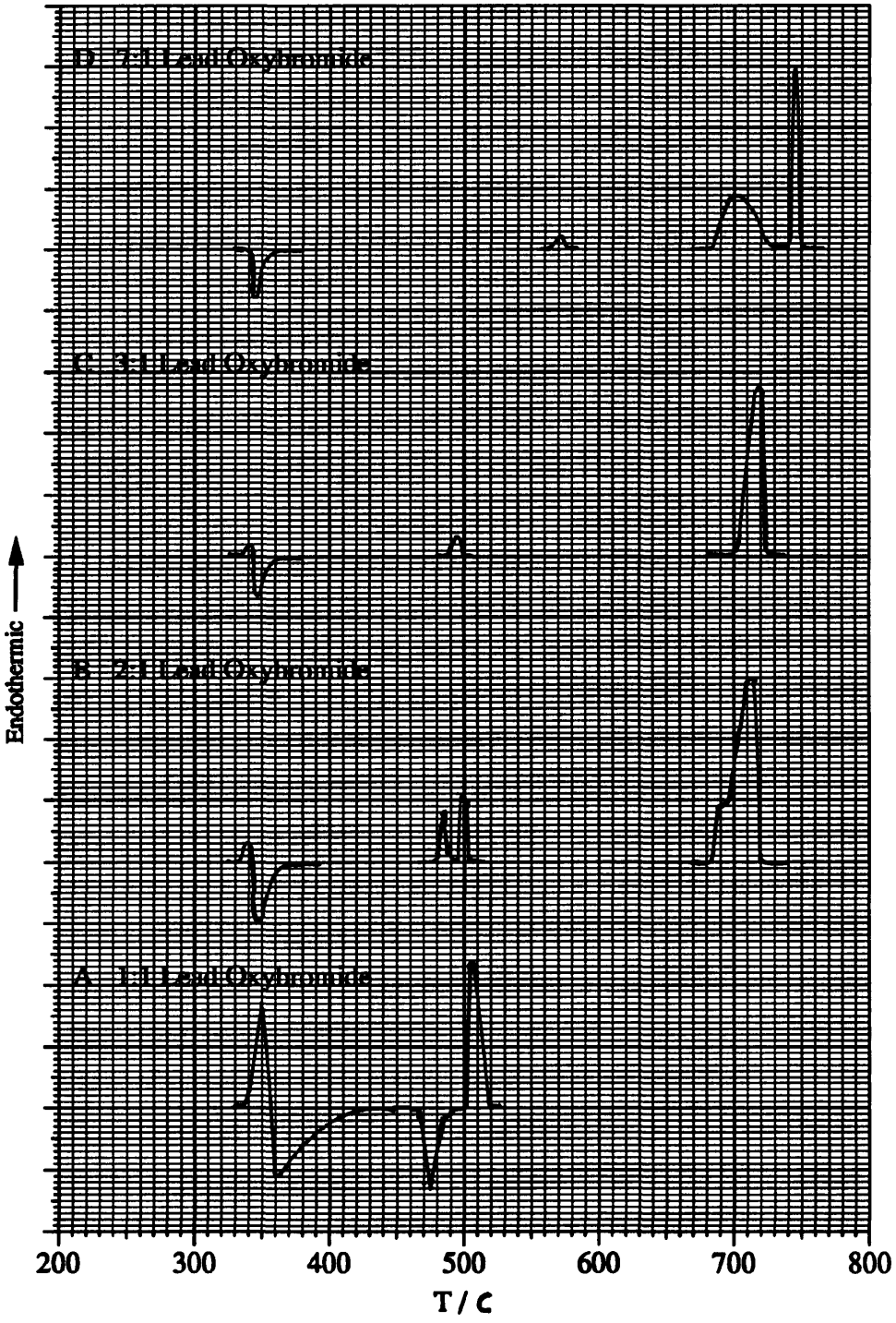

Figure 3.12: The differential thermal analysis traces for the lead oxide / lead bromide mixtures

X-ray diffraction pattern of the product shows that it is the N form 1:1 lead oxybromide.

The third and final feature in the thermogram is always endothermic and occurs at a temperature between 496 and 500 °C. This is the temperature at which 1:1 lead oxybromide is known to undergo a peritectic reaction to form solid 2:1 lead oxybromide and a lead oxide / lead bromide melt [5]. This feature is not removed by temperature cycling and hence the process is reversible.

The thermograms of 1:1 lead oxybromide prepared for use in the vapour pressure measurements contain only one peak. It is found at temperatures between 496 and 500 °C, this corresponds to the peritectic melting of 1:1 lead oxybromide. The X-ray powder diffraction patterns of these samples confirm that they are the N form of 1:1 lead oxybromide.

3.2.4 The Thermal Analysis of the 2:1 Lead Oxybromide

The thermograms for 2:1 lead oxide / lead bromide mixtures show three temperature regions in which endothermic or exothermic transitions take place and trace B of Figure 3.12 represents a typical thermogram. The first of the processes is observed at between 340 and 365 °C and reflects the formation of R form 1:1 lead oxybromide, as discussed in Section 3.2.3, although the shape of the trace is different. Typically there is a very small endothermic peak which almost instantly turns into an exothermic peak. This feature is absent when the sample is cooled and reheated, indicating that the reaction is irreversible. The X-ray powder diffraction pattern of the product shows it to be a mixture of the R form 1:1 lead oxybromide and another phase which is possibly lead oxide (See Section 3.2.4 and Figure 3.10).

The second temperature region in which the DTA traces indicate activity is 480 to 510 °C. The traces contain one or two endothermic peaks, the exact number depends upon sample preparation. In the majority of the experiments two endothermic peaks are present, the first begins at around 480 °C and the second at, or slightly above 492 °C. The first of the peaks occurs at the temperature at which R form 1:1 lead oxybromide is converted to the N form, the second corresponds to the formation of 2:1 lead oxybromide by the peritectic reaction which accompanies the melting of 1:1 lead oxybromide. These peaks are removed when the temperature is cycled between 400 and 520 °C, showing that the reactions are irreversible. The X-ray powder diffraction pattern of the product identifies it as 2:1 lead oxybromide.

The third and final feature in the thermogram is endothermic and is found at approximately 696 °C. This is the only peak which is unaffected by temperature cycling and is

due to the endothermic melting of 2:1 lead oxybromide. It should be noted that this peak always had a small shoulder on the side at lower temperature, although the cause was not identified.

The thermograms of 2:1 lead oxybromide prepared for use in the vapour pressure measurements contain only one peak. It is found at temperatures between 696 and 698 °C and shows that the formation of the 2:1 lead oxybromide is complete, incidentally, the shoulder mentioned above was also observed here. The complete formation of 2:1 lead oxybromide was also confirmed by the X-ray powder diffraction patterns.

3.2.5 The Thermal Analysis of the 3:1 Lead Oxybromide

The DTA results for 3:1 lead oxide / lead bromide mixtures (see trace C, Figure 3.12) show an exothermic reaction beginning between 348 and 350 °C, this is followed by an endothermic process which begins between 492 and 496 °C. These correspond to the formation of the R form of 1:1 lead oxybromide and the 2:1 lead oxybromide respectively. The next clear feature is found between 704 and 706 °C and results from the endothermic melting of 3:1 lead oxybromide.

The thermogram between 510 and 700 °C contains a very broad endothermic hump, which suggests that the transition of 2:1 lead oxybromide to 3:1 lead oxybromide is a slow endothermic process. When the sample is cooled and reheated only the large endotherm at 705 °C remains.

The thermal analysis of the 3:1 lead oxybromide prepared in this work shows its formation to be complete.

3.2.6 The Thermal Analysis of the 7:1 Lead Oxybromide

A typical thermogram obtained with 7:1 lead oxide / lead bromide mixtures is presented as trace D in Figure 3.12. The DTA results show the exothermic formation of the R form of 1:1 lead oxybromide between 348 and 350 °C. The next clear feature appears at 705 °C and corresponds to the melting of 3:1 lead oxybromide. Between these very pronounced peaks there are two very broad endothermic humps. These endotherms appear in the temperature regions where, (from studies of 2:1 and 3:1 lead oxybromide) the transition from 1:1 to 2:1 and 2:1 to 3:1 lead oxybromide occur.

The final peak in the thermogram at 737 °C results from the endothermic melting of the

7:1 lead oxybromide and is the only feature which remains if the sample is cooled and reheated.

The thermal analysis of samples of the 7:1 lead oxybromide prepared in this work show that the formation of 7:1 lead oxybromide was complete.

References

[1] Davies P.T., Garner E.V. and Caddock B.D., *An X-ray Study of the Lead Bromide Rich Region of the Lead Oxide-Lead Bromide System*, Acta. Cryst., 7, (1954), p. 640.

[2] Hyde J.L. *On the Melting Point, Oxidation and Vapour Pressure of Lead Bromide.* J. Am. Chem. Soc., 73, (1951), p. 1860.

[3] Joint Committee on Powder Diffraction Standards (Formerly the ASTM (American Society for Testing Materials) card file index).

[4] Julien H.P. and Ogilvie R.E., *High Temperature X-ray Study of Lead Halides and Oxyhalides*, J. Am. Chem. Soc., 82, (1960), p. 293.

[5] Knowles L.M., *Thermal Analysis of the System $PbBr_2$-PbO,* J. Chem. Phys., 19, (1951), p. 1128.

[6] Lamb F.W. and Niebylski L.M., *Formation of Engine Deposit Compounds by Solid-State Reactions*, Anal. Chem., 23 , (1951), p. 1388.

[7] Lamb F.W. and Niebylski L.M., *Phase Study of the PbO-$PbBr_2$ System by X-ray Diffraction*, J. Am. Chem. Soc., 75, (1953), p. 511.

[8] Linsey .C.W. *High Temperature Enthalpies of Lead Halides; Enthalpies and Entropies of Fusion.* North Texas State Univ., Denton Texas, (1970), 110 pp. Avail. Univ. Microfilms, Ann Arbor, Mich. Order no.71- 559. Diss. Abstr. Int B 1971, 31(7), p. 3958.

[9] *X-ray Diffraction Patterns of Lead Compounds*, The Shell Petroleum Company Limited, Thornton Research Centre, Chester, England, (1954).

Chapter 4

The Determination of the Vapour Pressure of Lead Bromide

The vapour pressure of lead bromide was measured in the temperature range 340 – 405 °C using the *Transpiration Method* described earlier in Chapter 2. Samples of approximately 0.6 g were accurately weighed into the sample basket and spread out evenly across its base. They were then loaded into the apparatus as described in Chapter 2.

The results of these experiments are summarised below in Table 4.1 and shown graphically in Figures 4.1 to 4.11. The error bars on the data points are equivalent to an error of ±0.05 mm in the measurement of the length of the quartz spring. This corresponds to the magnitude of the maximum discrepancy between repeat measurements of the spring extension during its calibration.

The extension changes plotted in each of the Figures 4.1 to 4.11 were "corrected" for variations in ambient atmospheric pressure. This correction was based on a constant mass flow of carrier gas and a constant partial pressure of lead bromide in the gas flow, so that the experimental measurements are expressed for a constant total pressure of 760 mmHg. The corrections were calculated by averaging the atmospheric pressure measured at two hourly intervals from the initial measurement to the time of each subsequent measurement, the atmospheric pressure being monitored using a recording barograph. In general the magnitude of this correction was very small. The "raw" and "corrected" data points are displayed in Figures 4.4 and 4.6 and illustrate the typical size of the correction.

The introduction of this correction produced a more accurate estimation of the overall vapour pressure when the data was analysed using a linear regression technique. The gradient resulting from the regression analysis of the corrected weight loss with respect to time was used along with the carrier gas flow rate and an atmospheric pressure of 760 mmHg to calculate the vapour pressure and an estimate of the experimental error.

Table 4.1: The results of the vapour pressure experiments with lead bromide

Figure No.	Temperature °C	Flow Rate cm^3min^{-1}	Vapour Pressure mmHg	Deviation mmHg	Error %
4.1	403	17.0	2.54×10^{-02}	1.2×10^{-03}	4.8
4.2	363	19.9	3.42×10^{-03}	3.4×10^{-05}	1.0
4.3	363	27.9	3.54×10^{-03}	3.2×10^{-05}	0.9
4.4	363	36.9	3.15×10^{-03}	1.8×10^{-05}	0.6
4.5	360.8	30.7	3.35×10^{-03}	4.8×10^{-05}	1.4
4.6	355.7	26.6	2.54×10^{-03}	6.9×10^{-06}	0.3
4.7	350.6	26.6	2.15×10^{-03}	2.8×10^{-05}	1.3
4.8	342.5	26.6	1.09×10^{-03}	6.7×10^{-06}	0.6
4.9	343.2	21.8	1.20×10^{-03}	1.3×10^{-05}	1.1
4.10	365.2	21.4	3.94×10^{-03}	2.1×10^{-05}	0.5
4.11	365.2	22.9	3.91×10^{-03}	2.3×10^{-05}	0.6

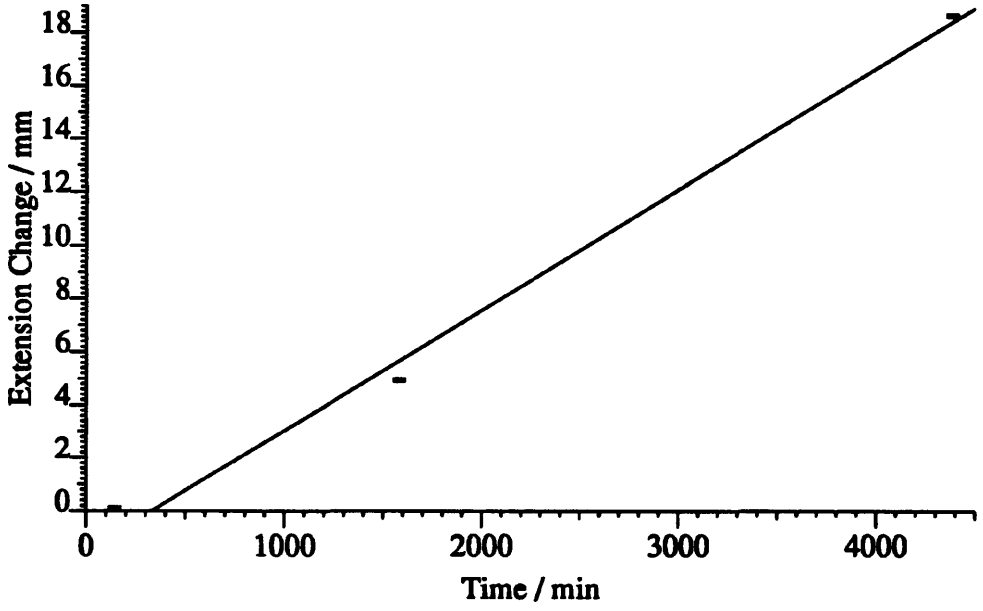

Figure 4.1: The change in extension of the quartz spring with respect to time for a lead bromide sample at 403 °C with a carrier gas flow rate of 17.0 cm^3 min^{-1}

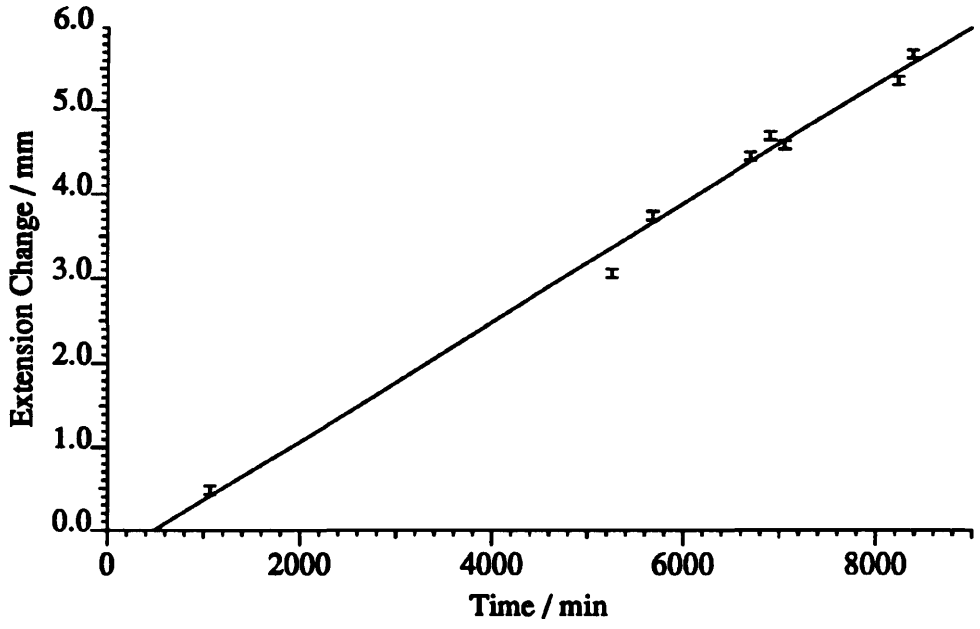

Figure 4.2: The change in extension of the quartz spring with respect to time for a lead bromide sample at 363 °C with a carrier gas flow rate of 19.9 cm^3 min^{-1}

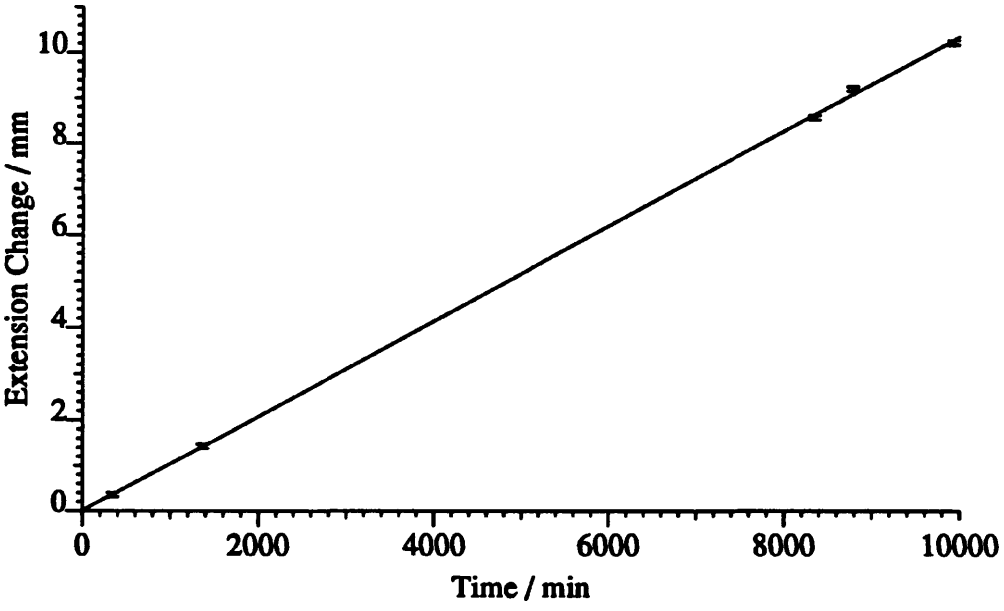

Figure 4.3: The change in extension of the quartz spring with respect to time for a lead bromide sample at 363 °C with a carrier gas flow rate of 27.9 cm^3 min^{-1}

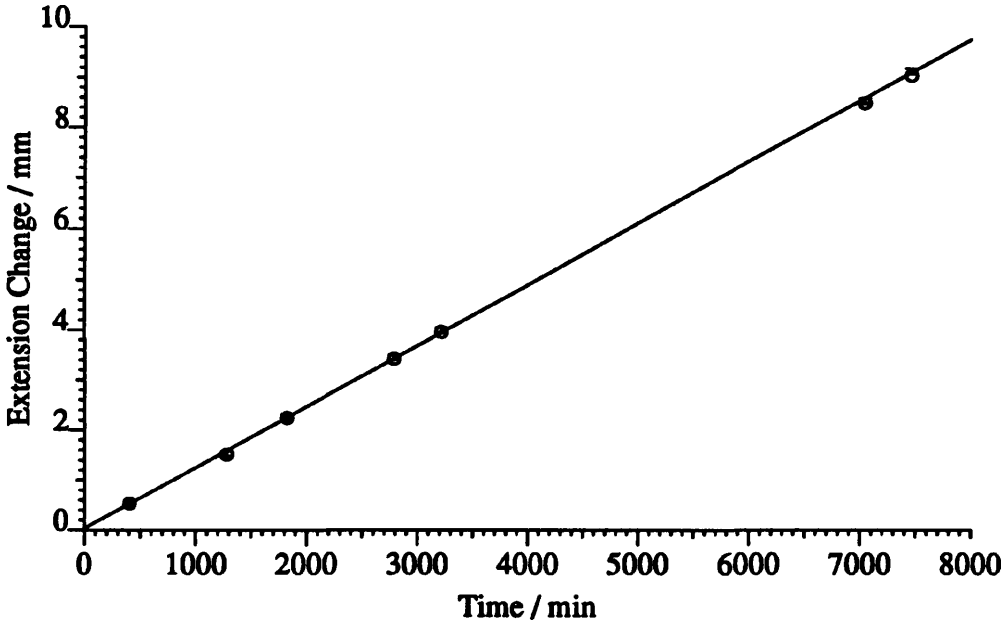

Figure 4.4: The change in extension of the quartz spring with respect to time for a lead bromide sample at 363 °C with a carrier gas flow rate of 36.9 cm^3 min^{-1}. Raw data points = o, corrected data points = I

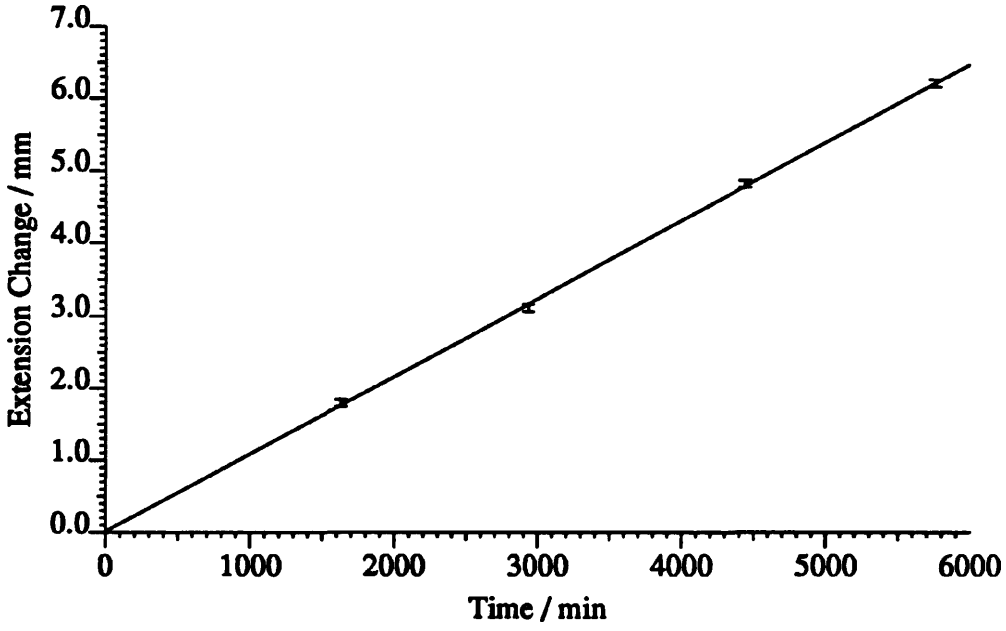

Figure 4.5: The change in extension of the quartz spring with respect to time for a lead bromide sample at 360.8 °C with a carrier gas flow rate of 30.7 cm^3 min^{-1}

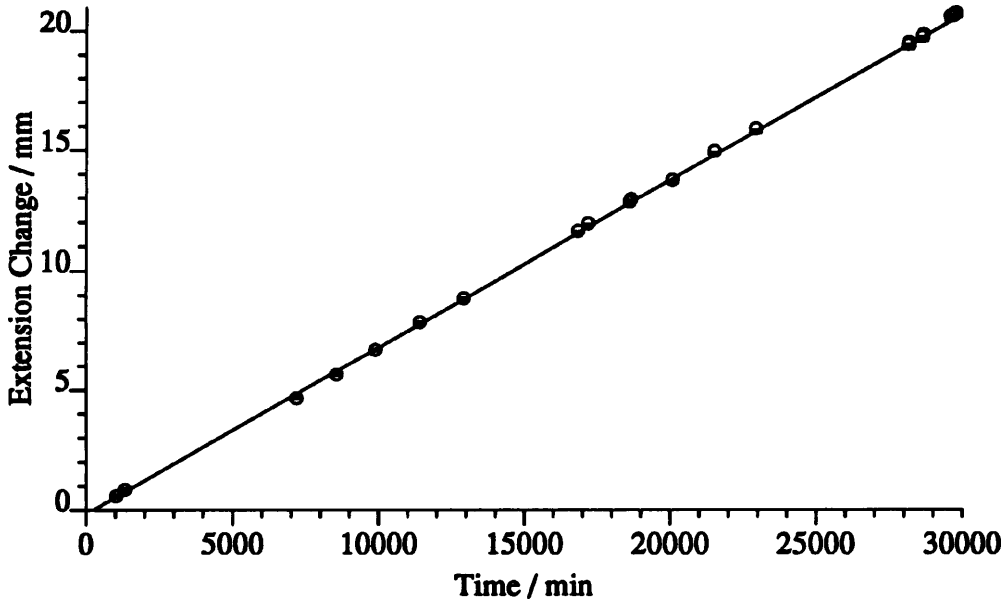

Figure 4.6: The change in extension of the quartz spring with respect to time for a lead bromide sample at 355.7 °C and a carrier gas flow rate of 26.6 cm^3 min^{-1}. Raw data points = o, corrected data points = I

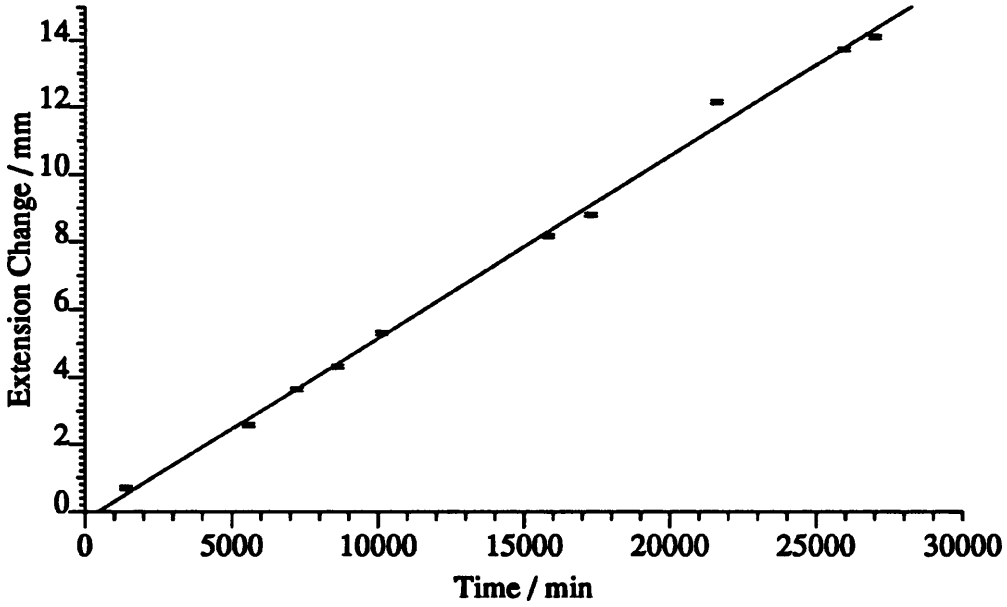

Figure 4.7: The change in extension of the quartz spring with respect to time for a lead bromide sample at 350.6 °C with a carrier gas flow rate of 26.6 cm^3 min^{-1}

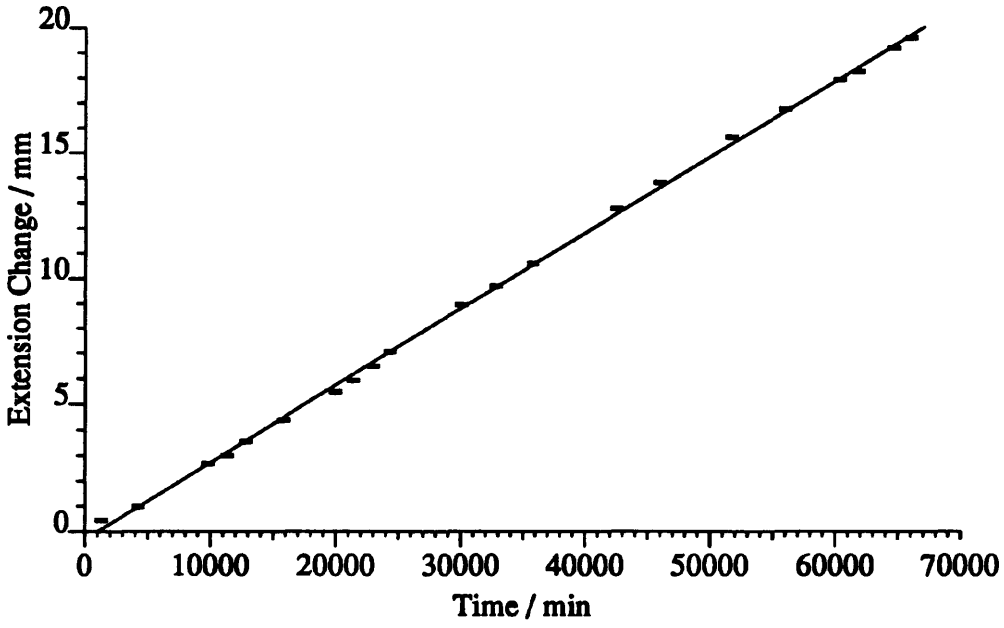

Figure 4.8: The change in extension of the quartz spring with respect to time for a lead bromide sample at 342.5 °C with a carrier gas flow rate of 26.6 cm^3 min^{-1}

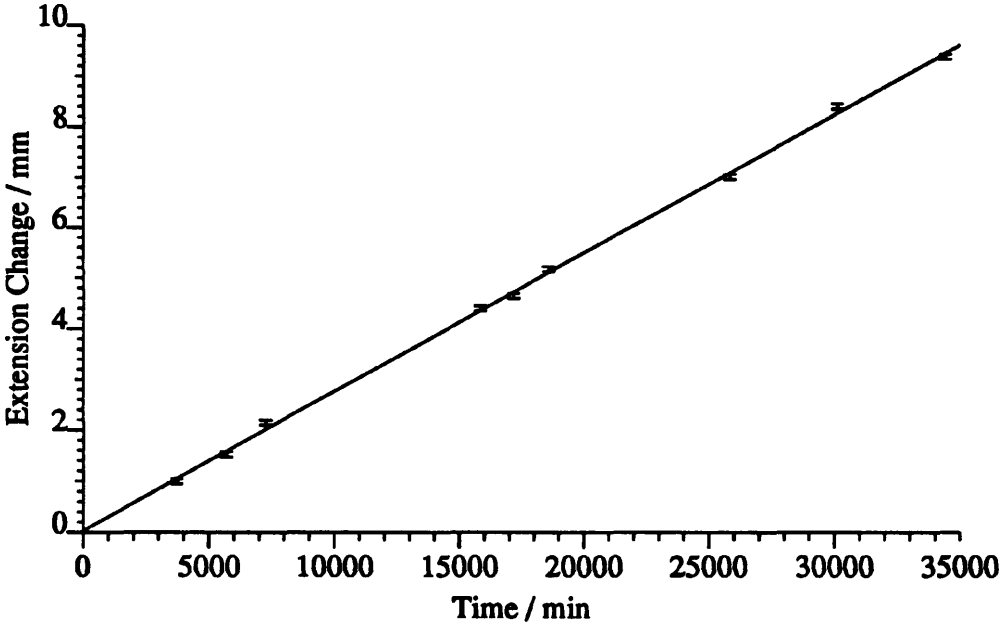

Figure 4.9: The change in extension of the quartz spring with respect to time for a lead bromide sample at 343.2 °C with a carrier gas flow rate of 21.8 cm^3 min^{-1}

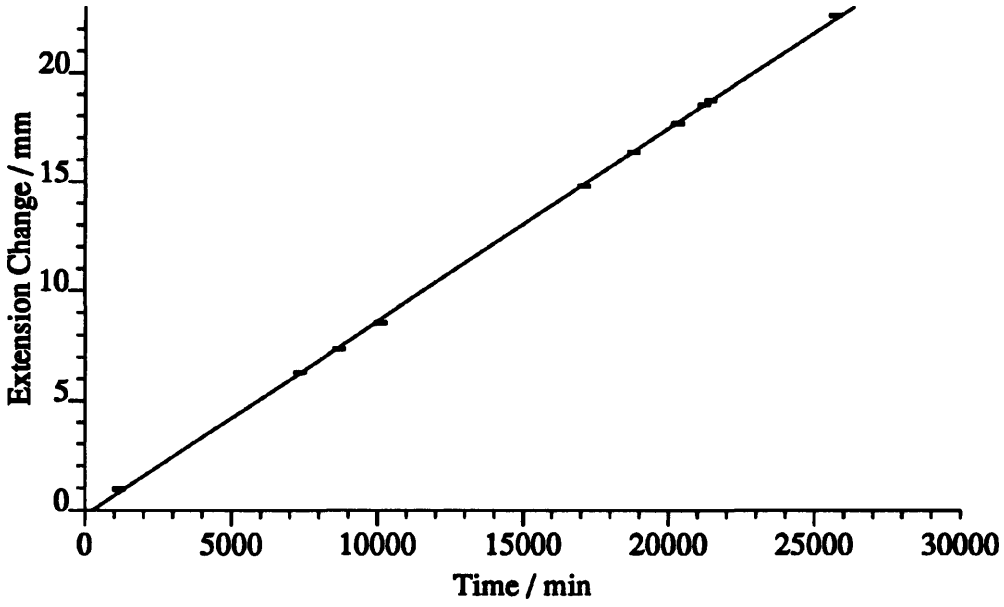

Figure 4.10: The change in extension of the quartz spring with respect to time for a lead bromide sample at 365.2 °C with a carrier gas flow rate of 21.4 cm^3 min^{-1}

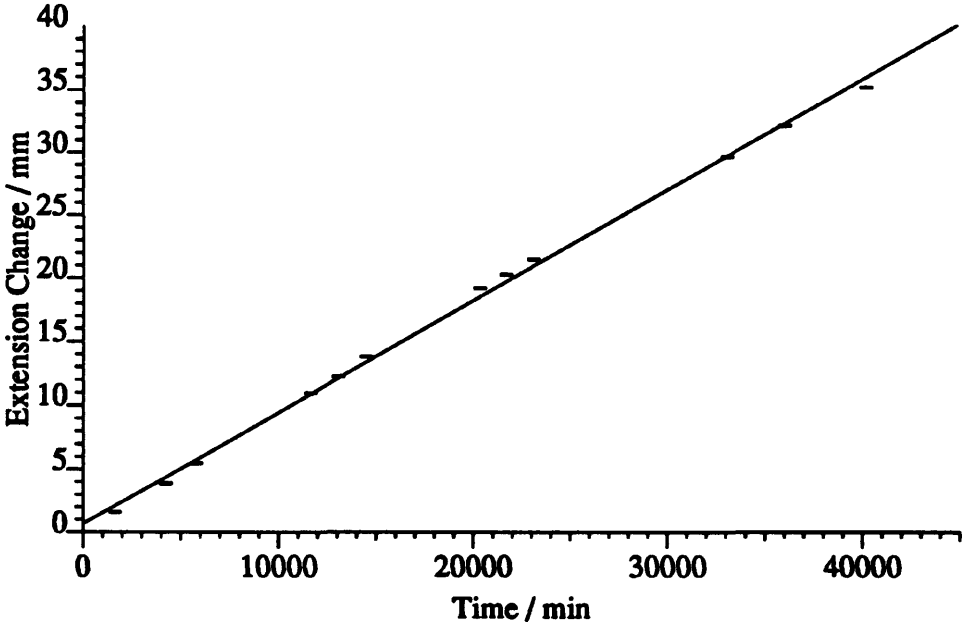

Figure 4.11: The change in extension of the quartz spring with respect to time for a lead bromide sample at 365.2 °C with a carrier gas flow rate of 22.9 cm^3 min^{-1}

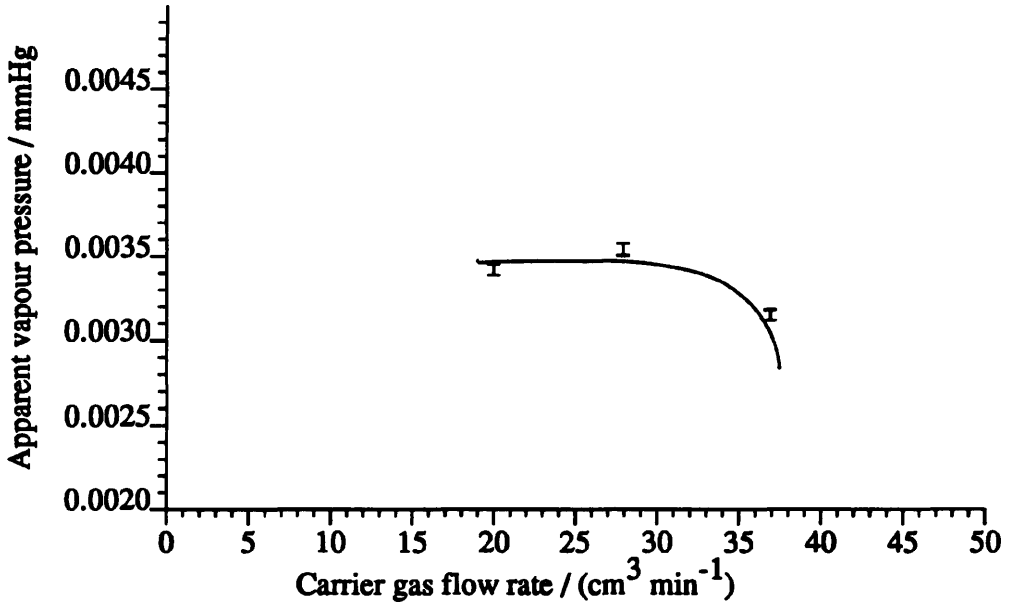

Figure 4.12: Apparent vapour pressure versus carrier gas flow rate at 363 °C

Figure 4.12 shows the effect of carrier gas flow rate on the apparent vapour pressure for experiments conducted at the same temperature but different flow rates of carrier gas. This graph indicates that within experimental error the apparent vapour pressure (that is the vapour pressure calculated from the experimental results for the specific experimental conditions of temperature, flow rate and pressure) was independent of the carrier gas flow rate between approximately 20 and 28 $cm^3\ min^{-1}$, but at higher flow rates the apparent vapour pressure decreased. This lowering of the vapour pressure was due to the residence time of the carrier gas in the saturation chamber being insufficient to allow the gas stream to become fully saturated with sample vapour.

The Clausius-Clapeyron equation

$$\frac{d(\ln(p))}{dT} = \frac{\Delta H_{evaporation,mol}}{RT^2} \tag{4.1}$$

expresses the relationship between the vapour pressure and the enthalpy of the transition between a condensed and vapour phase. It is more frequently discussed in terms of the enthalpy of evaporation of a liquid, but similarly describes the enthalpy of sublimation of a solid. The integrated form of equation 4.1

$$\ln(p) = constant - \frac{\Delta H_{evaporation,mol}}{RT} \tag{4.2}$$

predicts that a plot of log(p) versus $\frac{K}{T}$ will be a straight line with a slope directly related

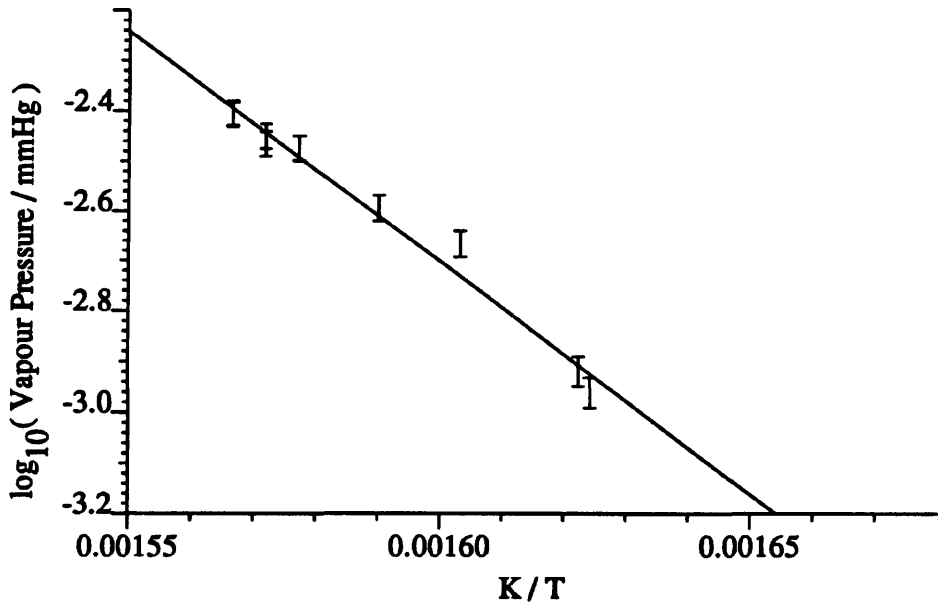

Figure 4.13: $\log_{10}$(vapour pressure / mmHg) versus $\frac{K}{T}$ from the experimental results for lead bromide

to the enthalpy of vaporisation.

Figure 4.13 is a plot of $\log_{10}$(vapour pressure / mmHg) versus $\frac{K}{T}$ for the present experimental results. The data obtained under conditions lying within the plateau region shown in Figure 4.12, were processed by linear regression and yielded the following vapour pressure equation

$$\log_{10}(p \ / \ \text{mmHg}) = 12.0 \pm 0.7 + \frac{-9200 \pm 480\,K}{T} \tag{4.3}$$

These results suggested that the calculated vapour pressure was subject to an error of between 0.3 % and 1.6 %, and the error bars shown in Figure 4.13 correspond to an uncertainty of 2 % in the vapour pressures.

The slope of the line shown in Figure 4.13 is related to the enthalpy of sublimation of lead bromide as follows

$$slope = -\frac{\Delta H_{sublimation,mol}}{(2.303R)} \tag{4.4}$$

and on substitution of the relevant values from equation 4.3 gives the enthalpy of sublimation for lead bromide as 176 ± 9 kJ mol^{-1}

Figure 4.14 compares the present experimental vapour pressures with those of other workers. The figure contains contributions from Von Wartenberg and Bosse [18], Volmer [17], Greiner and Jellinek [7], Kelley [10], Stull [16], Kubaschewski and Alcock [13], Bloom, Bockris, Taylor and Richards [2], and Spiridonova, Aleksandrov and Emel'yanov [15]. The temperature range covered by each of these workers is indicated by the horizontal line drawn beneath their name.

The Handbook of Chemistry and Physics 64^{th} edition [4] contains two references to the vapour pressure of lead bromide, a table of temperatures which correspond to a set of standard pressures (this appears to be a duplicate of the work of Stull) and an equation (which is analogous to equation 4.2) of the form

$$\log_{10}(\text{ Vapour pressure / mmHg}) = \frac{0.0552\ A\ \text{K}}{T} + B. \tag{4.5}$$

The constants of equation 4.5 appear to have been derived from the work of Von Wartenberg and Bosse. These data are also shown in Figure 4.14.

The vapour pressures presented in the present work clearly lie between those predicted by the equation of Kubaschewski and Alcock [13] and the experimental results of Spiridonova *et al.* [15]. The following discussion starts by outlining a little of the historical background surrounding the data shown in Figure 4.14.

The vapour pressure equation reported by Kubaschewski and Alcock is of the form

$$\log(p\ /\ \text{mmHg}) = \frac{A}{T} + B\log(T) + CT + D \tag{4.6}$$

and the values of the constant A, B, C and D are shown in Table 4.2. They were derived by Kubaschewski and Alcock from a combination of the works of Kelley [10], Brewer [3] and Stull [16], who had themselves used data provided by a number of the experimenters listed above to compile tables of vapour pressure data and other thermodynamic quantities such as enthalpy of fusion and heat capacity. A closer examination of the constants for both temperatures above and below the melting point of lead bromide reveals that they differ only slightly from those published by Kelley and that the tables of vapour pressure published by Stull are also in good agreement with the equation of Kubaschewski and Alcock.

Kelley based his equation on the work of Von Wartenberg, Greiner and Jellinek and Volmer, but in his discussion raised doubts as to the validity of some of Volmer's results.

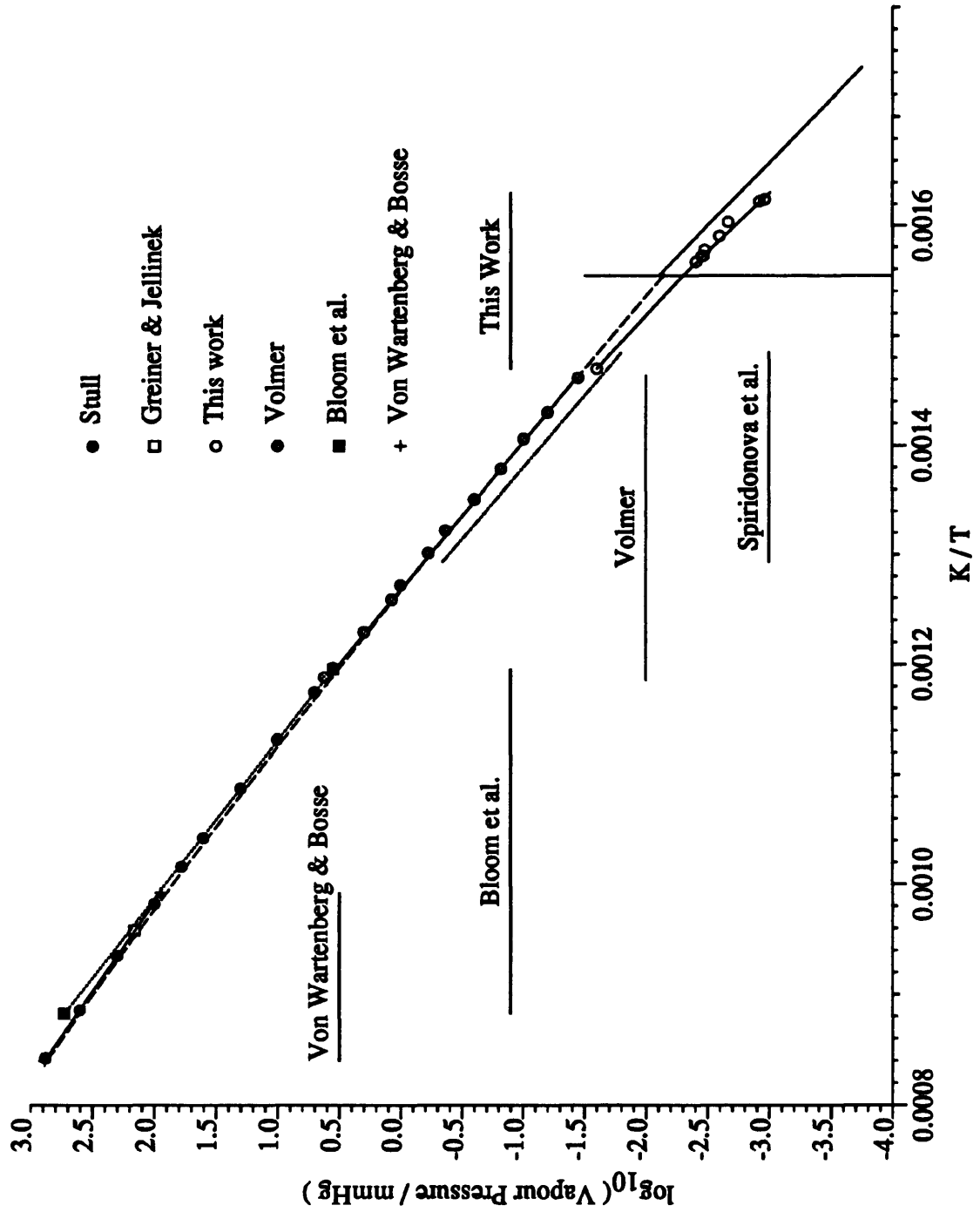

Figure 4.14: $\log_{10}$(vapour pressure / mmHg) versus $\frac{K}{T}$ for lead bromide. The temperature range covered by each worker is indicated by the horizontal line beneath the name. The melting point of lead bromide is indicated by the vertical line

Table 4.2: The coefficients of lead bromide vapour pressure equation 4.6

Phase	Temperature Range K	A	B	C	D
Solid	298-643	-9320	-2.08	-0.34×10^{-03}	18.44
Liquid	643-1187	-9540	-6.76	-	31.67

The discussion contains an explicit reference to results which Volmer obtained for *solid* lead bromide, which is very disturbing because the temperature range covered by Volmer was 410 to 570 °C and the melting point of lead bromide is 370 °C [12]. Thus, if Volmer was truly working with lead bromide then it ought to have been a *liquid*. Kelley also stated that the enthalpy of fusion produced from the reports of Volmer could not be reconciled with the directly measured value, and therefore based the vapour pressure equation of the solid on results for the liquid and other measured thermal data. Although Kelley refers to "the directly measured thermal data" he neglects to disclose his source.

Several years after Kelley published his compilation of vapour pressure and thermodynamic data Knowles [12] and Hyde [8] pointed out that he had used a value of 497 °C for the melting point of lead bromide. It is interesting to note that this is the temperature at which the 1:1 lead oxybromide undergoes a peritectic decomposition. This implies that prior to the publications of Knowles and Hyde many of the experiments may have been carried out with 1:1 lead oxybromide instead of lead bromide, which would explain the reference of Kelley to the results of Volmer for "solid lead bromide". Unfortunately there is no way of knowing for certain if this is the case.

Hyde presented an expression for the enthalpy of sublimation for lead bromide based on the heat capacity of the liquid and the enthalpy of fusion and cited Brewer [3] as the source of the thermal data. This expression is very similar to that reported by Kelley.

The discussion to this point implies that the vapour pressure equation for lead bromide was based primarily on the experimental data of Von Wartenberg and Bosse, a single experimental value obtained from Greiner and Jellinek and a set of results reported by Volmer. However, Kelley stated that because Von Wartenberg and Bosse had observed some dissociation near the boiling point, at first sight it seemed better to base the equation on the results of Volmer, unfortunately these data are also plagued by the uncertainty discussed above. Furthermore, the enthalpy of fusion from which the enthalpy of sublimation was calculated, was more than likely the enthalpy of the peritectic decomposition of the 1:1 lead oxybromide and not the enthalpy of fusion of lead bromide! It appears that an

Table 4.3: Comparison of calculated vapour pressures at the melting point of lead bromide

Source	Vapour Pressure / mmHg	Discrepancy %
Spiridonova *et al.*	4.62×10^{-3}	
		7.8
Present	5.01×10^{-3}	
		43.3
Kubaschewski and Alcock	7.18×10^{-3}	

equation based upon these data is due a certain amount of skepticism.

Fortunately two further sets of vapour pressure data are available, those of Bloom *et al.* and Spiridonova *et al.*, both of which were carried out after the reports of Knowles and Hyde and, hopefully are more reliable than the earlier works.

The vapour pressures reported by Bloom *et al.* are in good agreement with those of Volmer in the overlapping temperature ranges. In the higher temperature range covered by Von Wartenberg the results differ both in magnitude and in the enthalpy of evaporation, Bloom *et al.* reporting higher values for both.

In contrast, the vapour pressures reported by Spiridonova *et al.* are considerably lower than those measured by Volmer at the same temperature. The vapour pressure equation of Spiridonova *et al.*

$$p \ / \ \text{mmHg} = 10^{9.56} e^{\left(-\frac{35000}{RT}\right)} \tag{4.7}$$

gives a slightly higher enthalpy of evaporation when compared to that of Volmer. It should be noted also that there must be a misprint in equation given by Spiridonova *et al.* in the original journal; the value 35000 has become 3500.

The vapour pressures measured in the present work are in good agreement with those of Spiridonova *et al.* but are considerably lower than those measured by Volmer. Table 4.3 shows the absolute discrepancies. Because of the uncertainty surrounding the nature of lead bromide samples which Volmer used in his experiments it seems reasonable to favour the results of Spiridonova *et al.* and those from the present work. As a result, the vapour pressure equation of Kubaschewski and Alcock should be modified accordingly.

Inspection of the vapour pressure curves provided by equation 4.6 at the melting point of lead bromide (370.2 °C) reveals that the vapour pressures differ by approximately 7 %. A similar examination of the equations for several other compounds chosen at random from the vapour pressure tables showed that this discrepancy was comparable to that for other compounds exerting similar vapour pressures. It is interesting to note that as the vapour pressure decreases the relative magnitude of the discrepancy increases, presumably reflecting the experimental difficulties encountered in the measurement of very low vapour pressures.

The gradients of the vapour pressure curves on a Clausius-Clapeyron plot, for solid and liquid phases, reflect the enthalpies of sublimation and evaporation respectively. Thus, the enthalpy of fusion can be estimated from the data providing it straddles the melting point of the condensed phase.

A summary of the enthalpies of evaporation, sublimation and hence fusion is provided for lead bromide in Table 4.4. The earliest reported value for the enthalpy of fusion is that of Ehrhardt in 1885 [5] and Goodwin and Kalmus [6] also obtained a similar result. In his original work Kelley [10] reported an enthalpy of fusion for lead bromide which lay between the results of these workers. However, both Ehrhardt and Goodwin and Kalmus report a melting point for lead bromide of 488 °C although the true melting point is known to be 370.2 °C. Consequently the measured enthalpy of fusion cannot be that of pure lead bromide and this must cast serious doubts upon the thermodynamic calculations of Kelley. Kelley [11] later published a comprehensive compilation of thermal data in which he again refers to the work of Ehrhardt and Goodwin and Kalmus as a source of the thermal data for lead bromide, apparently unaware of the reports of Knowles and Hyde.

The value for the enthalpy of fusion of lead bromide reported by Blanc and Petit [1] is the source of the value provided in the JANAF [9] tables. Kubaschewski and Alcock used this enthalpy of fusion to update the original equations of Kelley. The most recent determination of the enthalpy of fusion of the lead halides has been reported by Linsey [14] and the reported melting point of the lead bromide used is 370 °C. Ironically this value is a little over 1 kJ mol^{-1} higher than that reported by Goodwin and Kalmus for a solid which, based on the findings of Hyde and Knowles, was probably the 1:1 lead oxybromide.

The enthalpy of sublimation and the enthalpy of evaporation determined in the present work gave a value for the enthalpy of fusion of lead bromide of 16 kJ mol^{-1}. This value was in excellent agreement with that of Linsey. However, it would be improper to place too much emphasis on this agreement, since the derived value for the enthalpy of fusion is small relative to the combined errors of the enthalpy of sublimation and evaporation.

Table 4.4: Values for the enthalpy of sublimation, evaporation and fusion of lead bromide at the melting point

Source	Sublimation kJ mol^{-1}	Evaporation kJ mol^{-1}	Fusion kJ mol^{-1}
Ehrhardt			18.8
Goodwin and Kalmus			15.3
Kelley	163.6	146.4	17.1
Hyde	167.0	-	20.6
Kubaschewski and Alcock	167.2	146.4	20.8
Blanc and Petit	-	-	20.8
Spiridonova *et al.*	-	146.5	-
Linsey			16.4
Present Work	176 ± 9	(169)	(16)

When the present work is taken in conjunction with that of Spiridonova *et al.*, an enthalpy of fusion of approximately 30 kJ mol^{-1} is obtained, this value is clearly much larger than the values listed in Table 4.4. However, vapour pressures obtained by extrapolation of the equation reported by Spiridonova *et al.* to the temperature range covered by Bloom *et al.* are lower than those reported by the latter workers; they also lie below the experimental values obtained in this work. In order to bring the vapour pressure equation reported by Spiridonova *et al.* into agreement with both the present work and that of Bloom *et al.* the vapour pressure at each temperature and the gradient of the line must be increased. When this is done the calculated enthalpy of fusion tends toward the most recent value of 16 kJ mol^{-1}.

The present work shows that the vapour pressure equation reported by Kubaschewski and Alcock for lead bromide requires modifying to reflect the vapour pressures measured both here and by Spiridonova *et al.* The new vapour pressure equation will necessarily give a higher enthalpy of evaporation at lower temperatures but the constants which result in the curvature can be adjusted to accommodate the majority of the results previously reported.

The results of the present work with lead bromide also showed that both the method and apparatus used were applicable to the measurement of vapour pressures of this magnitude and in light of this it was likely that they could be used to determine the vapour pressure of the lead oxyhalides.

References

[1] Blanc M. and Petit P., Compt Rend, 248, (1959), p. 1305-6.

[2] Bloom H., Bockris J.O., Richards N.E.and Taylor R.G. *Vapour Pressure and Heat of Vaporization of Some Simple Molten Electrolytes,* J. Am. Chem. Soc., 80, (1958), p. 2044.

[3] Brewer L. National Nuclear Energy. Series., Div. IV, 19B, p. 13.

[4] CRC press. *Handbook of Chemistry and Physics 64th Edition,* CRC press, 1983-1984.

[5] Ehrhardt Weid Ann, 24, (1885), p. 215.

[6] Goodwin H.M. and Kalmus T.H., *On the Latent Heat of Fusion and Specific Heat of Salts in the Solid and Liquid State,* Physics Review, 28, (1909), p. 1.

[7] Greiner B. and Jellinek K. *Uber die Dampfe des reziproken Salzpaares NaCl, KJ und der binaren Gemische $PbCl_2$, $PbBr_2$;$PbCl_2$, PbJ_2;PbJ_2, CuJ_2 und $CdCl_2$, $CdBr_2$,* Z. Physikal Chem., 165A, (1933), p. 97.

[8] Hyde J.L. *On the Melting Point, Oxidation and Vapour Pressure of Lead Bromide,* J. Am. Chem. Soc., 73, (1951), p. 1860.

[9] JANAF, *Thermochemical Tables,* 2nd Ed., US Dept. of Commerce, National Bureau of Standards, 1971.

[10] Kelley K.K. *The Free Energies of Vaporization and Vapor Pressures of Inorganic Substances,* U.S. Department of the Interior Bureau of Mines Bulletin, 383, (1935), p. 61.

[11] Kelley K.K. *High Temperature Heat Content, Heat Capacity and Entropy Data of the Elements and Inorganic Compounds,* U.S. Department of the Interior Bureau of Mines Bulletin, 584, (1960), p. 102.

[12] Knowles L. M. *Thermal Analysis of the System $PbBr_2$-PbO,* J. Chem. Phys., 19, (1951), p. 1128.

[13] Kubaschewski O. and Alcock C.B. *Metallurgical Thermochemistry,* 5th edition. Pergamon Press. ISBN 0 08 020897 5.

[14] Linsey .C.W. *High Temperature Enthalpies of Lead Halides; Enthalpies and Entropies of Fusion,* North Texas State Univ., Denton Texas, (1970), 110 pp. Avail. Univ. Microfilms, Ann Arbor, Mich. Order no. 71-559. Diss. Abstr. Int B, 1971, 31(7), p. 3958.

[15] Spiridonova M.N, Aleksandrov Y.U.A. and Emel'yanov B.V. *Vapour Pressure of Lead Chloride and Lead Bromide,* Trudy Po Khimii I Khimicheskoi Tekhnologii, (1971), p. 212.

[16] Stull D.R. *The Vapour Pressures of Pure Substances, Inorganic Compounds,* Ind. Eng. Chem., 39, (1947), p. 540.

[17] Volmer F. *Uber den Dampfdrück der Halogenide des Thalliums und Bleis,* Physical Z., vol. 30, (1929), p. 590.

[18] Wartenberg H. Von, and Bosse O. *Der Dampfdrück einig Salze,* Z. Electrochem, 28, (1922), p. 384.

Chapter 5

The Determination of the Vapour Pressure of 1:1 Lead Oxybromide

The vapour pressure of the N Form of the 1:1 lead oxybromide was measured using the transpiration method described in Chapter 2. In this technique, the amount of evaporating material is used to calculate its mole fraction in the gas stream and hence its partial pressure (i.e. vapour pressure). In the apparatus used here the *weight* of evaporating material was measured and the evaporating species had to be identified before the partial pressure could be calculated.

5.1 The Composition of the Vapour Phase Above 1:1 Lead Oxybromide

In order to identify the evaporating species, the deposit which accumulated in the outlet tube from the saturation chamber was collected following individual experiments. The X-ray powder diffraction patterns obtained from both the N form of the 1:1 lead oxybromide and the 2:1 lead oxybromide were virtually indistinguishable from those of lead bromide. Figure 5.1 shows the powder diffraction pattern of pure lead bromide and that of the condensed solid. It should also be noted that the powder diffraction pattern of a 1 % mixture of lead oxide in lead bromide shows the diffraction pattern of both components. This shows that these lead oxybromides effectively only lose lead bromide and do not evaporate intact.

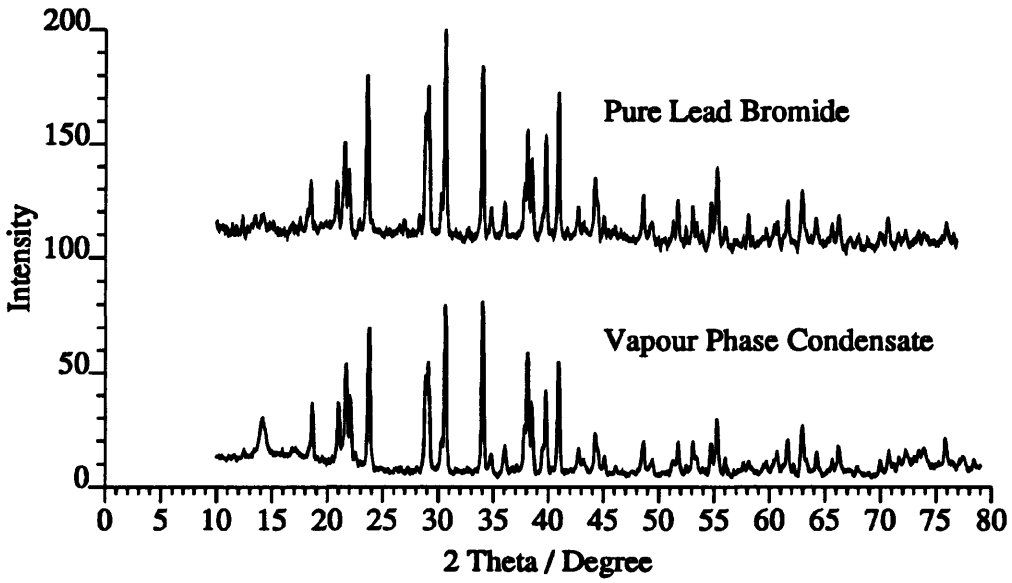

Figure 5.1: The powder diffraction pattern of pure lead bromide and the deposit from the saturation chamber outlet

5.2 The X-ray Diffraction Patterns of the Residual Solid

The evaporation of lead bromide from the 1:1 lead oxybromide during the measurements inevitably produced changes in the sample stoichiometry. Consequently, the composition of the material left in the sample holder at the end of the vapour pressure experiments was of especial interest and the X-ray diffraction patterns of the residual solids were examined to see if there was any evidence of compound formation, mixture production or phase change.

The residues from experiments with the N form of the 1:1 lead oxybromide showed a range of changes in the X-ray diffraction pattern. In some cases the diffraction pattern showed that the material was still the original 1:1 lead oxybromide, but in others the material was a mixture of the original 1:1 lead oxybromide and 2:1 lead oxybromide. The former, was not a particularly unexpected result, because the removal of a small amount of lead bromide might result in no detectable change in the diffraction pattern. The formation of the 2:1 lead oxybromide is reported to occur, albeit very slowly, at temperatures above 375 °C, and a number of experiments were conducted in the temperature range 400 – 480 °C. These were terminated when they had undergone similar weight losses (on a percentage basis). The powder diffraction patterns showed that the samples from the experiments conducted at the higher temperatures contained relatively less 2:1 lead oxybromide. Interestingly, the powder diffraction patterns of the samples containing very little 2:1 lead oxybromide

did not show any evidence of the diffraction pattern of lead oxide! In these cases, the *free* lead oxide which had been left behind by the vacating lead bromide must have remained locked in position with respect to the surrounding 1:1 lead oxybromide lattice. The 2:1 lead oxybromide was most noticeable in the samples where the rate of evaporation had been low and hence the experiment had been of a correspondingly longer duration. These results suggest that the 2:1 lead oxybromide formed in a slow reaction between lead oxide and the 1:1 lead oxybromide.

5.3 The Data from the Vapour Pressure Experiments Involving the N Form 1:1 Lead Oxybromide

It was shown in Section 5.1 that the gaseous species removed by the carrier gas was lead bromide, and the vapour pressure data presented here have been calculated accordingly. The experimental data cover the temperature range 360 – 511 °C and are summarised in Table 5.1.

In the vapour pressure experiments conducted at temperatures in excess of approximately 490 °C, the plots of weight loss versus time were linear, and some typical results are shown in Figure 5.2. In contrast, the experimental data obtained at lower temperatures showed a very slight but progressive decrease in the gradient with time. This behaviour is illustrated by Figures 5.3 and 5.4 and can be explained quite simply as follows. The 1:1 lead oxybromide is known to melt peritectically [2] at 497 °C; between this temperature and that at which the sample becomes completely molten it will consist of two phases, a molten solution of lead bromide and lead oxide, and solid 2:1 lead oxybromide. In this temperature range the composition of the solid phase remains constant, but the composition of the liquid phase (and hence the vapour pressure) is determined by the temperature and not the overall composition of the system. Thus, the evaporation of lead bromide from the liquid phase does not change its composition, it simply shifts the equilibrium between the amount of liquid and solid. In contrast, at temperatures below the melting point the sample exists as a single phase and the composition must change as the lead bromide evaporates; this produces the decrease in the observed vapour pressure. The implications of this change in behaviour are discussed in greater detail in Section 5.4.

Table 5.1: The results of the vapour pressure experiments with the N form of the 1:1 lead oxybromide

Run No.	Temperature °C	Flow Rate $cm^3\ min^{-1}$	Apparent Vapour Pressure (mmHg) Initial	Polynomial	Deviation % of Initial
20[1]	482.2	26.0	1.87×10^{-01}	linear	
21[1]	444.2	26.0	1.04×10^{-02}	1.03×10^{-02}	1
22[2]	425.3	26.0	9.08×10^{-03}		
23[3]	463.6	26.0	5.21×10^{-02}	5.01×10^{-02}	3.8
24[3]	480.7	26.0	9.70×10^{-02}	linear	
25[3]	499.8	26.0	1.98×10^{-01}	linear	
26	463.0	26.1	6.08×10^{-02}	6.14×10^{-02}	1
27	480.3	26.1	9.88×10^{-02}	linear	
28	511.6	26.1	3.70×10^{-01}	linear	
29	511.6	19.6	3.86×10^{-01}	linear	
30	511.6	19.3	3.86×10^{-01}	linear	
31	511.6	14.1	4.08×10^{-01}	linear	
32	511.5	29.5	3.52×10^{-01}	linear	
33	511.5	22.3	3.65×10^{-01}	linear	
34	480.4	22.3	1.11×10^{-01}	1.11×10^{-01}	0
35	480.4	22.1	1.06×10^{-01}	1.06×10^{-01}	0
36	480.4	22.1	1.10×10^{-01}	1.11×10^{-01}	0
37	480.3	16.9	1.16×10^{-01}	1.16×10^{-01}	0
38	463.4	16.9	6.37×10^{-02}	6.47×10^{-02}	1.6
39	463.4	16.9	6.67×10^{-02}	6.47×10^{-02}	3
40	463.4	16.9	6.47×10^{-02}	6.53×10^{-02}	0.9
41	463.5	16.5	7.16×10^{-02}	6.79×10^{-02}	5
42	463.3	21.7	5.67×10^{-02}	5.66×10^{-02}	0.2
43	463.3	29.1	5.54×10^{-02}	5.59×10^{-02}	0.9
44	463.3	30.0	5.33×10^{-02}	5.31×10^{-02}	0.4
45	463.3	34.7	4.75×10^{-02}	4.81×10^{-02}	1.3
46	463.3	10.1	7.59×10^{-02}	8.01×10^{-02}	5.5
47	463.3	25.7	5.57×10^{-02}	5.62×10^{-02}	0.9
48	463.3	11.5	7.38×10^{-02}	7.58×10^{-02}	2.7
49	463.3	21.1	5.88×10^{-02}	6.00×10^{-02}	2.0

[1], sample was not prepared in sealed container

[2], based on three data points!

[3], continuation of previous experiment (no sample change)

The results for the vapour pressure experiments with the N form of the 1:1 lead oxybromide, continued...

Run No.	Temperature °C	Flow Rate $cm^3\ min^{-1}$	Apparent Vapour Pressure (mmHg) Initial	Polynomial	Deviation % of Initial
50	463.3	21.1	6.05×10^{-02}	6.04×10^{-02}	0.2
51	441.0	21.1	2.28×10^{-02}	2.50×10^{-02}	10.0
52	441.0	21.4	2.37×10^{-02}	2.60×10^{-02}	9.7
53	441.0	24.6	2.33×10^{-02}	2.36×10^{-02}	1.3
54	441.0	24.6	2.34×10^{-02}	2.36×10^{-02}	0.8
55	440.8	24.6	2.28×10^{-02}	2.29×10^{-02}	0.4
62[4]	441.9	30.5	3.15×10^{-02}	2.80×10^{-02}	11.0
63	464.9	30.5	8.30×10^{-02}	8.52×10^{-02}	2.7
64	464.9	38.0	6.87×10^{-02}	6.87×10^{-02}	0.0
65	464.9	25.2	8.45×10^{-02}	7.78×10^{-02}	8.0
66	464.7	19.3	8.08×10^{-02}	8.61×10^{-02}	6.6
67	464.7	14.0	9.11×10^{-02}	9.42×10^{-02}	3.4
68	464.7	29.4	7.06×10^{-02}	7.00×10^{-02}	0.8
69	430.4	29.6	1.80×10^{-02}	1.87×10^{-02}	3.9
70	430.4	19.5	1.94×10^{-02}	2.24×10^{-02}	15.0
71	430.4	19.0	2.07×10^{-02}	2.03×10^{-02}	1.9
72	430.4	8.70	2.90×10^{-02}	3.02×10^{-02}	4.1
73	430.0	8.81	2.79×10^{-02}	2.90×10^{-02}	3.9
74	430.0	38.2	1.75×10^{-02}	1.75×10^{-02}	0.0
75	430.0	50.3	1.64×10^{-02}	1.55×10^{-02}	5.5
76	430.0	24.9	1.91×10^{-02}	1.98×10^{-02}	3.7
77	430.0	32.9	1.76×10^{-02}	1.77×10^{-02}	0.6
78	407.5	32.6	6.88×10^{-03}	6.93×10^{-03}	0.7
79	406.4	23.7	7.48×10^{-03}	7.27×10^{-03}	2.8
80	406.4	35.7	6.54×10^{-03}	6.00×10^{-03}	8.2
81	399.7	35.7	4.93×10^{-03}	5.12×10^{-03}	3.8
82	399.6	25.1	5.31×10^{-03}	4.96×10^{-03}	6.6
84	378.0	25.3	1.78×10^{-03}	2.04×10^{-03}	14.6
85	411.7	25.3	8.86×10^{-03}	9.25×10^{-03}	4.4
86	414.7	25.3	9.90×10^{-03}	9.17×10^{-03}	7.0
87	422.0	25.3	1.37×10^{-02}	1.40×10^{-02}	2.0
88	360.4	25.3	8.66×10^{-04}	8.67×10^{-04}	0.1

[4], twin pan sample holder introduced

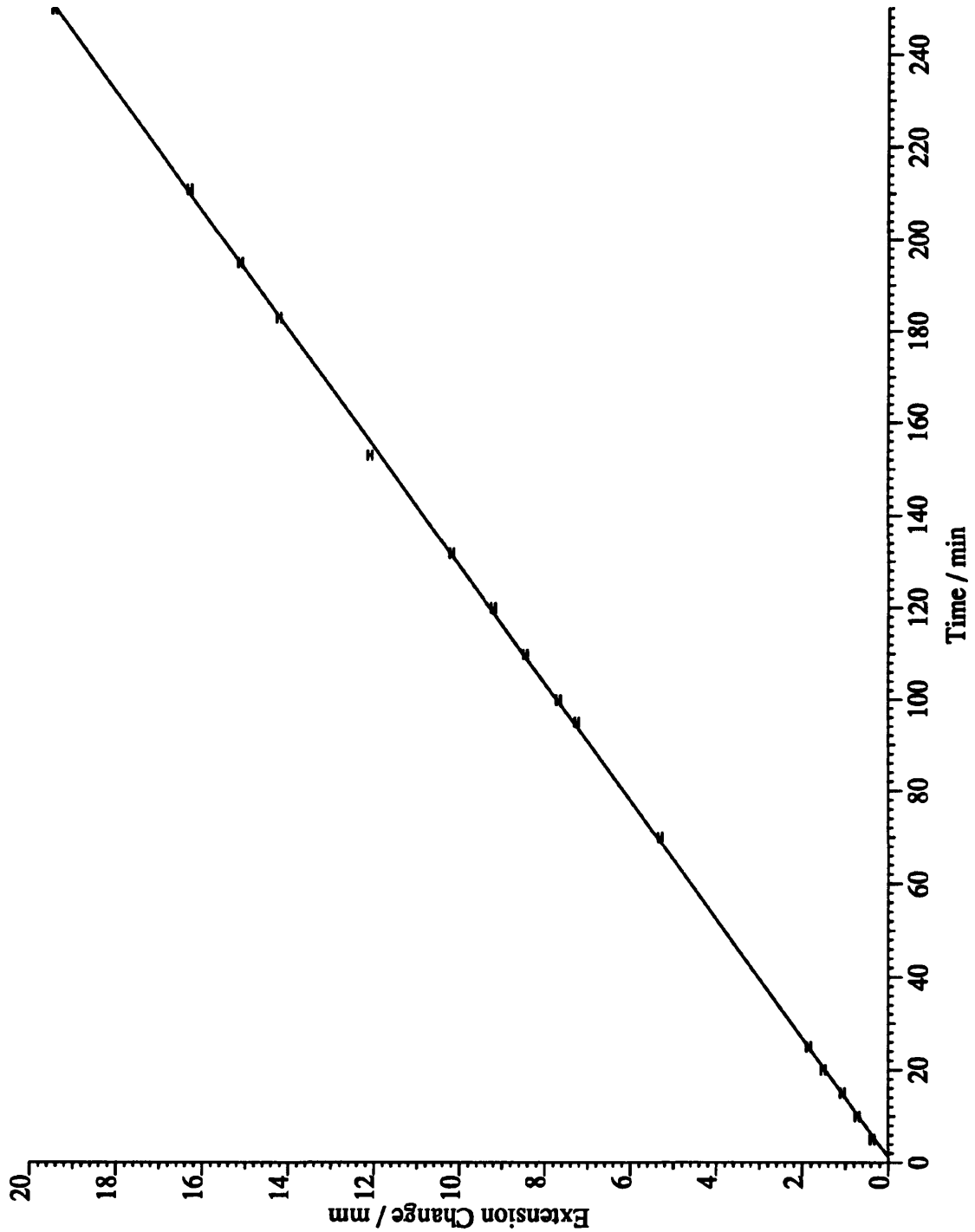

Figure 5.2: The change in extension of the quartz spring with respect to time for a 1:1 lead oxybromide sample at 511 °C with a carrier gas flow rate of 19.3 cm^3 min^{-1}

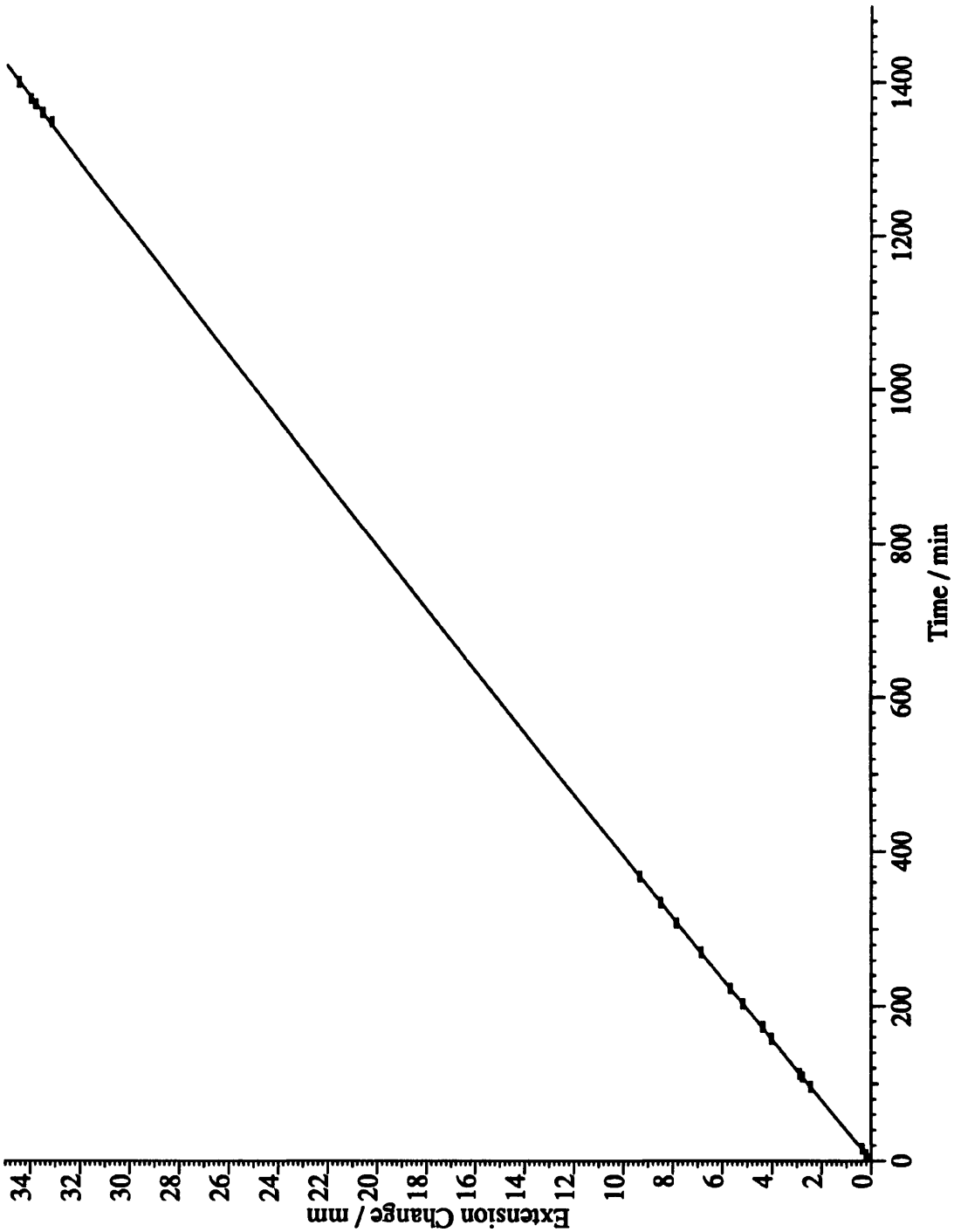

Figure 5.3: The change in extension of the quartz spring with respect to time for a 1:1 lead oxybromide sample at 480 °C with a carrier gas flow rate of 22.1 cm^3 min^{-1}

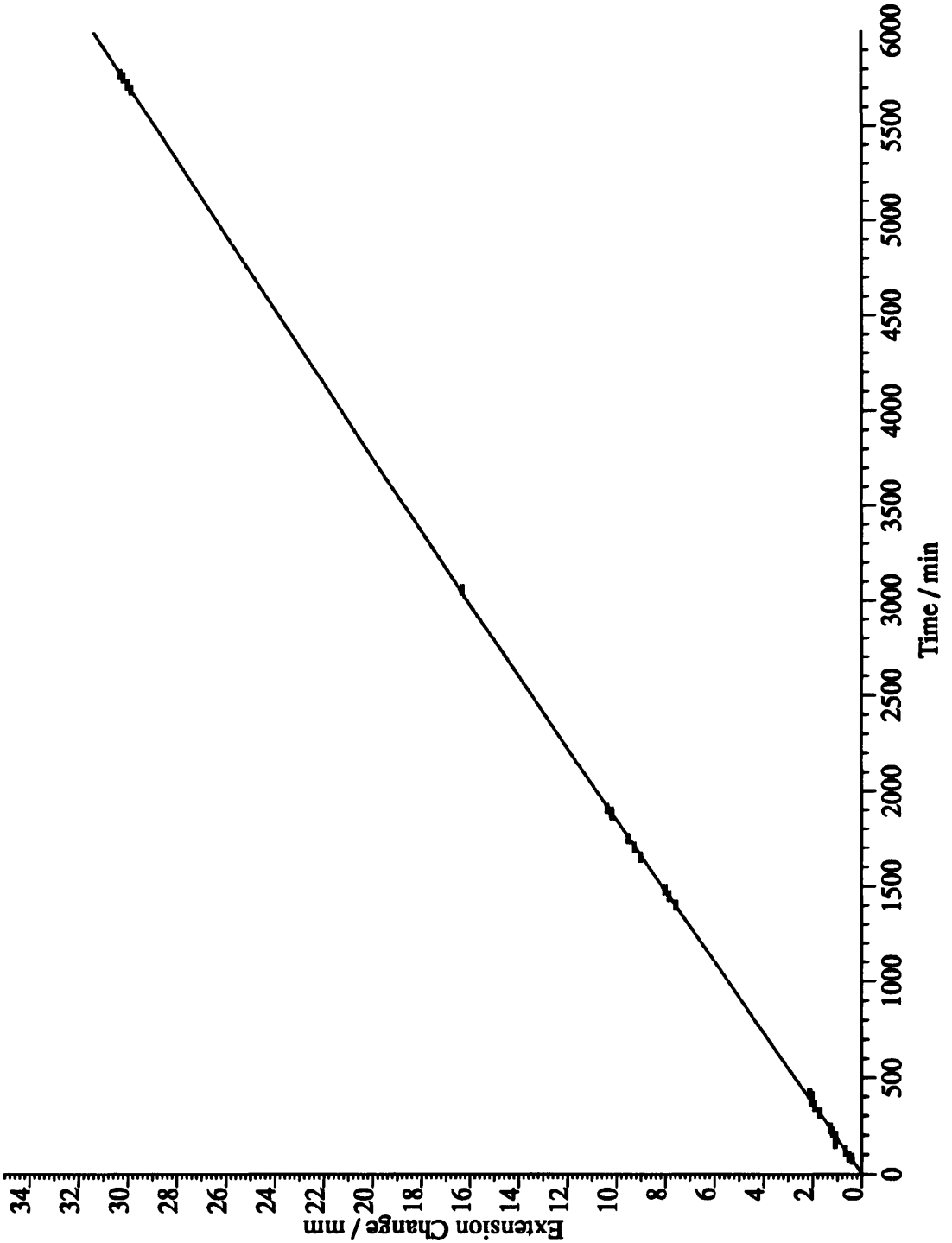

Figure 5.4: The change in extension of the quartz spring with respect to time for a 1:1 lead oxybromide sample at 441 °C with a carrier gas flow rate of 21.1 cm^3 min^{-1}

The data from experiments in which the observed rate of weight loss was constant were simply processed in the manner described for lead bromide in Chapter 4, but this was clearly inadequate for the remainder of the experimental results. The nonlinearity of the change in spring extension with time also made the correction for variation in atmospheric pressure (see Chapter 4) less reliable. In the majority of cases this correction was only of the order of 0.5 % of the total change in extension at any point, but when the corrections were applied the corrected curves were generally smoother.

In an attempt to determine the most reliable and realistic method of analysis two approaches were used. First of all a linear regression of the type $Y = MX + C$ was performed on sections of the data which approximated to a 2 mm change in extension. In addition, the complete set of data was fitted by a second degree polynomial regression analysis. In general, the vapour pressure calculated from the initial slope of the polynomial regression of all of the data and that resulting from a linear regression of the initial data points were in good agreement. In the five experiments where the slopes differed by 10 % or more, the plot of change in extension versus time showed that the initial gradient of the polynomial was too steep, and visual inspection of these plots showed that a small error in the measurement of the spring extension early in the experiment had dramatically altered the initial slope of the polynomial fit. The root mean square deviation of the vapour pressure calculated from the slopes of the polynomial and linear regression (excluding the five experiments in which the deviation was artificially high) was 3.8 % and this showed that both treatments give essentially the same result. In view of these findings the vapour pressures used in the remainder of this work were those calculated from the initial slope of the plot of extension versus time. In the cases where the initial slope provided by the polynomial fit differed markedly from that obtained from the linear regression of the initial set of data points, both values have been included in any calculations and/or graphs for completeness.

5.3.1 Confirmation of the Existence of a Plateau Region for the 1:1 Lead Oxybromide

The vapour pressure of the 1:1 lead oxybromide measured in these experiments was several orders of magnitude higher than those measured in the experiments involving pure lead bromide. In consequence, it was necessary to ascertain that a region existed in which the apparent vapour was independent of the flow rate of carrier gas for this solid.

Figures 5.5 - 5.7 show the variation of apparent vapour pressure with flow rate at temperatures between 430 and 512 °C. In all cases there is in effect a plateau region for flow rates between approximately 20 to 30 $cm^3\ min^{-1}$. The data in these figures were taken

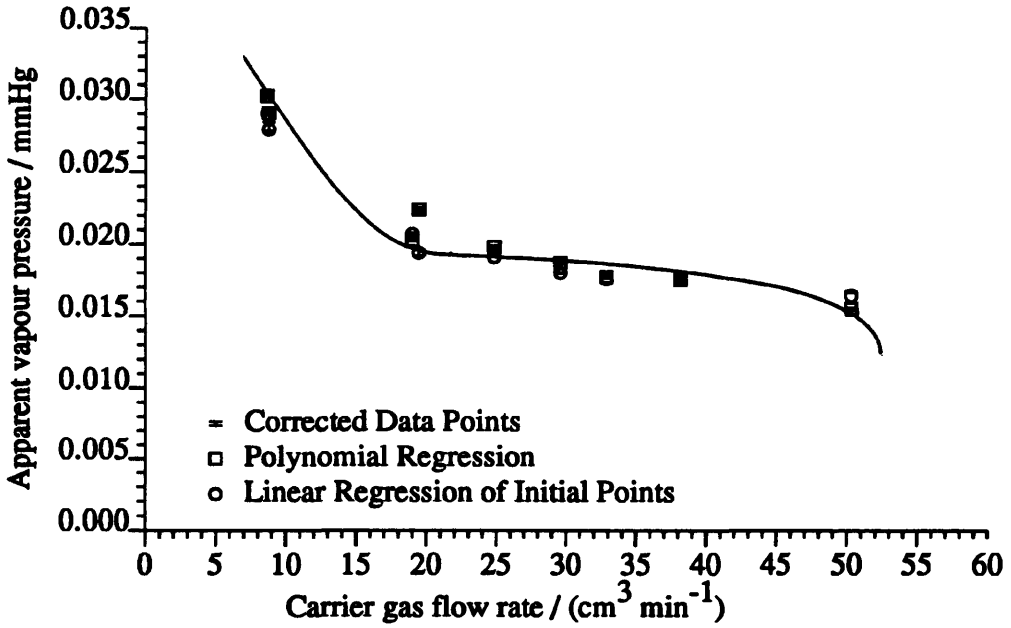

Figure 5.5: Apparent vapour pressure versus carrier gas flow rate at 430.4 °C

from Table 5.1, but a correction has been applied to account for the slight variation in temperature between experiments. The vapour pressure equation for the 1:1 lead oxybromide derived in this work was used to calculate the magnitude of the correction and the raw and corrected data are presented in Figure 5.5 to illustrate the magnitude of the correction.

Figure 5.8 shows the familiar plot of $\log_{10}(p/\text{mmHg})$ versus reciprocal temperature for the experimental data obtained in the temperature range 360 to 511 °C. A linear least squares regression of the data corresponding to temperatures between 360 and 497 °C provides the following vapour pressure equation for the 1:1 lead oxybromide

$$\log_{10}(p/\text{mmHg}) = 10.00 \pm 0.13 + \frac{-8293 \pm 91\ K}{T} \qquad (5.1)$$

and an enthalpy of sublimation of 158.8 ± 2 kJ mol^{-1}.

The 1:1 lead oxybromide melts peritectically at 497 °C to give a liquid solution of lead bromide and lead oxide, plus solid 2:1 lead oxybromide, but the sample becomes completely molten at approximately 680 °C. In this intermediate region the relative amounts of the two phases, and therefore the composition of the liquid is dictated by the temperature and the mole fraction of lead bromide in the liquid decreases as the temperature increases. It is important to note that the partial pressure of lead bromide comes predominantly from

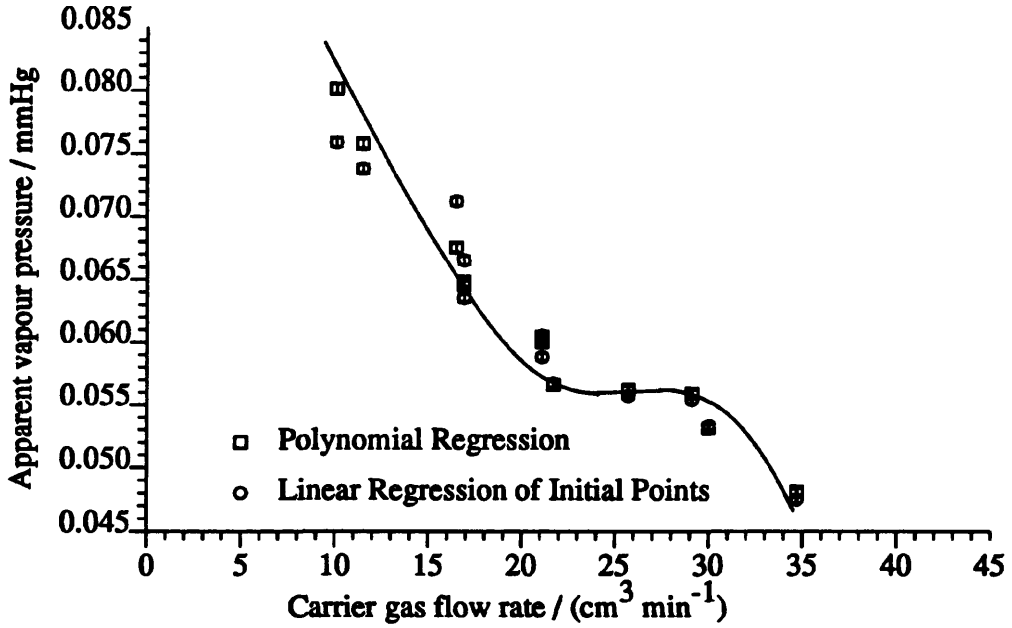

Figure 5.6: Apparent vapour pressure versus carrier gas flow rate at 463.3 °C

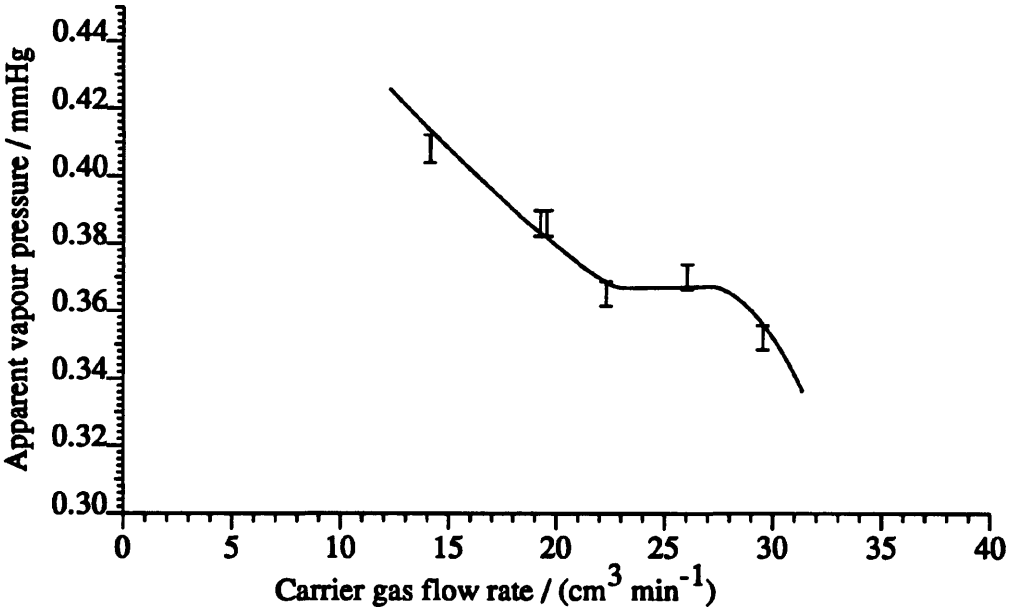

Figure 5.7: Apparent vapour pressure versus carrier gas flow rate at 511.6 °C

Table 5.2: Vapour pressure data for lead oxide - lead bromide mixtures, Belyaev and Mareskin.

Mole Fraction of lead bromide	A ±160	B ±0.003	Temperature Range / K
1.0	6789	8.672	819-1093
0.9	7054	8.854	882-1028
0.8	7054	8.854	913-1018
0.6	6830	8.486	918-1090
0.5	6819	8.424	971-1074
0.333	6965	8.373	993-1118
0.24	6882	8.204	993-1116
0.12	8718	9.474	1023-1127

the liquid; Raoult's law states that the partial pressure of any component in a mixture is directly proportional to its mole fraction and so in this system, the partial pressure of lead bromide is controlled by the composition of the liquid. The net effect is that the increase in the vapour pressure with temperature is opposed by the decrease in mole fraction of lead bromide in the liquid. It follows, that a plot of $\log_{10}(p/\text{mmHg})$ versus reciprocal temperature is not necessarily linear in this region and the data obtained in this work only extend a little into this temperature range.

The vapour pressure data obtained in this work are compared in Figure 5.9 with those obtained by Belyaev and Mareskin [1], and Maslennikov, Spiridonova, Aleksandrov and Emel'yanov [3]. The data of Belyaev and Mareskin and Maslennikov *et al.* are derived by the substitution of the constants A and B, given in Tables 5.2 and 5.3 respectively, into the equation $\log_{10}(p/\text{mmHg}) = -A/T + B$.

It must be noted, however, that the vapour pressure of lead bromide from the data of Maslennikov *et al.* is much greater for the mixtures of lead bromide and lead oxide than it is for pure lead bromide. For example, the calculated partial pressure of lead bromide above a mixture containing 0.9 mole fraction of lead bromide is approximately 100 times larger than that of pure lead bromide! As a result this data must be discounted.

Table 5.4 compares the partial pressure of lead bromide above a liquid mixture of lead bromide and lead oxide, measured by Belyaev and Mareskin at 750 K, with that calculated on the assumption that the molten mixture behaves ideally. With the exception of the mixture containing 0.12 mole fraction of lead bromide, the activity coefficient of lead

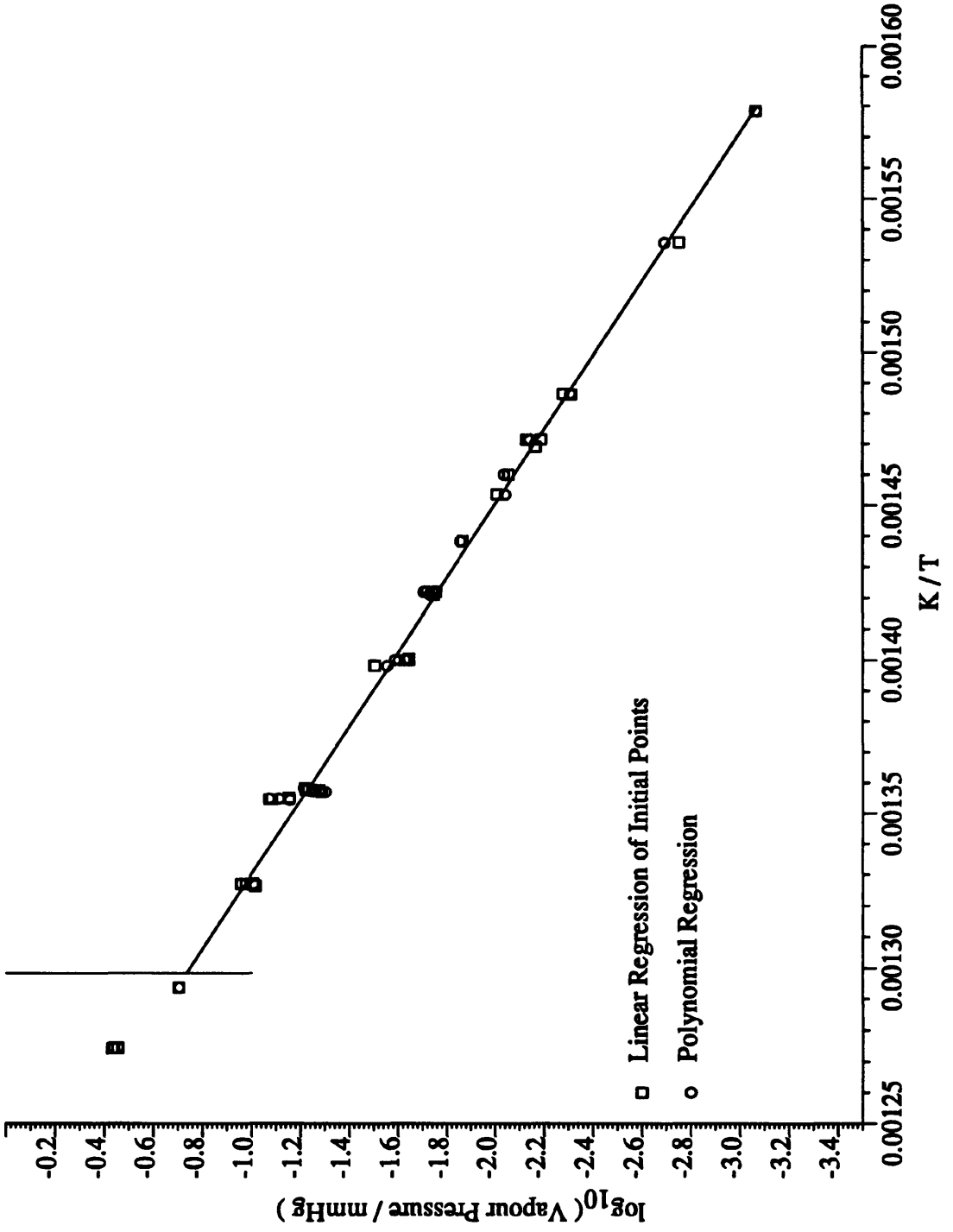

Figure 5.8: $\log_{10}$(vapour pressure / mmHg) versus $\frac{K}{T}$ for the N form of 1:1 lead oxybromide

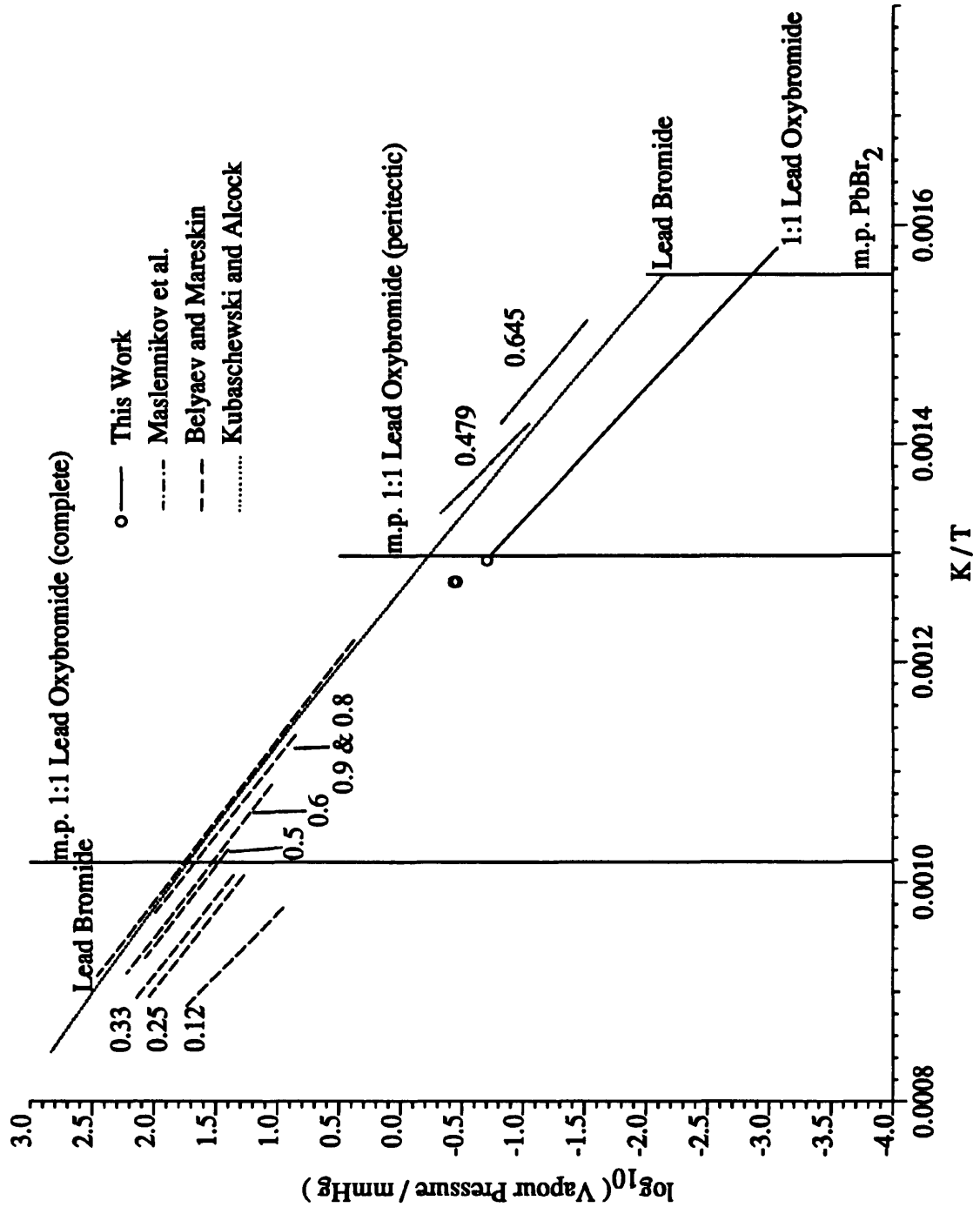

Figure 5.9: $\log_{10}$(vapour pressure / mmHg) versus $\frac{K}{T}$ data for the lead oxide / lead bromide system. The labels refer to the mole fraction of lead bromide.

Table 5.3: Vapour pressure data for lead oxide - lead bromide mixtures, Maslennikov *et al.*

Mole Fraction of lead bromide	A	B	Temperature Range / K	Enthalpy of Sublimation kJ mol^{-1}
0.479	8922	11.6065	705-748	158.6
0.6445	7462	9.7673	661-705	154.9
0.842	8232	12.4004	586-631	152.8
0.901	7222	11.0858	570-616	147.3

Table 5.4: Activity coefficient for lead bromide / lead oxide mixtures @ 750 °C

Mole Fraction of lead bromide	$\log_{10}$ (p/mmHg)	Vapour Pressure/mmHg Experimental	Predicted	Activity Coefficient
1.0	2.0366	108.8	108.8	1.00
0.9	1.9596	91.1	97.9	0.93
0.8	1.9596	91.1	87.0	1.05
0.6	1.8105	64.6	65.3	0.99
0.5	1.7593	57.4	54.4	1.06
0.333	1.5656	36.7	36.2	1.01
0.25	1.4777	30.0	27.2	1.10
0.12	0.9352	8.98	13.1	0.69

bromide is very close to unity, and it is likely that the observed scatter about unity reflects the experimental accuracy of the results. Table 5.5 contains similar data calculated by extrapolation of the data to the peritectic decomposition temperature of 497 °C. Here again the activity coefficient is close to unity.

In the present work the vapour pressure of the 1:1 lead oxybromide was measured above and below the peritectic melting point of 497 °C. The highest temperature at which a vapour pressure measurement was made was 512 °C and, at this temperature, the sample would have been molten. For the reasons discussed earlier, the composition of this liquid is governed by the temperature, and the mole fraction of lead bromide in the liquid phase at this temperature was estimated (from the phase diagram) to be 0.63. The measured vapour pressure at this composition is of the order expected from ideal behaviour and this suggests that the liquid phase is behaving as a solution of relatively involatile lead oxide

Table 5.5: Activity coefficient for lead bromide / lead oxide mixtures @ 497 °C

Mole Fraction of lead bromide	$\log_{10}$ (p/mmHg)	Vapour Pressure/mmHg Experimental	Predicted	Activity Coefficient
1.0	-0.1432	0.719	0.719	1.00
0.9	-0.3052	0.495	0.647	0.76
0.8	-0.3052	0.495	0.575	0.86
0.6	-0.3824	0.414	0.432	0.96
0.5	-0.4301	0.371	0.360	1.03
0.333	-0.6707	0.214	0.240	0.89
0.25	-0.7319	0.185	0.180	1.03
0.12	-1.846	0.014	0.086	0.162

in much more volatile lead bromide (i.e. Raoult's law behaviour). The activity coefficient of the lead bromide in the solution was estimated to be 0.3.

The activity coefficient calculated on the assumption that the solid 1:1 lead oxybromide behaved as a solution of lead bromide and lead oxide ranged from approximately 0.5 at the peritectic melting point of 497 °C to 0.1 at 360 °C. This suggests that the nature of the 1:1 lead oxybromide is somewhere between a solid solution and a true compound.

5.4 Possible Explanations for the Observed Decrease in Vapour Pressure of the N Form 1:1 Lead Oxybromide with Time

The observed decrease in the rate of evaporation of the sample in experiments conducted below 497 °C means that the partial pressure of lead bromide in the gas stream decreased as the experiment proceeded. One possibility which must be considered is that the evaporation of lead bromide depletes the surface layer to such an extent that equilibrium conditions within the saturation chamber are not maintained. However, this suggestion can be eliminated since a region exists in which the apparent vapour pressure is independent of the flow rate of carrier gas (see Section 5.3.1). This shows that equilibrium conditions have been maintained within the saturation chamber and that the carrier gas has become fully saturated with the vaporising species under these particular conditions.

It has already been shown that lead bromide is removed from the 1:1 lead oxybromide during a vapour pressure experiment and that this results in a change in the overall composition of the residual solid sample (see Sections 5.1 and 5.2). If this change in the mole fraction of lead bromide were sufficiently large, it could affect the apparent vapour pressure of the sample.

In principle there are three possible ways in which this might arise. The first is that the lead oxide left behind by the evaporating lead bromide simply acts as a diluent and another is that this lead oxide reacts with the residual 1:1 lead oxybromide to give 2:1 lead oxybromide. Support for these two possibilities comes from the X-ray diffraction patterns of the residual solids from the vapour pressure experiments (see Section 5.2). In some cases only the pattern for the 1:1 oxybromide was present, which implies free residual lead oxide, but in other cases both 1:1 and 2:1 lead oxybromide were present. The final possibility is that the 1:1 lead oxybromide is a solid solution of lead bromide in lead oxide, as discussed at the end of the previous section. In each of these cases the measured vapour pressure can be related to the composition of the solid, and the following section shows how they have been modelled.

5.5 Modelling of the Experimental Data

It was assumed that the change in vapour pressure was due to the change in composition of the sample and that the apparent vapour pressure of lead bromide was directly proportional to the mole fraction of one component in a multi-component mixture (Raoult's law behaviour). Each of the three possibilities was modelled with the aid of computer programs.

In the first case, it was considered that the evaporating lead bromide left behind a residual solid solution of lead oxide in the 1:1 lead oxybromide, as shown in Equation 5.2. Thus, the solid sample was thought of as 1:1 lead oxybromide diluted by lead oxide. Assuming Raoult's law behaviour, the partial pressure of lead bromide above the sample was directly proportional to the mole fraction of the lead oxybromide in the solid phase. As a result, the variation of vapour pressure with composition was given by Equation 5.3. The vapour pressure of the 1:1 lead oxybromide was calculated from the initial vapour pressure and the mole fraction of the 1:1 lead oxybromide in the sample at the given time, using the weight loss to calculate the mole fraction.

$$x\mathrm{PbO.PbBr}_{2(s)} \rightarrow y\mathrm{PbBr}_{2(g)} + (x-y)\mathrm{PbO.PbBr}_{2(s)} + y\mathrm{PbO}_{(s)} \qquad (5.2)$$

$$p = p^o \left(\frac{n_{\mathrm{PbO.PbBr_2}(s)}}{n_{\mathrm{PbO.PbBr_2}(s)} + n_{\mathrm{PbO}(s)}} \right) \tag{5.3}$$

Where p is the partial pressure of lead bromide in the vapour phase, p^o the vapour pressure of the pure 1:1 lead oxybromide and n_i the molar amount of species i.

In the second case, it was assumed that 2:1 lead oxybromide was formed by the reaction of the *free* lead oxide (left behind by the evaporating lead bromide) with the original 1:1 lead oxybromide. This process is summarised by Equation 5.4 and the vapour pressure relationship is then given by Equation 5.5.

$$x\mathrm{PbO.PbBr_{2(s)}} \rightarrow y\mathrm{PbBr_{2(g)}} + (x-2y)\mathrm{PbO.PbBr_{2(s)}} + y(2\mathrm{PbO.PbBr_{2(s)}}) \tag{5.4}$$

$$p = p^o \left(\frac{n_{\mathrm{PbO.PbBr_{2(s)}}}}{n_{\mathrm{PbO.PbBr_{2(s)}}} + n_{\mathrm{2PbO.PbBr_{2(s)}}}} \right) \tag{5.5}$$

In the third case which was envisaged, the 1:1 lead oxybromide behaved as a solid solution of lead oxide and lead bromide. This scheme is shown in Equation 5.6 and the vapour pressure relationship is shown in Equation 5.7.

$$x\mathrm{PbO_{(s)}} + x\mathrm{PbBr_{2(s)}} \rightarrow x\mathrm{PbO_{(s)}} + (x-y)\mathrm{PbBr_{2(s)}} + y\mathrm{PbBr_{2(g)}} \tag{5.6}$$

$$p = p^o \gamma \left(\frac{n_{\mathrm{PbBr_2}}}{n_{\mathrm{PbBr_2}} + n_{\mathrm{PbO}}} \right) \tag{5.7}$$

where γ is the activity coefficient for lead bromide in the solid solution.

In all three cases the partial pressure of the lead bromide in the vapour phase is also given by

$$p = p_A \left(\frac{n_{\mathrm{PbBr_2}}}{n_{\mathrm{PbBr_2}} + n_{\mathrm{Carrier\ Gas}}} \right) \tag{5.8}$$

where p_A is the atmospheric pressure.

Thus, if the system is at equilibrium, the known atmospheric pressure and partial pressure can be used to calculate the total amount of lead bromide removed by the carrier gas in

any time interval. The plots of the experimental data appeared to be quadratic in nature and in each case when a polynomial regression analysis was preformed on the data with a quadratic polynomial an excellent fit was obtained. It was not immediately obvious why this should be, but all three cases examined lead to a quadratic function for the amount of lead bromide (or mass) evaporating as a function of time. The derivation of these equations is shown in Section 5.5.1.

Two distinct types of computer program were used to simulate the experimental data; the first used a simple iterative calculation and the second solved the quadratic equations relating time to the amount of lead bromide removed by the carrier gas. The parameters supplied to these programs were the initial mass of the sample, the flow rate of carrier gas and the vapour pressure of pure 1:1 lead oxybromide at the particular temperature. A typical comparison of the theoretical change in extension of the spring as a function of time with the experimental data is shown in Figure 5.10. This figure gives the results for both the quadratic and iterative simulations for one experiment, assuming that the 1:1 lead oxybromide behaved as a simple solid solution and both are very close to the experimental results.

It was noted, however, that the curve from the iterative simulation always lay above the quadratic solution. The iterative calculations were performed with a time interval of 1 second, as experiments proved that consistent results were obtained provided a time interval of less than 6 seconds was employed. Thus, the difference in the quadratic and iterative simulations cannot be due to the use of a time step in the iterative calculation which was too large. However, it should be noted that any error in the calculated change in extension for the iterative calculation is cumulative, so that this simulation could become less accurate with time. Similarly, the magnitude of the terms in the quadratic equation are such that the calculations for the early points were being performed at the limit of numerical accuracy of the computer. In this case, the solutions become more accurate as time increases.

Having established that the computer programs did not contain any obvious errors, the results of the two types of simulation were compared to see if they provided any clues which could pinpoint the cause of the discrepancy. The simulation results for the experiment shown in figure 5.10 are given in Table 5.6. For each point in the table there is a discrepancy in the calculated change in extension, but the difference in both the mole fraction of lead bromide and the vapour pressure is extremely small. In view of the errors inherent in both simulations the results can be considered to be in reasonable agreement. Nevertheless, the quadratic solutions should become more accurate than those from the iterative simulation, and hence they have been used in the following discussion.

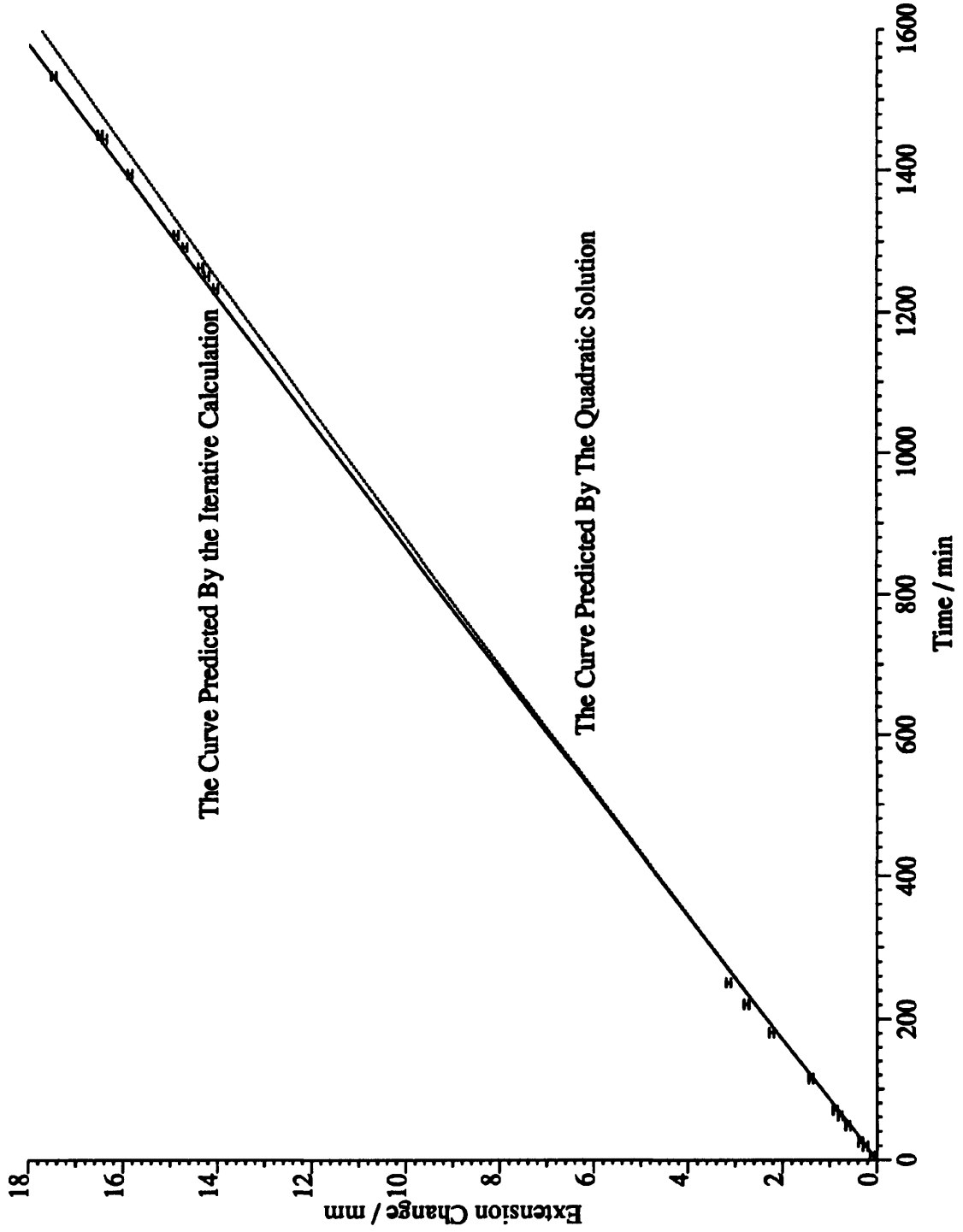

Figure 5.10: A comparison of the change in extension of the quartz spring with respect to time for the 1:1 lead oxybromide behaving as a solid solution of lead bromide and lead oxide as predicted by the iterative and quadratic simulations

Table 5.6: The results of a vapour pressure simulation for the N form of the 1:1 lead oxybromide

Time /min	Extension Change /mm			Mole Fraction of Lead Bromide		Vapour Pressure /mmHg	
	Experimental	Iterative	Quadratic	Iterative	Quadratic	Iterative	Quadratic
6	0.11	0.07	0.07	0.4999	0.4999	0.0679	0.0679
19	0.25	0.22	0.22	0.4996	0.4996	0.0679	0.0679
25	0.35	0.29	0.29	0.4995	0.4995	0.0678	0.0678
48	0.62	0.56	0.56	0.4992	0.4992	0.0678	0.0678
62	0.78	0.73	0.72	0.4989	0.4989	0.0678	0.0678
70	0.88	0.82	0.82	0.4988	0.4988	0.0677	0.0677
115	1.40	1.34	1.34	0.4980	0.4980	0.0676	0.0676
181	2.23	2.11	2.11	0.4969	0.4969	0.0675	0.0675
221	2.76	2.58	2.57	0.4963	0.4963	0.0674	0.0674
251	3.14	2.93	2.91	0.4958	0.4958	0.0673	0.0673
141	14.04	14.15	13.86	0.4790	0.4794	0.0651	0.0651
159	14.23	14.35	14.05	0.4787	0.4791	0.0650	0.0651
171	14.36	14.48	14.18	0.4785	0.4789	0.0650	0.0650
200	14.70	14.81	14.49	0.4780	0.4785	0.0649	0.0650
217	14.89	15.00	14.67	0.4777	0.4782	0.0649	0.0649
302	15.86	15.95	15.58	0.4762	0.4768	0.0647	0.0648
352	16.40	16.51	16.11	0.4753	0.4760	0.0646	0.0646
358	16.50	16.57	16.17	0.4752	0.4759	0.0645	0.0646
442	17.49	17.51	17.06	0.4738	0.4745	0.0643	0.0644

Table 5.7: The effect of the evaporation of 0.05 g of lead bromide from 0.5 g of 1:1 lead oxybromide on the residue

Compound	Mass /g	Amount /mol
$PbO.PbBr_2$	0.5	8.471×10^{-4}
$PbBr_2$	0.05	1.362×10^{-4}

The mole fraction of 1:1, in 1:1 and PbO

$$\frac{(8.471\times10^{-4} - 1.362\times10^{-4})_{1:1}}{(8.471\times10^{-4} - 1.362\times10^{-4})_{1:1}+(1.362\times10^{-4})_{PbO}} = 0.8392$$

The mole fraction of 1:1, in 1:1 and 2:1

$$\frac{(8.471\times10^{-4} - 2\times1.362\times10^{-4})_{1:1}}{(8.471\times10^{-4} - 2\times1.362\times10^{-4})_{1:1}+(1.362\times10^{-4})_{2:1}} = 0.7342$$

The mole fraction of $PbBr_2$, in $PbBr_2$ and PbO

$$\frac{(8.471\times10^{-4} - 1.362\times10^{-4})_{PbBr_2}}{(8.471\times10^{-4} - 1.362\times10^{-4})_{PbBr_2}+(8.471\times10^{-4})_{PbO}} = 0.4563$$

The results of the simulations for a typical experiment provided by each of the three models are compared in Figure 5.11 and these can be divided into two sets. The model in which the 1:1 lead oxybromide is assumed to decompose to give lead oxide and lead bromide, and the other in which the lead oxide released by the evaporating lead bromide is assumed to react with more 1:1 lead oxybromide to produce 2:1 lead oxybromide, gave very similar results and form one set. Significantly different results were obtained when the 1:1 lead oxybromide was treated as a simple solid solution and these form the second set. The data presented in Table 5.7 show how the evaporation of 0.05 g of lead bromide from 0.5 g of 1:1 lead oxybromide affects the mole fraction for each of the three systems under consideration. A comparable decrease in the partial pressure of lead bromide is predicted by the two models in which it is assumed to depend upon the mole fraction of 1:1 lead oxybromide in the solid phase. In the case of the solid solution, however, the decrease in the mole fraction of lead bromide is proportionally less, as the initial mole fraction of lead bromide is only 0.5. Thus, the decrease in vapour pressure will be also less in this case.

In 86 % of the simulations the experimental data were more accurately reproduced using the simple lead oxide / lead bromide mixture model. Some typical simulation results are shown in Figure 5.12, which is representative of a reasonable simulation, and Figures 5.14

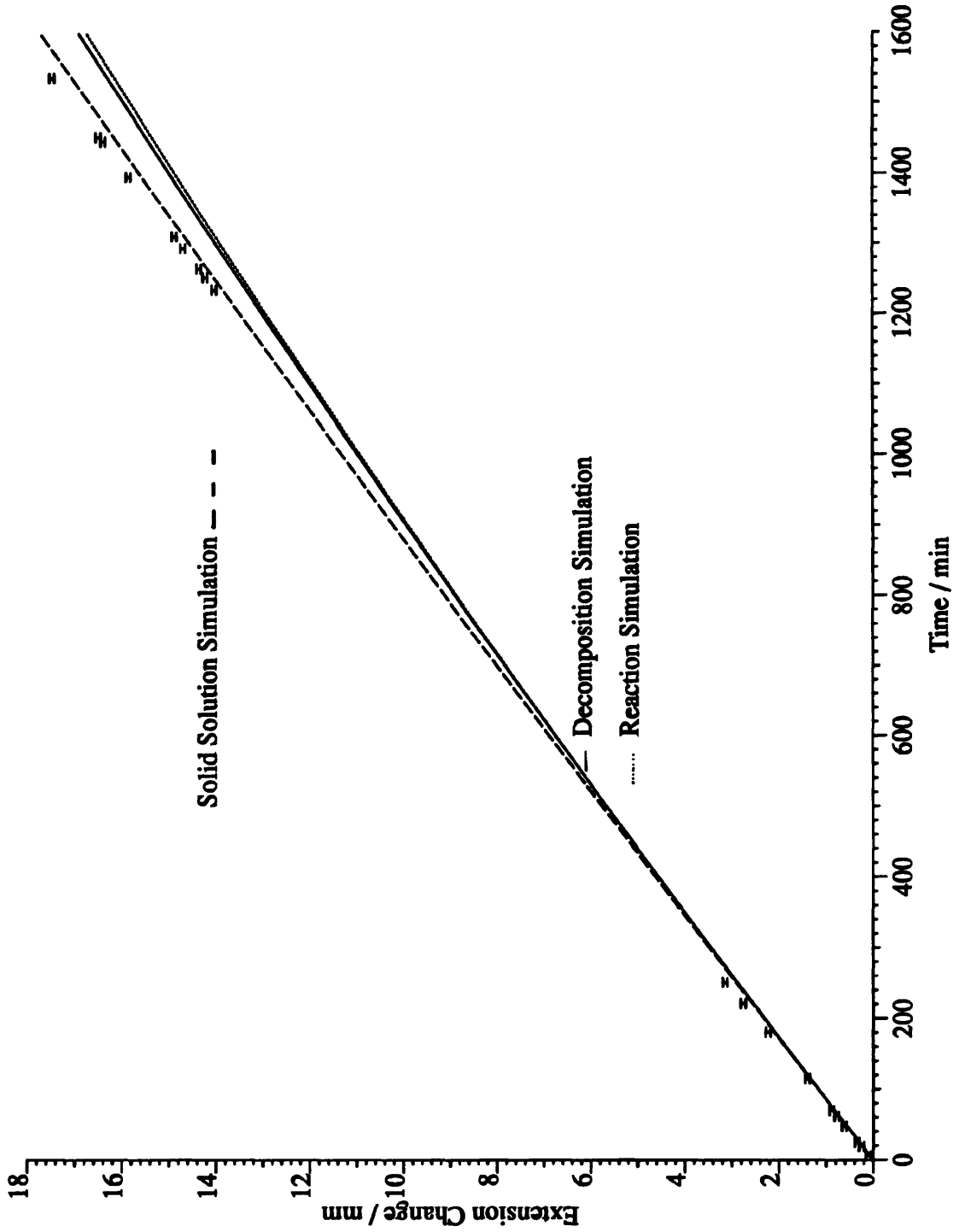

Figure 5.11: A comparison of the change in extension of the quartz spring with respect to time for the 1:1 lead oxybromide as predicted by the three models

and 5.13 which show two of the more disappointing fits. Even in these latter examples the discrepancy in the final change in extension is only 5 %. In the majority of cases the changes in extension predicted by this model were slightly less than those measured experimentally. Thus, the simulations suggest that the behaviour of the 1:1 lead oxybromide was more akin to that of a solid solution than a compound, in accord with the suggestion made earlier in this Chapter.

5.5.1 The Derivation of the Quadratic Equations used in the Simulation of the Vapour Pressure Variation with Composition for the N form 1:1 Lead Oxybromide

Consider the first case where the vapour pressure is assumed to be proportional to the mole fraction of the 1:1 lead oxybromide in a solid solution of the 1:1 lead oxybromide and lead oxide. The process and the variation of the vapour pressure with composition are described by Equations 5.2 and 5.3.

The relationship between the partial pressure of lead bromide p and the total pressure has already been given in Equation 5.7 (reproduced here as Equation 5.9 for convenience)

$$p = p_A \left(\frac{n_{B(g)}}{n_{B(g)} + n_{C(g)}} \right) \tag{5.9}$$

but the partial pressure of lead bromide is also related to the composition of the solid solution as follows

$$p = p^o \left(\frac{n_{OB(s)}}{n_{OB(s)} + n_{O(s)}} \right) \tag{5.10}$$

where the subscripts B, O, OB and C denote lead bromide, lead oxide, 1:1 lead oxyhalide and carrier gas respectively and n the molar amount.

At all times the amount of free lead oxide is equal to the amount of evaporated lead bromide and hence

$$n_B = n_O \tag{5.11}$$

Thus

$$p_A \left(\frac{n_{B(g)}}{n_{B(g)} + n_{C(g)}} \right) = p^o \left(\frac{n_{OB(s)}}{n_{OB(s)} + n_{B(s)}} \right) \tag{5.12}$$

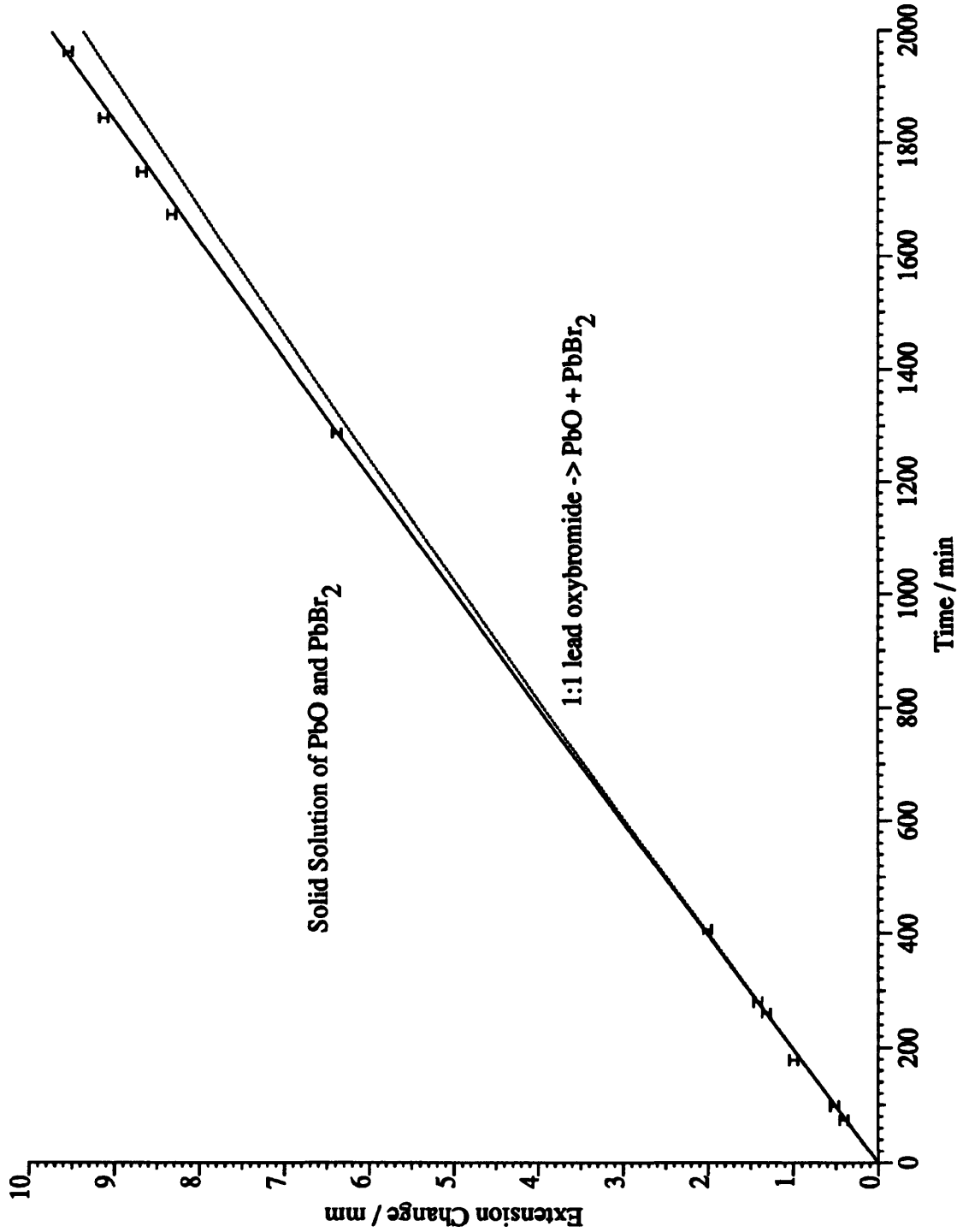

Figure 5.12: The results of the quadratic equation based simulations for a 1:1 lead oxybromide sample at 430 °C with a carrier gas flow rate of 24.9 cm^3 min^{-1}

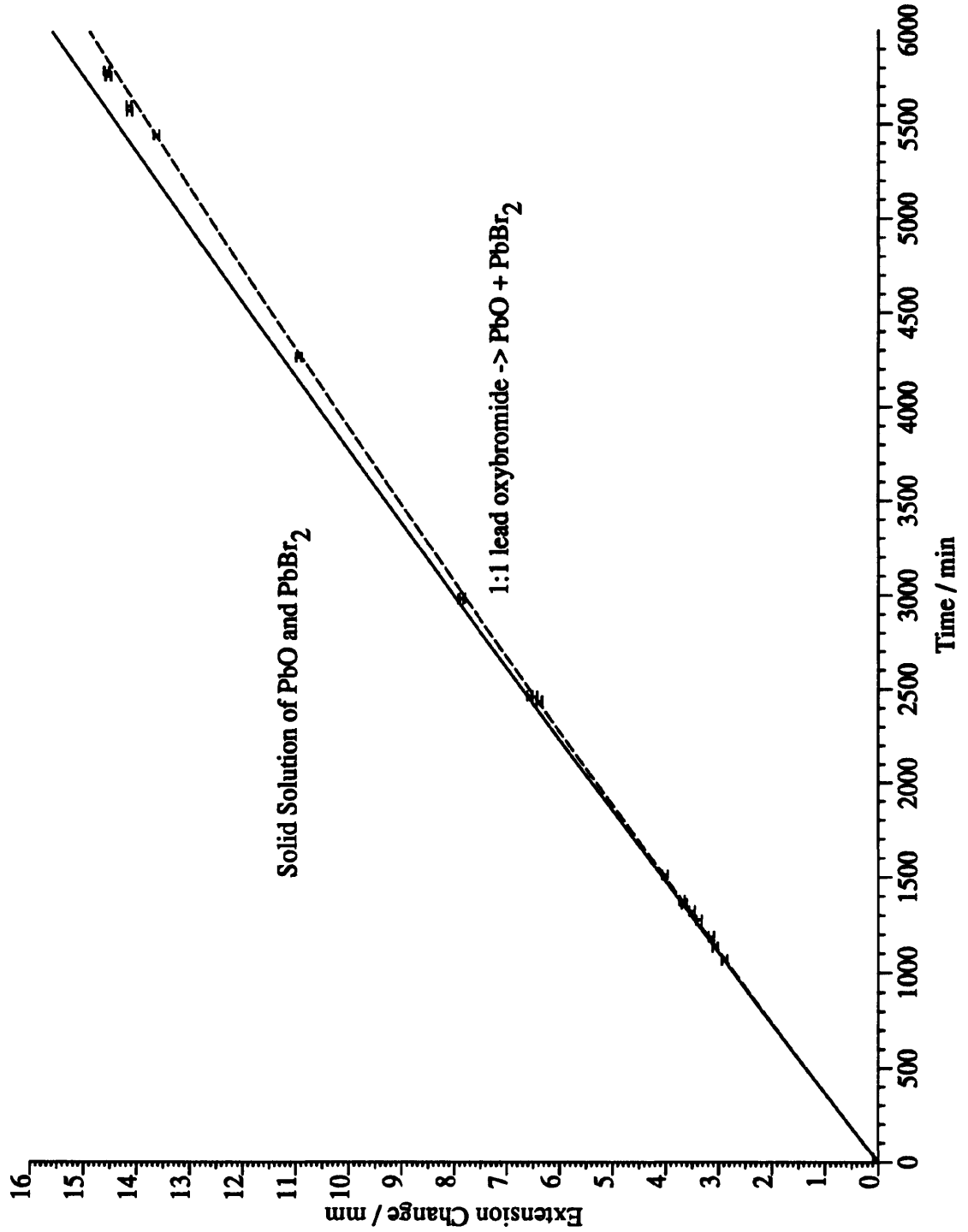

Figure 5.13: The results of the quadratic equation based simulations for a 1:1 lead oxybromide sample at 430 °C with a carrier gas flow rate of 8.8 cm^3 min^{-1}

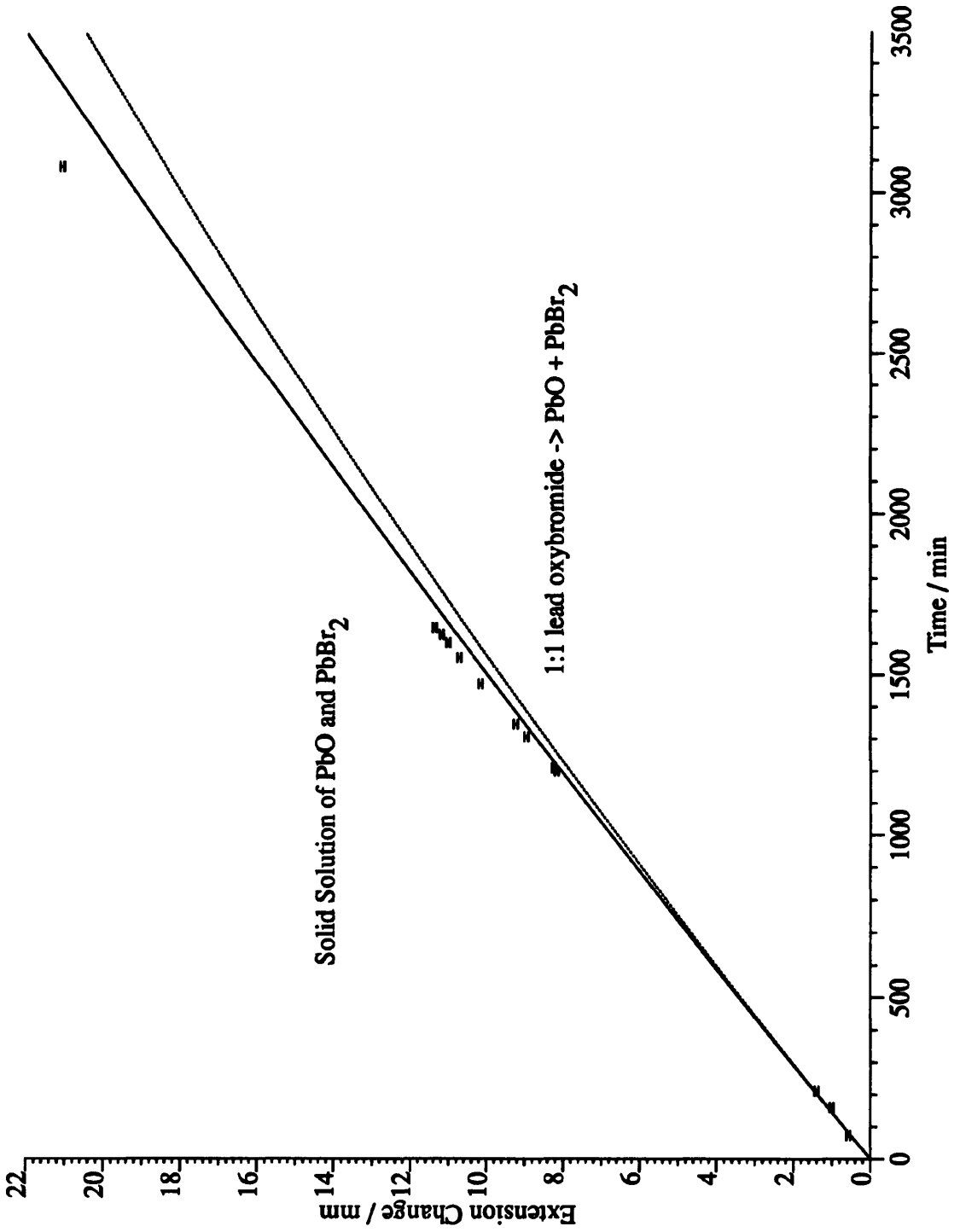

Figure 5.14: The results of the quadratic equation based simulations for a 1:1 lead oxybromide sample at 430 °C with a carrier gas flow rate of 38.2 cm^3 min^{-1}

Rearranging gives

$$p_A(n_{B(g)})(n_{OB(s)} + n_{B(s)}) = p^o(n_{OB(s)})(n_{B(g)} + n_{C(g)}) \tag{5.13}$$

From Equation 5.2 the amount of the 1:1 lead oxybromide $n_{OB(s)}$ at any time is related to the initial amount $n^o_{OB(s)}$ by

$$n_{OB(s)} = n^o_{OB(s)} - n_{B(g)} \tag{5.14}$$

Substituting into Equation 5.13 gives

$$p_A n_{B(g)}(n^o_{OB(s)} - n_{B(g)} + n_{B(g)}) = p^o(n^o_{OB(s)} - n_{B(g)})(n_{B(g)} + n_{C(g)}) \tag{5.15}$$

Expanding

$$p_A n_{B(g)} n^o_{OB(s)} = p^o n_{B(g)} n^o_{OB(s)} + p^o n^o_{OB(s)} n_{C(g)} - p^o n^2_{B(g)} - p^o n_{B(g)} n_{C(g)} \tag{5.16}$$

Rearranging into a quadratic form and substituting for $n_{C(g)} = \frac{Ft}{V_m}$, gives

$$n^2_{B(g)} p^o + n_{B(g)}(n^o_{OB(s)}(p_A - p^o) + p^o \frac{Ft}{V_m}) - P^o n^o_{OB(s)} \frac{Ft}{V_m} = 0 \tag{5.17}$$

The positive root of Equation 5.17 where p^o/mmHg is the vapour pressure of pure 1:1 lead oxybromide, p_A/mmHg the atmospheric pressure, F /cm^3 min^{-1} the flow rate of carrier gas, and V_m/cm^3 mol^{-1} the molar gas volume gives the amount of lead bromide removed by the carrier gas stream in a time t. The quadratic is of the form $ax^2 + bx + c$ where b and c are functions of time and the root was found through the standard formula

$$n_{B(g)} = \frac{-b \pm \sqrt{b^2 - 4ac}}{2a} \tag{5.18}$$

A similar treatment of the system described by Equations 5.4 and 5.5, in which the lead oxide left behind by the evaporating lead bromide is assumed to react with the 1:1 lead oxybromide to form the 2:1 lead oxybromide, furnishes the following quadratic equation

$$n^2_{B(g)}(p_A - 2p^o) + n_{B(g)}(p^o n^o_{OB(s)} - 2p^o n_{C(g)} - p_A n^o_{OB(s)}) + p^o n^o_{OB(s)} n_{C(g)} = 0 \tag{5.19}$$

The third system which was described by Equations 5.6 and 5.7 is subtly different. The vapour pressure over the sample is assumed to be proportional to the mole fraction of lead bromide in a solid solution of lead bromide in lead oxide. In this case the vapour pressure is related to the vapour pressure of pure lead bromide. If the activity coefficient is assumed to remain constant over the limited range of composition covered by the experiment, a quadratic equation can be derived as follows

$$p = p_A \left(\frac{n_{B(g)}}{n_{B(g)} + n_{C(g)}} \right) \tag{5.20}$$

let the activity coefficient be represented by γ

Then

$$p = p^{o}\gamma\left(\frac{n_{B(s)}}{n_{B(s)} + n_{O(s)}}\right) \tag{5.21}$$

Thus

$$p_A\left(\frac{n_{B(g)}}{n_{B(g)} + n_{C(g)}}\right) = p^{o}\gamma\left(\frac{n_{B(s)}}{n_{B(s)} + n_{O(s)}}\right) \tag{5.22}$$

But from equation 5.6

$$n_{B(s)} = n^{o}_{B(s)} - n_{B(g)} \tag{5.23}$$

Thus

$$p_A n_{B(g)}(n^{o}_{B(s)} - n_{B(g)} + n_{O(s)}) = p^{o}\gamma(n_{B(t)-n_{B(g)}})(n_{B(g)} + n_{C(g)}) \tag{5.24}$$

Expanding

$$p_A n_{B(g)} n^{o}_{B(s)} - p_A n^{2}_{B(g)} + p_A n_{B(g)} n_{O(s)} = p^{o}\gamma n_{B(g)} n^{o}_{B(s)} - p^{o}\gamma n^{o}_{B(s)} n_{C(g)} - p^{o}\gamma n_{B(g)} n_{C(g)} \tag{5.25}$$

Rearranging into a quadratic form and substituting $\frac{Ft}{V_m}$ for $n_{C(g)}$ gives

$$n^{2}_{B(g)}(p^{0}\gamma - p_A) + n_{B(g)}(p_A n^{o}_{B(s)} + p_A n_{O(s)} - p^{o}\gamma n^{o}_{B(s)} + p^{o}\gamma\frac{Ft}{V_m}) - p^{o}\gamma n^{o}_{B(s)}\frac{Ft}{V_m} \tag{5.26}$$

which can be solved to obtain the mass of lead bromide in the gaseous phase at any time t.

References

[1] Belyaev I.N. and Mareskin S.A., *Thermodynamics of Lead Oxide Lead Halide Melts. II. Tensimetric Study of the Lead Bromide-Lead Oxide System*, Russian Journal of Physical Chemistry, 49, (4), (1975) p. 619.

[2] Knowles L.M., *Thermal Analysis of the System $PbBr_2$-PbO*, J. Chem. Phys., 19, (1951), p. 1128.

[3] Maslennikov V.P., Spiridonova M.N., Aleksandrov Y.U.A., and Emel'yanov B.V., *Volatility of Lead Compounds*, Trudy Po Khimii I Khimicheskoi Tekhnologii, 2, (1973), p. 146.

Chapter 6

The Determination of the Vapour Pressure of the 2:1 Lead Oxybromide

6.1 The Composition of the Vapour Phase Above 2:1 Lead Oxybromide

The same apparatus was used to measure the vapour pressures of lead bromide, the 1:1 lead oxybromide and the 2:1 lead oxybromide (see Chapter 2). The species evaporating from the 2:1 lead oxybromide was lead bromide. As a result, the effect of its preferential evaporation from the 2:1 lead oxybromide was studied using X-ray powder crystallography. In particular, the diffraction patterns of the residues were examined for evidence of compound formation, mixture production and/or a phase change, and the results are presented in the following section.

6.2 The X-ray Diffraction Patterns of the Residue from the Vapour Pressure Experiments with the 2:1 Lead Oxybromide

The X-ray powder diffraction patterns of the residue from the vapour pressure experiments with 2:1 lead oxybromide demonstrated that in some experiments the 3:1 lead oxybromide was formed when lead bromide was removed by evaporation. In contrast, the powder diffraction pattern of lead oxide was never seen. Thus, the lead oxide left behind by the evaporation of lead bromide, either remained locked into the crystal lattice of the 2:1 lead oxybromide, or reacted with neighbouring 2:1 lead oxybromide to form the 3:1 lead oxybromide.

It should be noted that the diffraction pattern of the 3:1 lead oxybromide was found only with residues which had undergone considerable weight loss. Because the vapour pressure of the 2:1 lead oxybromide is very low, these weight losses were attained in a reasonable length of time only in the experiments conducted at the higher temperatures. Therefore, it is impossible to say with any certainty whether the temperature and duration of the experiment or merely the composition of the sample controlled the formation of the 3:1 lead oxybromide.

6.3 The Data Obtained from the Vapour Pressure Experiments with the 2:1 Lead Oxybromide

The rate of evaporation of lead bromide from the 2:1 lead oxybromide was effectively constant throughout all but one of the experiments and this allowed the vapour pressures presented in Table 6.2 to be calculated using the method described for lead bromide in Chapter 4. The vapour pressures were comparable to those obtained for the 1:1 lead oxybromide, although the temperatures were much higher. In the vapour pressure experiments with both lead bromide and the 1:1 lead oxybromide, the apparent vapour pressure was shown to be independent of the flow rate of carrier gas between approximately 20 and 30 $cm^3\ min^{-1}$. In these cases, the plots of apparent vapour pressure versus flow rate had the expected profile, namely, the apparent vapour pressure rose at low flow rates due to diffusion with the flow of carrier gas, fell at higher flow rates due to incomplete saturation, but remained constant in the intermediate region. Thus, to confirm that the 2:1 lead oxybromide followed the same pattern of behaviour, a number of experiments was conducted at the same temperature but with differing flow rates of carrier gas. Figure 6.1 shows the results of these experiments and confirms the existence of a plateau region for the 2:1 lead oxybromide for flow rates from approximately 20 - 35 $cm^3\ min^{-1}$.

The linearity of the plots of weight loss versus time for the 2:1 lead oxybromide is illustrated by Figure 6.2 and this behaviour is in marked contrast to that of the 1:1 lead oxybromide. In the experiments with the 1:1 lead oxybromide, the rate of evaporation began to decrease long before the overall weight loss displayed in this figure was reached. Table 6.1 compares the effect of evaporating 0.05 g of lead bromide from, firstly, 0.5 g of the 1:1 lead oxybromide and then from 0.5 g of the 2:1 lead oxybromide. In all cases, the change in the mole fraction of the lead oxybromide in the residual solid for comparable systems is greater with the 2:1 lead oxybromide than with the 1:1 lead oxybromide. Hence, the vapour pressure of the 2:1 lead oxybromide was expected to decrease more rapidly than that of the 1:1 lead oxybromide in a vapour pressure experiment, but, surprisingly,

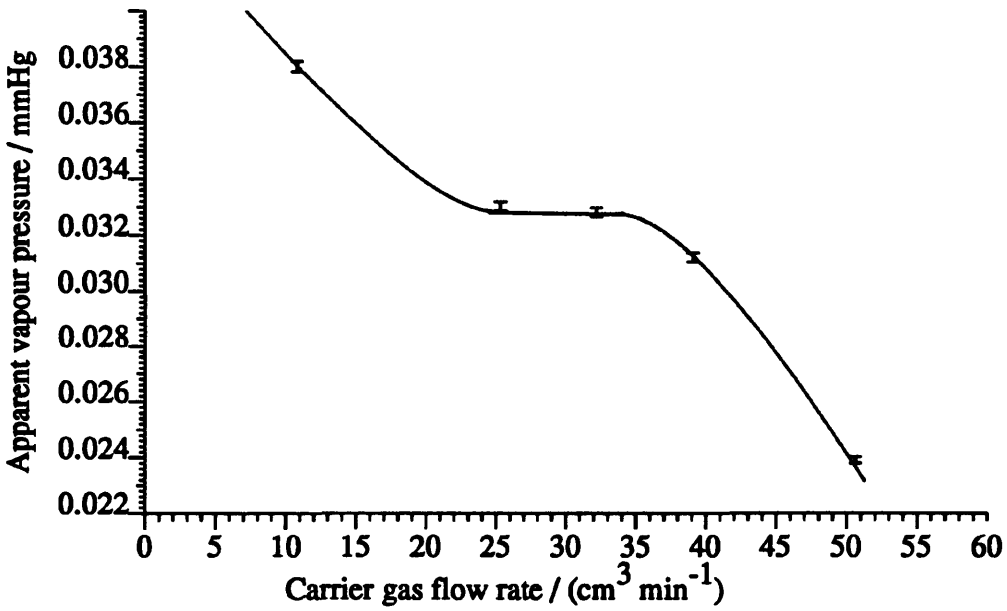

Figure 6.1: Apparent vapour pressure versus carrier gas flow rate at 595 °C

this was not the case.

It was thought, however, that this change in composition must eventually cause the rate of evaporation to decrease; hence, one experiment was allowed to continue until a much greater weight loss than normal had been attained. The results from this extended experiment are given in Figure 6.3, which shows a constant rate of weight loss up to at least a change in extension of 28 mm, but a pronounced curvature for higher weight losses. The data for this experiment (number 95) presented in Table 6.2 contain the vapour pressure calculated from the data points in this region. The experimental results span three days, which accounts for the spacing of the data points. Confirmation that the rate of evaporation was constant up to a change in extension of 28 mm was obtained in other experiments and a typical set of data is presented in Figure 6.4.

A 30 mm change in the extension of the spring corresponds to a weight loss of 0.063 g. As the initial mass of 2:1 lead oxybromide in experiment 95 was 0.342 g, this represented an 18 % loss in mass and it reduced the mole fraction of 2:1 lead oxybromide in the sample to 0.4, (assuming that the lead oxide left behind by the evaporation of lead bromide, did not react with more 2:1 lead oxybromide to produce 3:1 lead oxybromide). In the remaining 15 mm change in extension, the mole fraction of the 2:1 lead oxybromide fell to 0.2 and so the accompanying decrease in vapour pressure was not surprising. Thus, the data clearly show that the vapour pressure of the solid 2:1 lead oxybromide is not affected by the

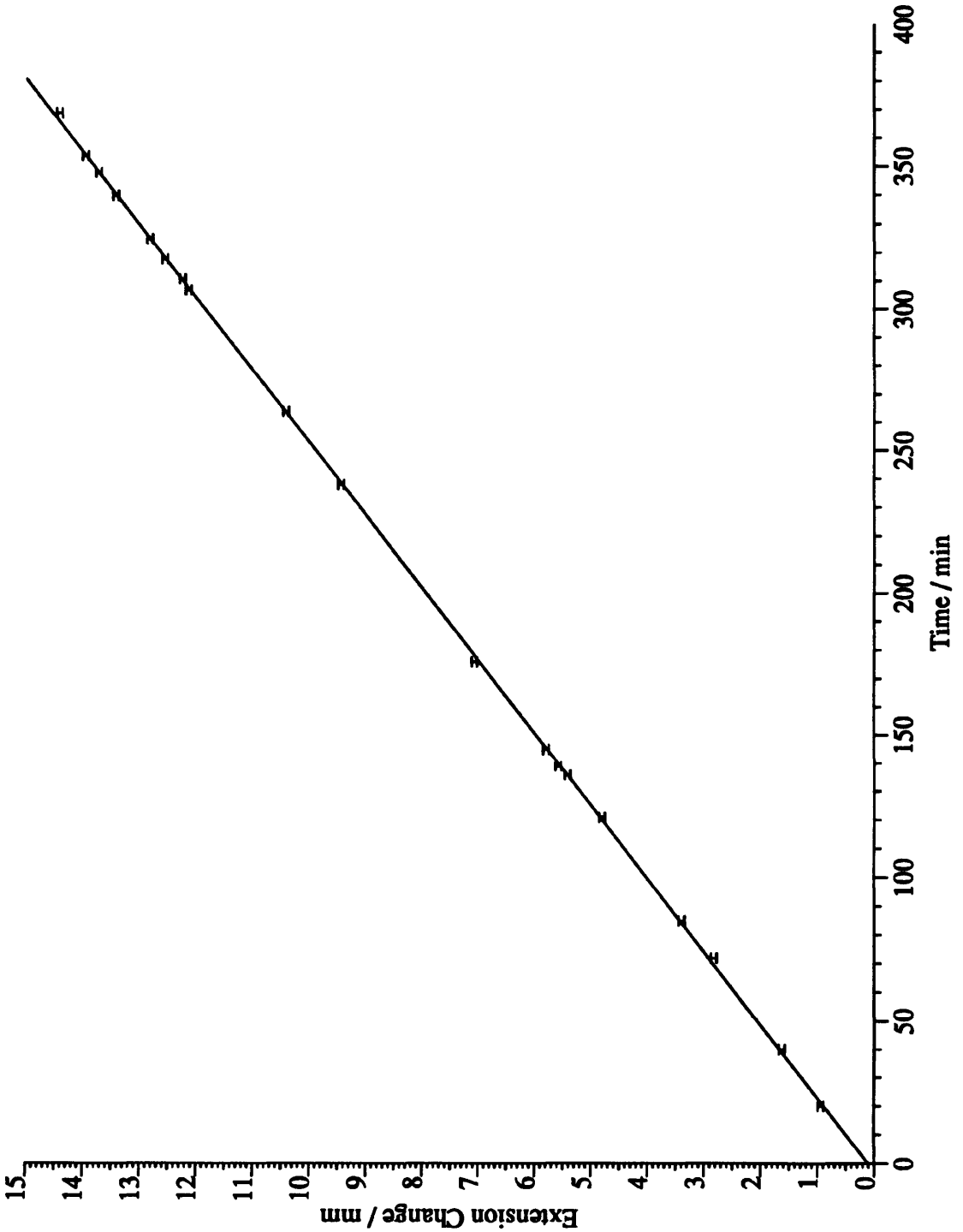

Figure 6.2: A typical plot of spring extension versus time for the 2:1 lead oxybromide at 646 °C and with a flow rate of 24.6 cm^3 min^{-1}

Table 6.1: The effect of the evaporation of 0.05 g of lead bromide from 0.5 g of the 1:1 lead oxybromide and 2:1 lead oxybromides on the residue

Compound	Mass /g	Amount /mol
$PbO.PbBr_2$	0.5	8.471×10^{-4}
$2PbO.PbBr_2$	0.5	6.147×10^{-4}
$PbBr_2$	0.05	1.362×10^{-4}

For the 1:1 lead oxybromide

The mole fraction of 1:1, in 1:1 and PbO

$$\frac{(8.471\times10^{-4} - 1.362\times10^{-4})_{1:1}}{(8.471\times10^{-4} - 1.362\times10^{-4})_{1:1}+(1.362\times10^{-4})_{PbO}} = 0.8392$$

The mole fraction of 1:1, in 1:1 and 2:1

$$\frac{(8.471\times10^{-4} - 2\times1.362\times10^{-4})_{1:1}}{(8.471\times10^{-4} - 2\times1.362\times10^{-4})_{1:1}+(1.362\times10^{-4})_{2:1}} = 0.7342$$

The mole fraction of $PbBr_2$, in $PbBr_2$ and PbO

$$\frac{(8.471\times10^{-4} - 1.362\times10^{-4})_{PbBr_2}}{(8.471\times10^{-4} - 1.362\times10^{-4})_{PbBr_2}+(8.471\times10^{-4})_{PbO}} = 0.4563$$

For the 2:1 lead oxybromide

The mole fraction of 2:1, in 2:1 and PbO

$$\frac{(6.147\times10^{-4} - 1.362\times10^{-4})_{2:1}}{(6.147\times10^{-4} - 1.362\times10^{-4})_{2:1}+(2\times1.362\times10^{-4})_{PbO}} = 0.6371$$

The mole fraction of 2:1, in 2:1 and 3:1

$$\frac{(6.147\times10^{-4} - 2\times1.362\times10^{-4})_{2:1}}{(6.147\times10^{-4} - 2\times1.362\times10^{-4})_{2:1}+(1.362\times10^{-4})_{3:1}} = 0.7153$$

The mole fraction of $PbBr_2$, in $PbBr_2$ and PbO

$$\frac{(6.147\times10^{-4} - 1.362\times10^{-4})_{PbBr_2}}{(6.147\times10^{-4} - 1.362\times10^{-4})_{PbBr_2}+(6.147\times10^{-4})_{PbO}} = 0.4377$$

Table 6.2: The vapour pressure results for the 2:1 lead oxybromide

Run No.	Temperature °C	Flow Rate $cm^3\ min^{-1}$	Vapour Pressure mmHg	Deviation mmHg	Error %
13	530.98	22.6	2.87×10^{-03}	2.93×10^{-05}	1.0
14	530.98	25.8	2.93×10^{-03}	1.32×10^{-05}	0.4
15	530.72	31.6	2.56×10^{-03}	3.17×10^{-05}	1.2
16	541.02	25.7	4.06×10^{-03}	7.73×10^{-05}	1.9
17	511.14	25.7	1.17×10^{-03}	8.07×10^{-05}	6.9
18	511.23	26.0	1.17×10^{-03}	1.47×10^{-05}	1.3
19	530.62	26.0	3.02×10^{-03}	1.57×10^{-05}	0.5
56	571.15	24.6	1.29×10^{-02}	3.72×10^{-05}	0.3
57	523.99	24.6	1.96×10^{-03}	2.52×10^{-05}	1.3
58	608.32	24.6	4.83×10^{-02}	1.26×10^{-04}	0.3
59	646.03	24.6	1.53×10^{-01}	3.86×10^{-04}	0.3
60	548.41	25.0	5.31×10^{-03}	5.00×10^{-05}	0.9
61	548.77	29.8	5.26×10^{-03}	1.68×10^{-05}	0.3
89	547.42	25.3	6.69×10^{-03}	6.10×10^{-05}	0.9
90	595.18	25.3	3.30×10^{-02}	3.31×10^{-04}	1.0
91	595.17	32.2	3.28×10^{-02}	1.68×10^{-04}	0.5
92	595.30	39.1	3.12×10^{-02}	8.17×10^{-05}	0.3
93	595.42	10.8	3.80×10^{-02}	1.84×10^{-04}	0.5
94	595.42	50.6	2.39×10^{-02}	8.28×10^{-05}	0.3
95	617.00	32.1	5.91×10^{-02}	5.24×10^{-05}	0.1
96	619.54	32.1	6.30×10^{-02}	4.63×10^{-04}	0.7
97	592.63	32.1	2.56×10^{-02}	2.23×10^{-04}	0.9

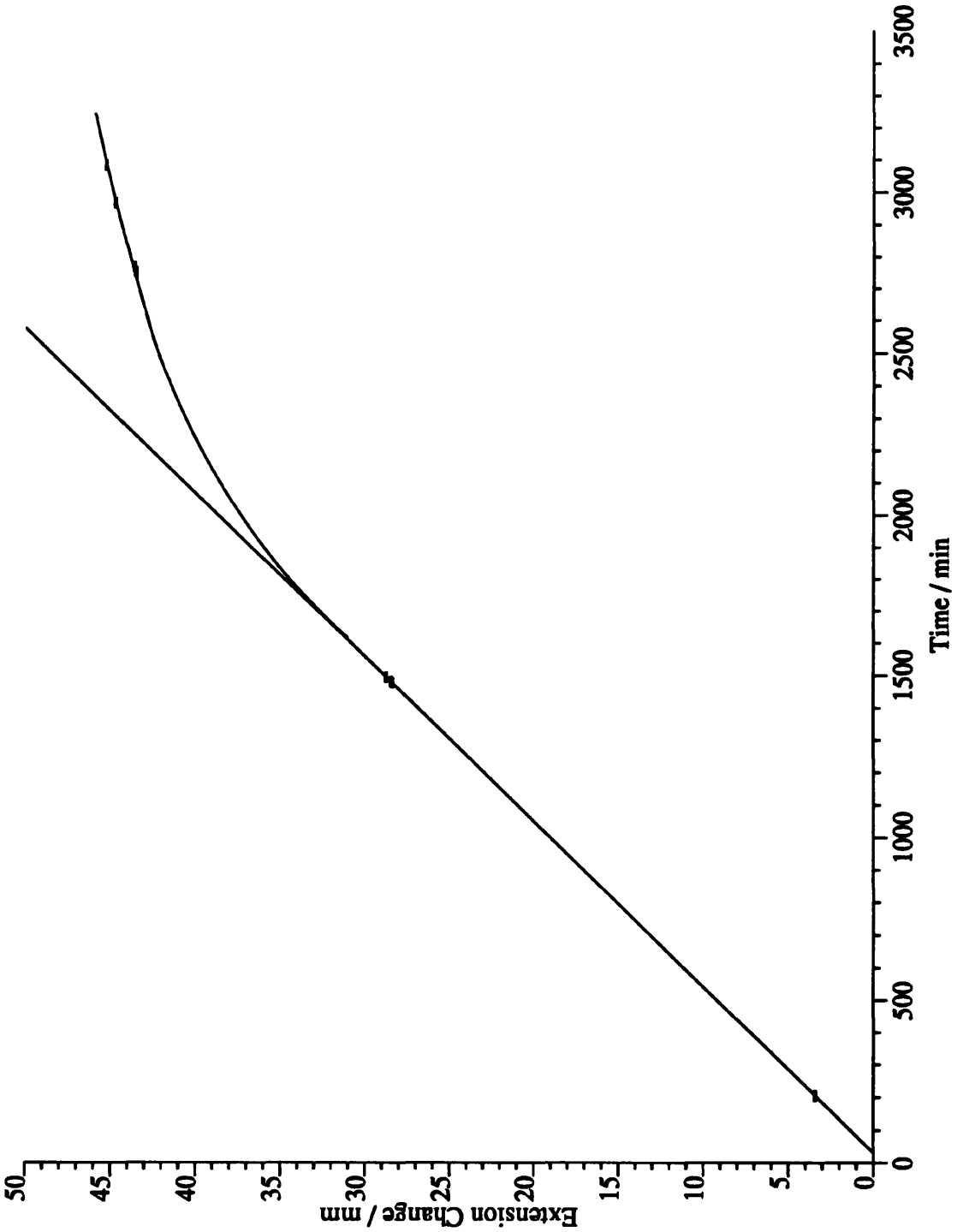

Figure 6.3: The plot of spring extension versus time for the 2:1 lead oxybromide at 617 °C and with a flow rate of 32.1 cm^3 min^{-1}

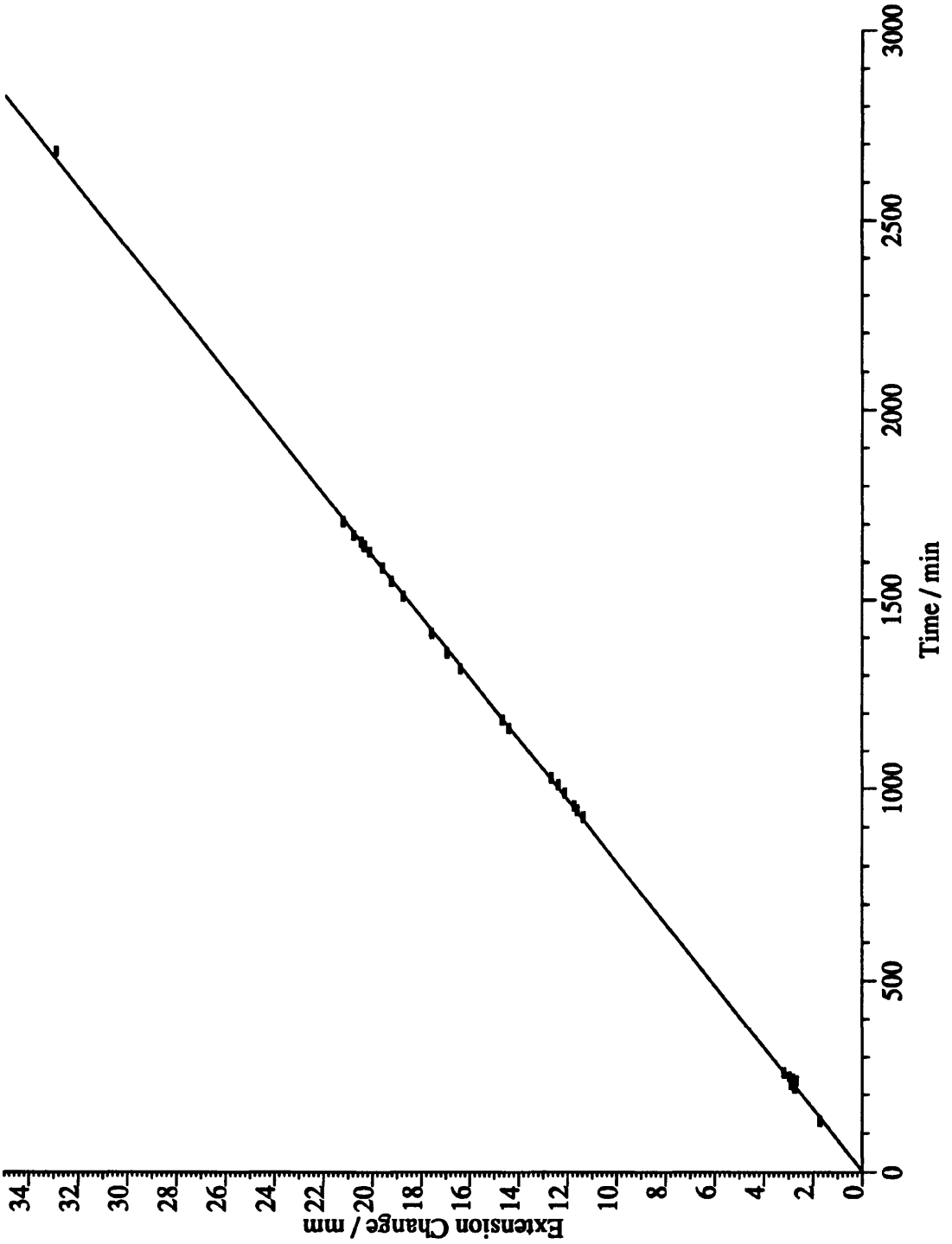

Figure 6.4: The plot of spring extension versus time for the 2:1 lead oxybromide at 524 °C and with a flow rate of 24.6 cm^3 min^{-1}

presence of a relatively large amount of lead oxide impurity. In turn, this suggests that the 2:1 lead oxybromide does not behave as a solid solution and that there is very little interaction between the free lead oxide and 2:1 lead oxybromide other than the reaction to form the 3:1 lead oxybromide.

6.4 The Vapour Pressure Curve for the 2:1 Lead Oxybromide

The vapour pressure of the 2:1 lead oxybromide was determined over the temperature range 530 – 646 °C. The vapour pressure curve derived from the experimental data is shown graphically in Figure 6.5 and a linear least squares regression gave the equation

$$\log_{10}(p/\text{mmHg}) = 11.42 \pm 0.18 + \frac{-11240 \pm 149\,\text{K}}{T} \qquad (6.1)$$

The slope of this plot gave the enthalpy of sublimation for lead bromide from the 2:1 lead oxybromide as 215.2 $\pm$ 3 kJ mol^{-1}

The apparent activity coefficient of lead bromide which was calculated from the vapour pressure data was 0.026 at 646 °C, assuming that the 2:1 lead oxybromide was a solid solution of lead oxide and lead bromide, and this decreased dramatically to 0.003 at 500 °C. In comparison with the values of 0.3 and 0.1 for the 1:1 lead oxybromide at its melting point of 497 and 360 °C, these are much smaller and decrease much more rapidly with decreasing temperature. This shows that there is significant interaction between lead oxide and lead bromide and suggests that 2:1 lead oxybromide is a true compound.

The rate of evaporation of lead bromide from the 2:1 lead oxybromide was found to be independent of the sample composition (see Section 6.3) and this is in keeping with the belief that the 2:1 lead oxybromide is a compound. However, if this is the case the lead bromide which evaporates from the 2:1 lead oxybromide must be formed by the decomposition of the 2:1 lead oxybromide and Equation 6.2 gives a possible decomposition process.

$$2\text{PbO.PbBr}_{2(s)} \rightleftharpoons 2\text{PbO}_{(s)} + \text{PbBr}_{2(g)} \qquad (6.2)$$

Another possibility is that the decomposition of the 2:1 lead oxybromide leads to the formation of lead bromide in the bulk phase, so that the vapour pressure arises from its sublimation. Thermodynamically, however, this is identical to the situation represented by Equation 6.2.

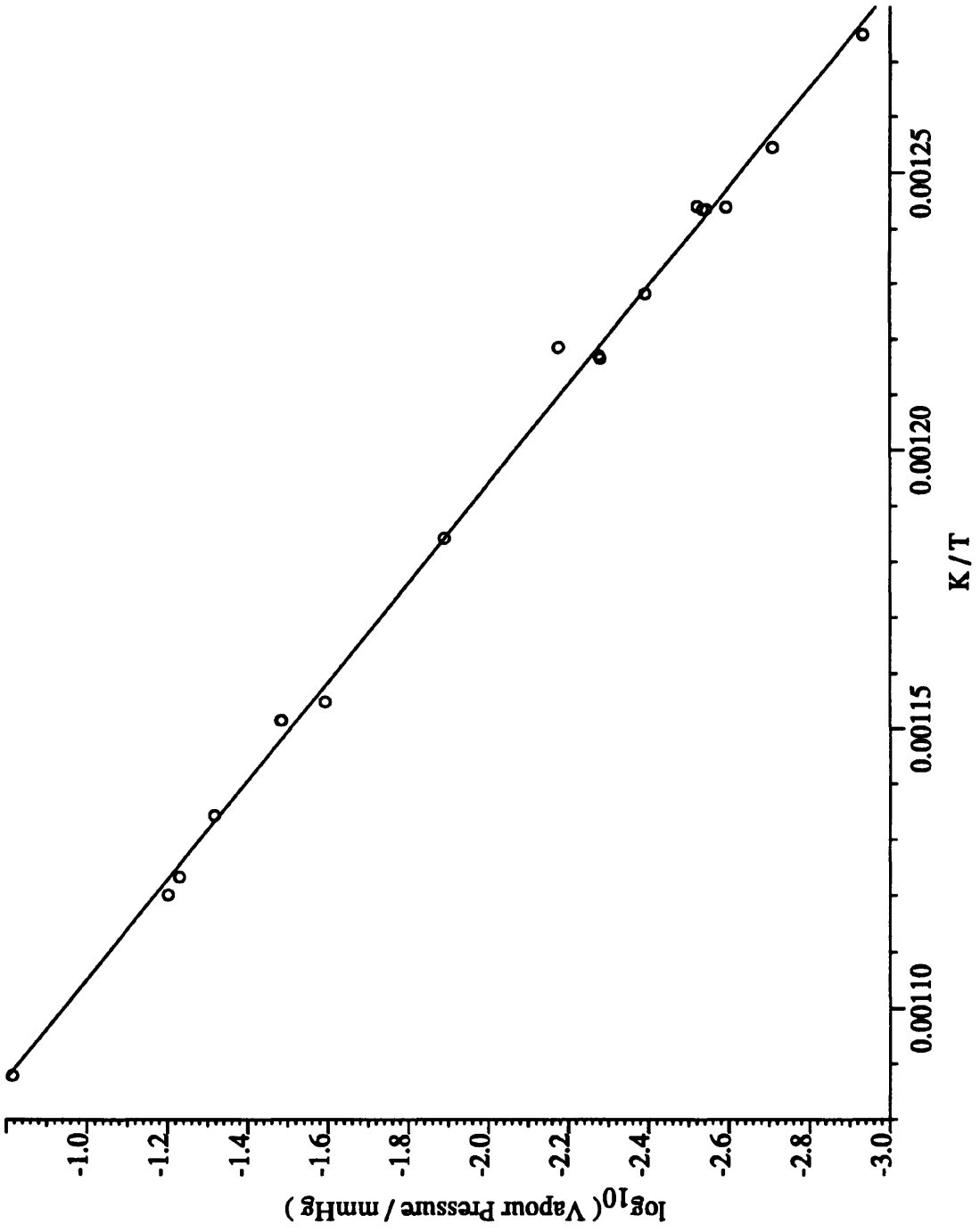

Figure 6.5: $\log_{10}$(vapour pressure / mmHg) versus $\frac{K}{T}$ for the 2:1 lead oxybromide

Table 6.3: Thermodynamic data for 2:1 lead oxybromide

T/K	$p\mathrm{PbBr_2}$	$\Delta G^{\ominus}_{6.2}$	$\Delta G^{\ominus}_f$/kJ mol^{-1}		
	mmHg		$\mathrm{PbO_{(s)}}$	$\mathrm{PbBr_{2(g)}}$	$\mathrm{2PbO.PbBr_{2(s)}}$
800	2.34×10^{-3}	84.4	-138.1	-156.3	-516.8
850	1.572×10^{-2}	76.2	-133.0	-157.2	-499.4
900	8.53×10^{-2}	68.1	-128.0	-158.1	-482.2
982	9.42×10^{-1}	54.7	-119.7	-159.5	-453.6
Using the data of Buck and Ryason [2]:					
982		50			-455.9

The evaporation of lead bromide during the vapour pressure experiments took place under essentially equilibrium conditions (i.e. in the plateau region). It follows, that the decomposition reaction is also at equilibrium, as this controls the partial pressure of the lead bromide. The Gibbs energy of reaction can be calculated from the equilibrium constant using the following relationship

$$\Delta G^{\ominus}_T = -RT \ln (K_p/\mathrm{atm}) \tag{6.3}$$

where $\Delta G^{\ominus}_T$ is the standard Gibbs energy change at the temperature T and K_p is the equilibrium constant for the reaction. This is given by

$$K_p/\mathrm{atm} = p\mathrm{PbBr_2} \tag{6.4}$$

where $p_{\mathrm{PbBr_2}}$ is the partial pressure of lead bromide.

Table 6.3 shows the change in the Gibbs energy for the decomposition of the 2:1 lead oxybromide calculated from the equilibrium vapour pressure of lead bromide at temperatures of 800, 850, 900 and 982 K. Having calculated the Gibbs energy change for this decomposition reaction, the Gibbs energy of formation for the 2:1 lead oxybromide was calculated from Equation 6.5

$$\Delta G^{\ominus}_{6.2} = 2\Delta G^{\ominus}_f \mathrm{PbO_{(s)}} + \Delta G^{\ominus}_f \mathrm{PbBr_{2(g)}} - \Delta G^{\ominus}_f \mathrm{2PbO.PbBr_{2(s)}} \tag{6.5}$$

These values are listed in Table 6.3 together with the Gibbs energy of formation of solid lead oxide and gaseous lead bromide [3] used in the calculation.

$$\mathrm{2PbO_{(s)} + PbBr_{2(s)} \rightleftharpoons 2PbO.PbBr_{2(s)}} \tag{6.6}$$

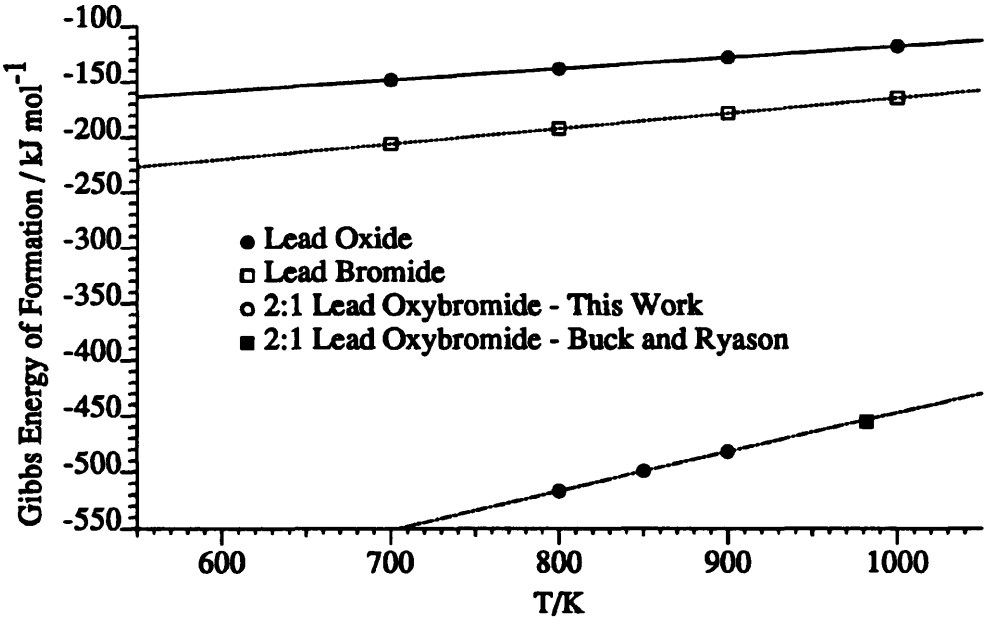

Figure 6.6: A plot of the standard Gibbs energy of formation of lead oxide, lead bromide and the 2:1 lead oxybromide

Buck and Ryason [2] have estimated the Gibbs energy of the Reaction 6.6 between solid lead bromide and solid lead oxide in which the 2:1 lead oxybromide is formed, to be -50 ± 4 kJ mol^{-1} at 982 K. This value was calculated from the phase diagram by Wagner's method [8]. The corresponding Gibbs energy of formation for the 2:1 lead oxybromide is -448.4 kJ mol^{-1}. Figure 6.6 shows that the literature values for the Gibbs energy of formation of solid lead oxide and solid lead bromide vary linearly with temperature over the range 700 – 1000 K. It also compares the Gibbs energies of formation for the 2:1 lead oxybromide calculated from the present vapour pressure measurements with that derived from the theoretical estimate of Buck and Ryason for the Gibbs energy change for Reaction 6.6. Within experimental error, these last three values lie on a straight line, which shows that they are consistent.

Ting-Man Li and Simmons [7] have calculated the change in the Gibbs energy for the reaction of hydrogen bromide gas with each of $6PbO.PbBr_2$, $3PbO.PbBr_2$, $2PbO.PbBr_2$ and $PbO.PbBr_2$ over the temperature range 600 – 1000 K in 100 K intervals. They assumed that the Gibbs energy of the reaction between lead oxide and lead bromide to form $6PbO.PbBr_2$ was reasonably constant in the temperature range of interest and used the value of -58.6 kJ mol^{-1} calculated by Buck and Ryason for a temperature of 948 K. Using the data of Ting-Man Li and Simmons, the Gibbs energy of formation of the 2:1 lead oxybromide was calculated as -518.4 kJ mol^{-1} at 800 K and -484.3 kJ mol^{-1} at

900 K; these values are in remarkable agreement with the corresponding values of −516.8 and −482.2 kJ mol^{-1} which were derived from the vapour pressure data obtained in this work.

It may be concluded, therefore, that the earlier assumption that the equilibrium vapour pressure of lead bromide from the 2:1 lead oxybromide is controlled by the equilibrium Reaction 6.2 is correct. Using Equation 6.7, the enthalpy of sublimation for the 2:1 lead oxybromide of 215.2 kJ mol^{-1} can be used to calculate its enthalpy of formation at the average temperature of the vapour pressure measurements, namely 850 K.

$$\Delta H_{6.2} = \Delta H_f^{\ominus} PbBr_{2(g)} + 2\Delta H_f^{\ominus} PbO_{(s)} - \Delta H_f^{\ominus} 2PbO.PbBr_{2(s)} \qquad (6.7)$$

The standard enthalpy of formation of gaseous lead bromide at 850 K was taken to be −141.3 kJ mol^{-1} and that of solid lead oxide was −218.6 kJ mol^{-1} [3], using these values and the enthalpy of the decomposition reaction given above, the standard enthalpy of formation of the 2:1 lead oxybromide was calculated to be −794.5 kJ mol^{-1}.

Thus, the thermodynamic data relating to the 2:1 lead oxybromide which has been derived from the vapour pressure data up to this point, shows that the 2:1 lead oxybromide is a true compound, that the evaporating lead bromide is produced by the decomposition reaction 6.2 and that the partial pressure of lead bromide is dictated by the equilibrium position of the reaction.

6.5 Comparison of the Vapour Pressure Data for the 2:1 Lead Oxybromide

Belyaev and Mareskin [1] have published vapour pressure data for molten mixtures of lead oxide and lead bromide, and these data indicate that molten 2:1 lead oxybromide behaves as an ideal solution of lead bromide and lead oxide. It should be noted that Belyaev and Mareskin also measured the vapour pressure of lead bromide and their results are in good agreement with all of the previously reported values; there is no reason why the measurements for the lead oxide and lead bromide mixtures should be any less reliable. These data for molten 2:1 lead oxybromide are compared with the present results in Figure 6.7.

The vapour pressure of lead bromide and of the 1:1 lead oxybromide obtained in this work are also included in Figure 6.7 for reference, and the substantial difference in the vapour pressures of the 1:1 and 2:1 lead oxybromides is evident.

The vapour pressure of solid 2:1 lead oxybromide at its melting point of 709 °C (982 K,

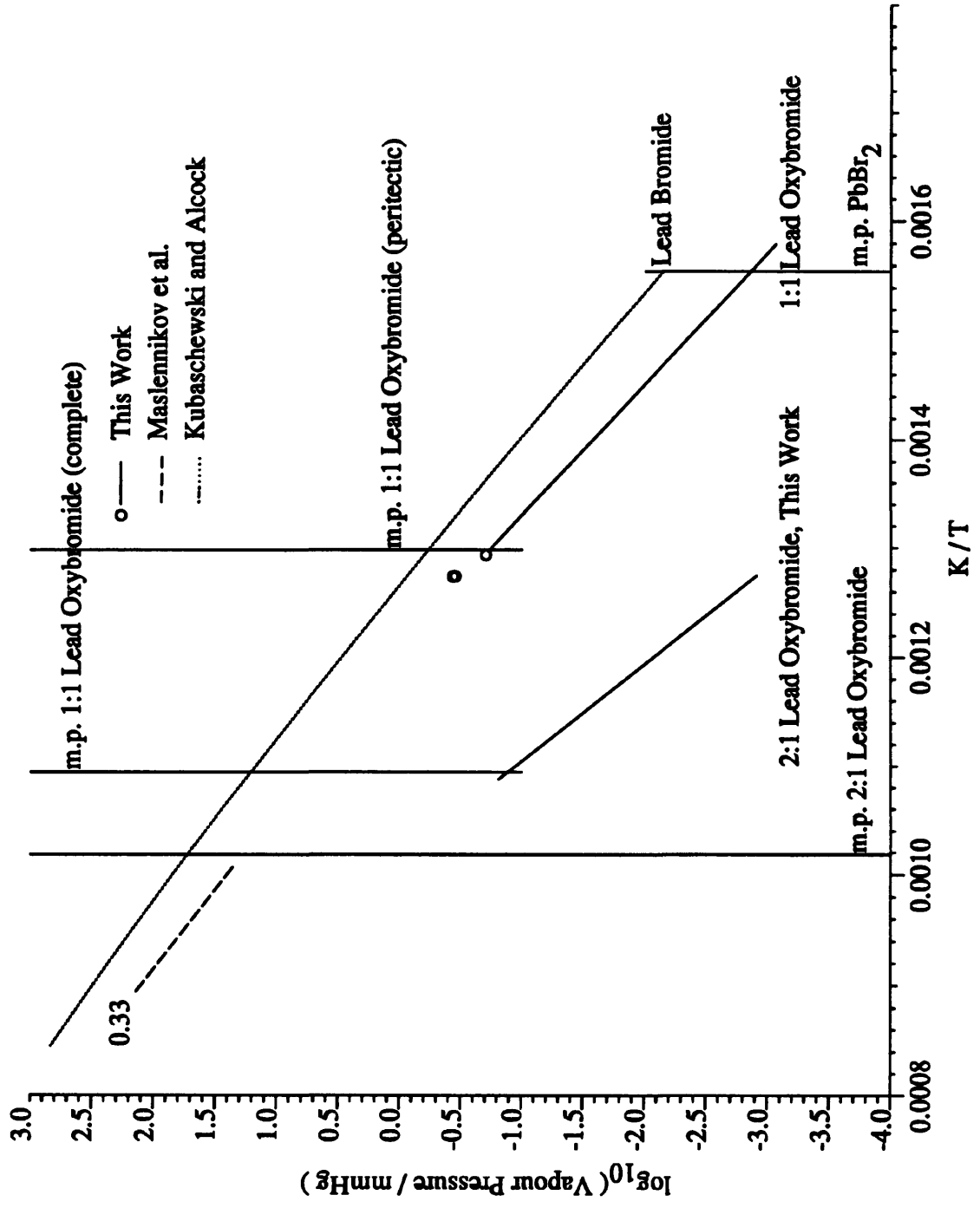

Figure 6.7: $\log_{10}$(vapour pressure / mmHg) versus $\frac{K}{T}$ data for the lead oxide / lead bromide system

obtained by extrapolation of the present data) should be in reasonable agreement with the value obtained by the corresponding extrapolation of the data for the molten material. Figure 6.7 shows that this is not the case, and the two values differ by a factor of 30! This sudden increase in the vapour pressure of the 2:1 lead oxybromide at the melting point cannot be accounted for by the uncertainty in the experimental measurements and it requires explanation. A number of situations can be envisaged that might affect the vapour pressure of 2:1 lead oxybromide near its melting point, and these will now be considered in turn to see if they provide a plausible explanation of the apparent discrepancy.

The first situation that can be envisaged is that when the 2:1 lead oxybromide melts it forms a molten mixture of lead bromide and lead oxide, which contains a significant proportion of undecomposed 2:1 lead oxybromide. Under these circumstances, the residual 2:1 lead oxybromide might produce a depression of the vapour pressure of the molten mixture of lead bromide and lead oxide. Such an explanation, however, would require that all the residual 2:1 lead oxybromide in the melt decomposes over a very narrow temperature range if the present results are to be reconciled with those of Belyaev and Mareskin. Thermodynamic considerations suggest that this is unlikely.

$$2PbO.PbBr_{2(s)} \rightleftharpoons 2PbO_{(s)} + PbBr_{2(s)} \qquad (6.8)$$

If the decomposition of the 2:1 lead oxybromide is formulated as occurring by Reaction 6.8 in the bulk phase, combination of the present data with the known Gibbs energies of formation for gaseous and solid lead bromide leads to an extrapolated value for its mole fraction equilibrium constant (K_x) of 3.06×10^{-3} at 982 K, i.e. the melting point of 2:1 lead oxybromide. Assuming ideal behaviour, this corresponds to approximately 11 % dissociation. However, the temperature dependence obtained in the present study for the enthalpy of sublimation of lead bromide from the 2:1 lead oxybromide was only 215.2 kJ mol^{-1}, of which 176 kJ mol^{-1} can be attributed to the actual enthalpy of sublimation of lead bromide. It follows that the enthalpy change associated with Reaction 6.8 is only about 39 kJ mol^{-1}; this is insufficient to produce the dissociation required to reconcile the present results with those of Belyaev and Mareskin.

The above situation assumes that the 2:1 lead oxybromide dissociates into solid lead oxide and solid lead bromide, although the temperature is above the melting point of lead bromide. It seems unlikely, however, that any resulting uncertainty in the precise state of the lead bromide will change the conclusion. Perhaps a more important assumption was that the system behaves as an ideal mixture and this may not be correct. The results of Belyaev and Mareskin show that at about 1000 K molten 2:1 lead oxybromide behaves as an ideal mixture, while the present results show that the apparent activity coefficient of the solid is only 0.026 at 920 K. The latter value is clearly a consequence of compound formation and thus any increase in the apparent activity coefficient with temperature

between 900 and 1000 K must arise from the dissociation of the 2:1 lead oxybromide into lead oxide and lead bromide. This is essentially the same situation as described above and it seems unlikely that the ideality of the system will change sufficiently abruptly to reconcile the two sets of data.

The final situation which must be considered is that the partial pressure of lead bromide above a solid sample of the 2:1 lead oxybromide is not controlled by just the equilibrium position of Reaction 6.8 in the vicinity of its melting point. While, the present experimental results show that this is the case at lower temperatures, the X-ray powder diffraction patterns of the residues showed that under certain circumstances the 3:1 lead oxybromide was formed. This must be produced by reaction of solid lead oxide with the 2:1 lead oxybromide and the reaction scheme below gives a plausible route for its formation (the first of the reactions is identical to Reaction 6.8 and has been reproduced for convenience). More importantly, this overall reaction produces free lead bromide and, therefore, it can affect its partial pressure.

$$2PbO.PbBr_{2(s)} \rightleftharpoons 2PbO_{(s)} + PbBr_{2(s)} \tag{6.9}$$

$$PbO_{(s)} + 2PbO.PbBr_{2(s)} \rightarrow 3PbO.PbBr_{2(s)} \tag{6.10}$$

Combining these two reactions gives

$$3(2PbO.PbBr_{2(s)}) \rightleftharpoons 2(3PbO.PbBr_{2(s)}) + PbBr_{2(s)} \tag{6.11}$$

The changes in the Gibbs energy associated with these three reactions are tabulated in Table 6.4 for the temperature range of interest. The Gibbs energy of formation of the 3:1 lead oxybromide used to derive these values was calculated from the combined data of Buck and Ryason, and Ting-Man Li and Simmons. It is listed in Table 6.4, together with the corresponding Gibbs energy of formation of the 2:1 lead oxybromide calculated from the present vapour pressure data. The Gibbs energies of formation of solid lead oxide and solid lead bromide are also listed for completeness.

Two particular points should be noted. First of all, the change in the Gibbs energy associated with the formation of the 3:1 lead oxybromide by reaction of solid lead oxide with the 2:1 lead oxybromide is negative. Thus, once free lead oxide is present in the system, the formation of the 3:1 lead oxybromide becomes possible, although it may not be kinetically fast. Secondly, the change in the Gibbs energy associated with overall reaction is less than that for the dissociation of the 2:1 lead oxybromide to solid lead oxide and solid lead bromide. Thus, thermodynamically, once the formation of the 3:1 lead oxybromide begins to occur, the overall equilibrium position will favour its formation.

Table 6.5 lists the partial pressure of lead bromide obtained in the present work and that expected if Reaction 6.11 reaches its equilibrium position. At any given temperature, the

Table 6.4: Thermodynamic data for 3:1 lead oxybromide

	T/K			
$\Delta G_f^{\ominus}$/kJmol^{-1}	700	800	900	982
$3PbO.PbBr_{2(s)}$	-706.9	-661.6	-617.9	581.9
$2PbO.PbBr_{2(s)}$	-551.7	-516.9	-482.2	-453.6
$PbO_{(s)}$	-148.3	-138.1	-128.0	-119.7
$PbBr_{2(s)}$	-206.1	-192.0	-178.2	-166.9
$\Delta G^{\ominus}_{Reaction\ 6.8}$	48.99	48.7	48.2	47.2
$\Delta G^{\ominus}_{Reaction\ 6.10}$	-6.88	-6.6	-7.7	-8.6
$\Delta G^{\ominus}_{Reaction\ 6.11}$	35.2	35.4	32.7	30.1

Table 6.5: A comparison of the partial pressure of lead bromide measured in this study with the values predicted assuming that the formation of 3:1 lead oxybromide from 2:1 lead oxybromide reaches equilibrium

T/K	$2PbO.PbBr_{2(s)}$ (exptl)		Reaction 6.11	
	$p PbBr_2$/mmHg	$\log_{10}(p/\text{mmHg})$	$p PbBr_2$/mmHg	$\log_{10}(p/\text{mmHg})$
800	2.34×10^{-3}	-2.63	1.7×10^{-2}	-1.77
900	8.53×10^{-2}	-1.07	0.66	-0.18
982			7.69	0.88

latter is about eight times greater than the partial pressure obtained in the present work. It is clear, however, that the formation of the 3:1 lead oxybromide cannot be important in the range of temperatures over which the present measurements were made. Presumably, this must be due partly to the low degree of dissociation of the 2:1 lead oxybromide in this temperature range and partly to kinetic limitations on its formation. In contrast, at the melting point of the 2:1 lead oxybromide the conditions may well favour the formation of the 3:1 lead oxybromide, in which case the partial pressure of lead bromide could be raised significantly above the value expected by extrapolation of the present results.

These two sets of partial pressures are compared graphically in Figure 6.8. The uncertainty in the Gibbs energy of formation of the 3:1 lead oxybromide is about 4 kJ mol^{-1}, and the corresponding uncertainty in the equilibrium partial pressure of lead bromide is shown by the dotted lines. When these data are compared with those of Belyaev and Mareskin one

important fact must be borne in mind, namely, that their paper does not report original data but only an equation for the partial pressure of lead bromide. Thus there is no way of knowing if there was any slight curvature downwards in their data as the melting point of 2:1 lead oxybromide was approached. Even without such an eventuality, it is clear that the formation of the 3:1 lead oxybromide as the melting point of the 2:1 lead oxybromide is approached could go a long way to explaining the apparent discrepancy between the present measurements and those of Belyaev and Mareskin.

Some independent support for such a situation comes from the thermal analysis traces for the 2:1 lead oxybromide presented in Chapter 2. These contained an unexplained shoulder on the peak corresponding to the melting of the 2:1 lead oxybromide. The presence of such a shoulder is consistent with the occurrence of an endothermic reaction just below its melting point and it could be explained by the formation of the 3:1 lead oxybromide.

Clearly, the data of Belyaev and Mareskin refer to conditions where dissociation of the 2:1 lead oxybromide is complete, as their activity coefficients are unity, while the present data refer to the situation which exists between 530 and 646 °C, i.e. up to about 60 °C below the melting point of 2:1 lead oxybromide. Unfortunately there are no experimental measurements within the grey area shown in Figure 6.8, and such measurements are needed to place the hypothesis outlined above on a more secure foundation; but an explanation of this type is required to reconcile these two sets of experimental data. The thermodynamic implications of such a situation will be considered further in the final chapter of this thesis.

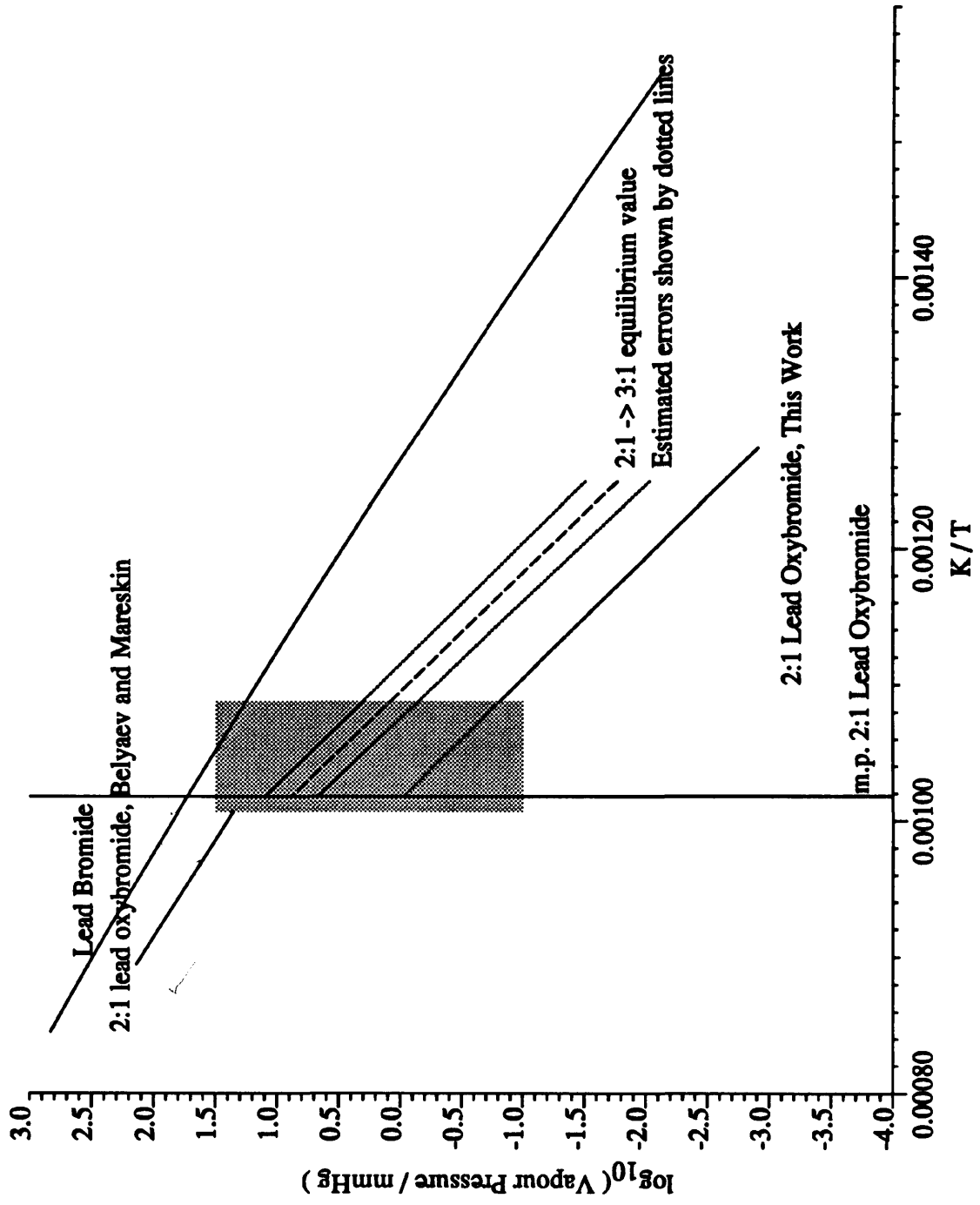

Figure 6.8: The $\log_{10}$(vapour pressure / mmHg) versus $\frac{K}{T}$ for the 2:1 lead oxybromide with estimated values for the vapour pressure of the 3:1 lead oxybromide

References

[1] Belyaev I.N. and Mareskin S.A., *Thermodynamics of Lead Oxide Lead Halide Melts. II. Tensimetric Study of the Lead Bromide-Lead Oxide System*, Russian Journal of Physical Chemistry, 49, (4), (1975), p. 619.

[2] Buck R.P. and Ryason P.R., *Lead Scavenging, A Quasithermodynamic Approach*, Am. Chem. Soc. Div. Petrol. Chem. Preprints, Vol. 10, part 2, (1965), p. 21.

[3] JANAF, *Thermochemical Tables*, 2nd Ed. US Dept. of Commerce, National Bureau of Standards, 1971.

[4] Knowles L.M., *Thermal Analysis of the System $PbBr_2$-PbO*, J. Chem. Phys., 19, (1951), p. 1128.

[5] Kubaschewski O. and Alcock C.B., *Metallurgical Thermochemistry*, 5th edition. Pergamon Press. ISBN 0 08 020897 5.

[6] Maslennikov V.P., Spiridonova M.N., Aleksandrov Y.U.A., and Emel'yanov B.V., *Volatility of Lead Compounds*, Trudy Po Khimii I Khimicheskoi Tekhnologii, 2, (1973), p. 146.

[7] Ting-Man Li and Simmons. R.F., *The Mechanism of Lead Scavenging by Bromoethane*, Nineteenth Symposium (International) on Combustion/The Combustion Institute, (1982), p. 1487-1494.

[8] Wagner C., *Thermodynamics of Phase Diagrams of Binary Systems Involving Compounds*, Acta Metallurgica, 6, (1958), p. 309.

Chapter 7

Conclusions

In the course of this present study, samples of the 1:1, 2:1, 3:1 and 7:1 lead oxybromides (and also 1:1 and 2:1 lead oxychlorides) were prepared in a platinum lined gas-tight vessel. Hence, in contrast to other previous studies the precise elemental composition of the material formed was known.

7.1 The X-ray Powder Diffraction Studies

The authenticity of the samples of lead bromide, lead oxide and lead chloride used in this work were confirmed by X-ray powder diffraction.

The X-ray powder crystallographic study confirmed that two forms (N and R) of the 1:1 lead oxybromide can be prepared from lead oxide and lead bromide. The N form is produced by melting an intimate mixture of lead oxide and lead bromide (of the correct stoichiometry) and then cooling slowly through the peritectic decomposition temperature. The R form of the 1:1 lead oxybromide is produced by heating an equivalent mixture of lead oxide and lead bromide to a temperature above 375 °C but below the peritectic decomposition temperature of 497 °C, this explains the report of Julien and Ogilvie who believed that the R form was the only stable form of the 1:1 lead oxybromide, as it appears that they did not melt their sample. The X-ray diffraction patterns of the N and R forms of the 1:1 lead oxybromide prepared in this work were in reasonable agreement with those of previous workers.

Only one form of the 2:1 lead oxybromide was prepared in this work and it appeared to be the only stable form. This is in accord with the findings of previous workers. The most consistent and satisfactory samples were prepared by slow cooling of a melt of lead bromide and lead oxide.

Samples of the 3:1 and 7:1 lead oxybromides were prepared by slowly cooling melts containing appropriate stoichiometric amounts of lead oxide and lead bromide. The 3:1 lead oxybromide is thought to exist in at least two forms (D and E) and the powder diffraction pattern of the samples prepared in this work resembled that which has been previously referred to as the E form. Similarly, the T form as opposed to the Q from of the 7:1 lead oxybromide was prepared here. The powder diffraction pattern of this 7:1 lead oxybromide was very clean. This implied that it was quite pure, but a sample with the alternative stoichiometry 6:1 was not prepared in this work and the correct formula is therefore still open to debate.

7.2 Thermal Analysis

Differential thermal analysis of the lead bromide, lead chloride and lead oxide used in the present study confirmed the nature and purity of the starting materials. Similarly, the traces obtained with the samples of the lead oxybromides prepared in this work showed that in all cases their formation was complete. The trace for the 1:1 lead oxybromide contained an endothermic peak at 497 °C and this confirmed that the 1:1 lead oxybromide undergoes a peritectic reaction at this temperature. The samples of the 2:1 lead oxybromide furnished traces which contained a single endothermic peak at temperatures between 696 and 698 °C, while the 3:1 and 7:1 lead oxybromides also gave only a single endothermic peak at their respective melting points.

The results obtained in experiments in which intimate mixtures of lead oxide and lead bromide were heated showed that, regardless of stoichiometry, the solid R form of the 1:1 lead oxybromide is formed in an exothermic reaction at a temperature of approximately 350 °C and that this was transformed to the solid N form in an endothermic process which occurs at approximately 492 °C. In mixtures with a lead oxide to lead bromide ratio of less than 2:1 the N Form of the 1:1 lead oxybromide then undergoes a peritectic reaction at around 500 °C to form solid 2:1 lead oxybromide and a molten mixture of lead oxide and lead bromide. Mixtures in which this ratio was 3:1 also gave an endothermic peak at this temperature, but the results obtained here do not show whether this corresponds to the formation of 3:1 lead oxybromide or 2:1 lead oxybromide (in both cases a molten solution of lead oxide and lead bromide must also be present). The 7:1 lead oxybromide showed no sign of a corresponding peritectic reaction, and the trace was virtually flat up to the melting point.

Thus, the lead oxybromides are formed from solid lead oxide and solid lead bromide in a stepwise fashion and the reactions occur at fixed temperatures. However, with the

Table 7.1: A summary of the vapour pressure data obtained in this work, $\log_{10}$ (p/mmHg) $= A + B$ K/T

	Temperature Range K	A	B
lead bromide	613 - 645	12.0 ± 0.7	-9200 ± 480
1:1 lead oxybromide	630 - 770	10.0 ± 0.13	-8293 ± 91
2:1 lead oxybromide	803 - 919	11.4 ± 0.18	-11240 ± 149

exception of the peritectic decomposition occurring in mixtures with stoichiometries of between 1:1 and 2:1 (lead oxide / lead bromide), the reactions are normally irreversible.

7.3 Vapour Pressure Measurements

In the course of this work, a transpiration apparatus was constructed and used to measure successfully the vapour pressure of lead bromide the 1:1 and 2:1 lead oxybromides. The vapour pressure equations have been obtained for specific temperature ranges and the data are summarised in Table 7.1. Lead bromide was identified as the species evaporating from both the 1:1 and 2:1 lead oxybromides and this shows that these lead oxybromides do not evaporate intact, i.e. lead oxide was not detected in the condensate which collected in the outlet of the saturation chamber.

The present vapour pressure measurements of solid lead bromide are the only experimentally determined data for this compound and they are in good agreement with the published data for molten lead bromide. The enthalpy of sublimation calculated from this data was 176 ± 9 kJ mol^{-1} and this is in good agreement with the values estimated previously of 163.6, 167.0 and 167.2 kJ mol^{-1}. Table 7.2 gives the enthalpy of sublimation of lead bromide, the 1:1 lead oxybromide and the 2:1 lead oxybromide calculated from the vapour pressure data.

In the temperature range covered by this work, the partial pressure of lead bromide above solid 2:1 lead oxybromide has been shown to be controlled by the equilibrium position of the following decomposition reaction

$$2PbO.PbBr_{2(s)} \rightleftharpoons 2PbO_{(s)} + PbBr_{2(g)} \qquad (7.1)$$

As discussed in Chapter 6, the partial pressure of the 2:1 lead oxybromide at its melting

Table 7.2: A summary of the enthalpy of sublimation of lead bromide from lead bromide, 1:1 lead oxybromide and 2:1 lead oxybromide

	Temperature Range K	$\Delta H_{sublimation}$ kJ mol^{-1}
lead bromide	613 - 645	176 ± 9
1:1 lead oxybromide	630 - 770	159 ± 2
2:1 lead oxybromide	803 - 919	215 ± 2

point of 982 K, obtained by an extrapolation of this vapour pressure equation is approximately 1/30th of the value obtained by the corresponding extrapolation of data for the molten material back to the melting point. Hence, at some temperature in the 60 K region between the two sets of experimental measurements, there must be a change in the character of the system which increases dramatically the partial pressure of lead bromide. It was shown that a plausible explanation is that the free lead oxide produced in the decomposition Reaction 7.1 reacts with the 2:1 lead oxybromide to form 3:1 lead oxybromide

$$PbO_{(s)} + 2PbO.PbBr_{2(s)} \rightarrow 3PbO.PbBr_{2(s)} \qquad (7.2)$$

The increase in the partial pressure of lead bromide calculated on the assumption that this reaction reached equilibrium, accounts almost completely for the difference in the two sets of experimental data, provided it only becomes important as the melting point of the 2:1 lead oxybromide is approached. This is not unreasonable, as this reaction is likely to be kinetically slow at lower temperatures where the degree of dissociation of the 2:1 lead oxybromide is also lower.

The thermal analysis traces of the 2:1 lead oxybromide contained a shoulder on the low temperature side of the endothermic peak at the temperature corresponding to the melting point. The presence of such a shoulder is consistent with the occurrence of a reaction and it could be explained by the formation of the 3:1 lead oxybromide. It is known that the 1:1 lead oxybromide melts incongruently and it is not unreasonable that the 2:1 lead oxybromide should melt in a similar way.

In Chapter 5, the vapour pressure data for the 1:1 lead oxybromide was presented and it was noted that the rate of evaporation of lead bromide decreased slowly with increasing time in many of the vapour pressure experiments. The resulting decrease in the vapour pressure was reproduced quite successfully using a model which was based on the assumption that the 1:1 lead oxybromide behaved as a simple solid solution of lead bromide in

lead oxide. The magnitude of the observed partial pressure of lead bromide at the higher temperatures was consistent with this view, but there was no obvious explanation for the marked decrease in the activity coefficient of the lead bromide as the temperature decreased. The suggestion that the partial pressure of lead bromide in equilibrium with the 2:1 lead oxybromide is controlled by the equilibrium position of the decomposition reaction for the 2:1 lead oxybromide, however, requires this initial conclusion to be reexamined.

There are two possibilities which must be considered and the first is that the vapour pressure of the 1:1 lead oxybromide is controlled by a decomposition reaction analogous to that which occurs with the 2:1 lead oxybromide i.e.

$$PbO.PbBr_{2(s)} \rightleftharpoons PbO_{(s)} + PbBr_{2(g)} \qquad (7.3)$$

Table 7.3 gives the Gibbs energy change for this decomposition reaction calculated using the thermodynamic data for lead oxide [1], lead bromide [1] and 1:1 lead oxybromide [2], along with the corresponding equilibrium vapour pressure. Figure 7.1 compares graphically these calculated vapour pressures with the present experimental values. It is clear that the measured vapour pressures are much larger than the calculated values, so that the partial pressure of lead bromide above the 1:1 lead oxybromide cannot be controlled by the equilibrium position of the decomposition Reaction 7.3.

The second possibility is analogous to the suggested behaviour of the 2:1 lead oxybromide near its melting point, in that the 1:1 lead oxybromide is in equilibrium with the 2:1 lead oxybromide and lead bromide. In this case, however, two adjacent molecules of 1:1 lead oxybromide in the solid lattice can interact to form 2:1 lead oxybromide and lead bromide. If this is the case, the partial pressure of lead bromide in equilibrium with the 1:1 lead oxybromide is controlled by the reaction

$$2(PbO.PbBr_{2(s)}) \rightleftharpoons 2PbO.PbBr_{2(s)} + PbBr_{2(g)} \qquad (7.4)$$

The Gibbs energy change for this reaction is given along with the corresponding partial pressure of lead bromide in Table 7.3 and shown graphically in Figure 7.1. The figure shows that the agreement between the calculated and experimentally determined values is excellent. Similarly, the Gibbs energy change for Reaction 7.4 calculated using the experimentally determined partial pressures of lead bromide is 63.4 kJ mol^{-1} at 700 K and 49.7 kJ mol^{-1} at 800 K and these are in excellent agreement with the corresponding values of 61.5 and 45.7 kJ mol^{-1} calculated using the data of Ting-Man Li and Simmons [2]. Thus, Reaction 7.4 provides a plausible explanation for the vapour pressure behaviour and suggests that, like the 2:1 lead oxybromide, the 1:1 lead oxybromide is a true compound. The X-ray powder diffraction patterns, however, show that the 1:1 lead oxybromide has a distinct crystal lattice at room temperature and that this is not the same as the 2:1

Table 7.3: A summary of the thermodynamic data associated with the reactions which could control the vapour pressure of 1:1 lead oxybromide

		Reaction 7.3	
T/K	ΔG / kJ mol^{-1}	pPbBr$_2$ / mmHg	$\log_{10}(p$ / mmHg)
700	81.12	6.72×10^{-4}	-3.17
800	65.06	4.3×10^{-2}	-1.37

		Reaction 7.4	
T/K	ΔG / kJ mol^{-1}	pPbBr$_2$ / mmHg	$\log_{10}(p$ / mmHg)
700	61.48	1.96×10^{-2}	-1.71
800	45.65	7.95×10^{-1}	-0.10

lead oxybromide. Thus, the present results suggest that as the temperature rises, the structure of the 1:1 lead oxybromide changes to an equilibrium mixture of 1:1 and 2:1 lead oxybromides and free lead bromide.

It should be noted that the evaporation of lead bromide from the 2:1 lead oxybromide should have little effect on the equilibrium position of the unimolecular decomposition Reaction 7.1 as the degree of dissociation is small. It follows that the resulting change in sample composition should have very little effect on its vapour pressure, and hence the plots of weight loss against time should be good straight lines as observed experimentally. In contrast, if the vapour pressure of the 1:1 lead oxybromide is controlled by the equilibrium position of Reaction 7.4, the vapour pressure of the 1:1 lead oxybromide could well be affected by changes in the sample composition, as the mole fraction equilibrium constant for the corresponding solid phase reaction involves the square of the mole fraction of the 1:1 lead oxybromide. The experimental vapour pressure data was simulated in Chapter 5 and one of the models considered corresponded to Reaction 7.4. The results of this particular model showed that the average weight loss achieved in the vapour pressure experiments reduces the mole fraction of 1:1 lead oxybromide in the solid phase to approximately 0.9 and this could have a marked effect on the equilibrium position of Reaction 7.4.

Many of the X-ray powder diffraction patterns of the residues from the vapour pressure experiments with the 1:1 lead oxybromide contained the diffraction pattern of the 2:1 lead oxybromide and this could have been produced by Reaction 7.4, with the mole fraction of the 2:1 lead oxybromide increasing with the loss of lead bromide from the system.

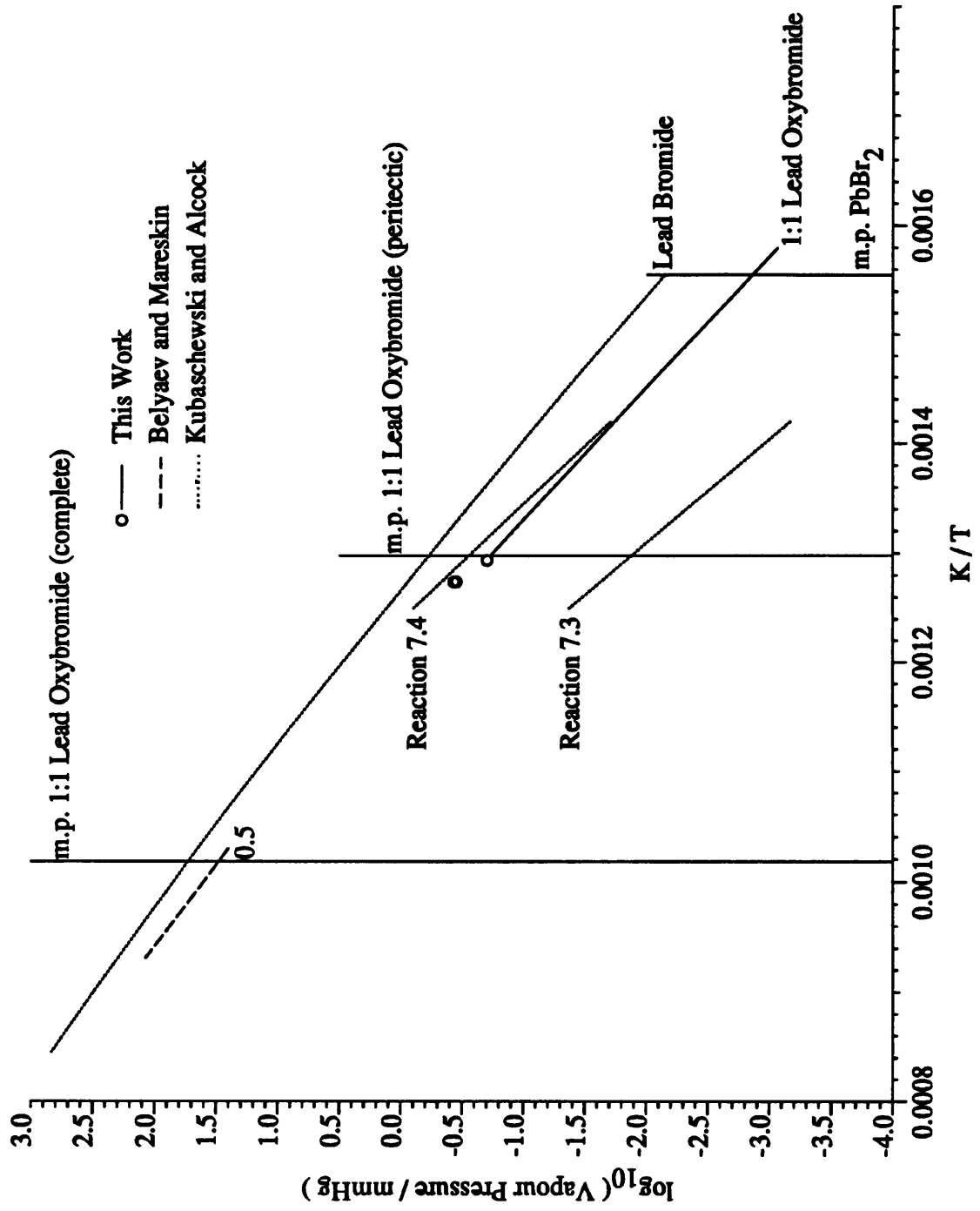

Figure 7.1: The calculated partial pressures of lead bromide for the reactions which could control the vapour pressure of the 1:1 lead oxybromide

It should also be noted that the 1:1 lead oxybromide melts incongruently and that the resulting solid phase is known to be 2:1 lead oxybromide. Thus, the present results suggest that the 2:1 lead oxybromide is formed progressively as the temperature is increased and not suddenly at the melting point, so that it is the residual 1:1 lead oxybromide which melts, leaving the solid 2:1 lead oxybromide in suspension.

It can be concluded, therefore, that both the 1:1 and 2:1 lead oxybromides are compounds in the accepted sense of the word and that they both behave in the same way with increasing temperature. The vapour pressure of the 1:1 lead oxybromide (manifest as the partial pressure of lead bromide above the oxybromide) is controlled by the thermodynamic equilibrium position of the reaction in which lead bromide and the 2:1 lead oxybromide are formed by the reaction of two moles of the 1:1 lead oxybromide. In contrast, the vapour pressure of the 2:1 lead oxybromide is controlled by the thermodynamic equilibrium position of the decomposition reaction in which one mole of the 2:1 lead oxybromide dissociates into two moles of solid lead oxide and one mole of gaseous lead bromide. This decomposition reaction controls the vapour pressure up to a temperature within 60 K of the melting point of the 2:1 lead oxybromide, but at some temperature in between the vapour pressure becomes dependent upon the equilibrium position of the reaction in which the 2:1 lead oxybromide and the lead oxide combine to form the 3:1 lead oxybromide. The overall reaction obtained by combining these latter two reactions is analogous to that described for the 1:1 lead oxybromide although the mechanism is different.

It follows that the lead oxybromides which are richer in lead oxide become progressively more stable as the temperature is raised, so that they have a tendency to form free lead bromide with increasing temperature. This is analogous to the conclusion of Ting-Man Li and Simmons concerning the nature of the lead deposits in an exhaust filter of a petrol engine. They used the available thermodynamic data and showed that the lead oxyhalides produced by the reaction of the lead deposits in an exhaust filter with the hydrogen bromide in the gas stream depended on the temperature. They predicted that the lead oxybromides with the higher lead oxide content were formed at the higher temperatures and that as the temperature was decreased the lead oxybromides with a higher lead bromide content were formed. However, they were unable to predict the level of retention of lead in the filter as the vapour pressures of these compounds were not known. They intuitively assumed that the conversion of the 1:1 lead oxybromide to the 2:1 lead oxybromide when the temperature reached a particular level led to the formation of free lead bromide which could then evaporate into the exhaust stream. Thus, a period of motorway driving after a period of urban driving would result in an increased emission of lead through the exhaust system. The present study has provided the missing vapour pressure data and shows that the situation in the exhaust is somewhat more complex than

that envisaged by Ting-Man Li and Simmons. Unfortunately, in this context, it is now effectively superfluous, as lead alkyls are being eliminated from petrol.

The results of this work are unlikely to reverse the decision to remove lead based anti-knock compounds from petrol. The more stringent controls on the emission of NO_x, unburnt hydrocarbons, carbon dioxide and carbon monoxide introduced in November 1991 will undoubtedly become tougher in the future and automobile manufacturers will be forced to add catalytic converters to the exhaust system in order to meet these standards. The catalysts present in these converters are readily poisoned by very low levels of lead compounds and it is doubtful that the lead filter technology will be improved to the extent where lead alkyls can used as anti-knock agents.

References

[1] JANAF, *Thermochemical Tables*, 2nd Ed. US Dept. of Commerce, National Bureau of Standards, 1971.

[2] Ting-Man Li and Simmons. R.F., *The Mechanism of Lead Scavenging by Bromoethane,* Nineteenth Symposium (International) on Combustion/The Combustion Institute, (1982), p. 1487-1494.